

An Experimental Investigation on the Transport Characteristics of Rough Fractures in the
Presence of Proppants

by

Raimbay Aigerim

A thesis submitted in partial fulfillment of the requirements for the degree of

Master of Science

in

Petroleum Engineering

Department of Civil and Environmental Engineering
University of Alberta

© Raimbay Aigerim, 2015

Abstract

Since the introduction of hydraulic fracturing technique, industry has been attempted to enhance production of hydrocarbon from tight reservoirs by selecting optimum design of hydraulic fracturing treatment. One of the essential parameters in hydraulic fracturing design is the proper selection and injection of proppants. They not only provide fracture permeability but also prevent “healing” of fractures. Hence, the quantification of proppant transport characteristics is highly critical in a sustainable production from hydraulically fractured wells. Previous studies in this regard were limited to smooth (parallel) fracture surfaces to a great extent ignoring the effect of roughness of fractures, which may have significant impact in controlling the permeability of hydraulic fractures in the presences of proppants.

In this thesis, effect of surface roughness to fluid flow and transportation/distribution of propping agents were investigated through experimental work. Water and polymer solutions representing typical rheological properties of hydraulic fracturing fluids were injected through transparent models of the fractures of different origin rocks (granite, marble, and limestone) with and without propping agents. The permeability changes due to proppant distribution caused by the roughness of fracture surfaces were quantified and correlated to different fractal characteristics of surface roughness. Qualitative and quantitative analyses were supported by visualization of experiments.

Acknowledgements

Uncountable number of people starting from parents, friends, professors, technicians and volunteer students were involved in the creation process of this research project. I would like to thank everyone of those for their support and assistance in developing of this master thesis. First and foremost, I would like to express my most profound gratitude to my supervisors Dr. Tayfun Babadagli and Dr. Ergun Kuru for their valuable guidance, encouragement and advices that they provided through my research study. Without their constant support and motivation this project would never have been carried out. In addition, I am infinitely thankful to Engineering Technologist Todd Kinnee for his help and suggestions in conducting laboratory experiments. With the guidance of him I learned to use a lot of tools and machines, which I would never have imagined, and thought I will learn to use them.

I gratefully acknowledge the financial support from Dr. Tayfun Babadagli's NSERC Industrial Research Chair in Unconventional Oil Recovery (industrial partners are CNRL, SUNCOR, Petrobank, Sherritt Oil, APEX Eng., PEMEX, Statoil, and Husky Energy), the Helmholtz Alberta Initiative (HAI) project funded by the Alberta Government for funding equipment used in the experiments. Also, I am thankful to JCS "Center for International Programs" funded by the government of the Republic of Kazakhstan for the MSc scholarship granted.

I am also thankful to EOGRRRC research group members for their constant help and advices in resolving any issues. Furthermore, I would like to thank Pamela Keegan for being patient in editing my papers. I am also thankful to Georgeta Istratescu for providing necessary items for an experiments. I would also like to thank summer volunteer student Yu Wang for assisting in processing data and laboratory experiments.

Special thanks to my entire graduate program friends and roommates without them my stay in Canada would not be full of warm memories. In particular I would like to thank my friends Doszhan Mamedulanov, Kais Ben Abdallah, Yevgenii Zagayevskii and Amin Jorati for being with me in my ups and downs of my life and most importantly, for providing moral support in my stay in Canada.

Last but most significant thank goes to my father Raimbay Siyazov, who is inspiring and supporting any my decisions through my life. I am also very grateful to my mother for her endless love and belief in me. Also, I would like to thank my brothers and all my extended family for giving me the best blessings and wishes.

Table of Content

CHAPTER 1: INTRODUCTION.....	1
Overview.....	2
Statement of the Problem.....	3
Objectives of the Study.....	5
Structure of the Thesis.....	5
References.....	6
CHAPTER 2: EFFECT OF FRACTURE ROUGHNESS, SHEAR DISPLACEMENT, FLUID TYPE AND PROPPANT ON THE PERMEABILITY OF A SINGLE FRACTURE: A VISUAL AND QUANTITATIVE ANALYSIS.....	8
Preface.....	9
1. Introduction.....	10
2. Experimental Methodology.....	11
3. Results and Discussion.....	12
3.1 Water Injection on Joint Fracture Models.....	13
3.2 Water Injection on 5 mm Shear Displaced Models.....	14
3.3 Xanthan Gum Injection on Joint Fracture Models.....	15
3.4 Xanthan Gum + Proppant Injection on Joint Fractures.....	16
4. Conclusions and Remarks.....	17
References.....	19
CHAPTER 3: FRACTAL ANALYSIS OF SINGLE-PHASE WATER AND POLYMER SOLUTION FLOW IN ROUGH FRACTURES.....	39
Preface.....	40
1. Introduction.....	41
2. Experimental Methodology	43
3. Results and Discussion	44
3.1 Effect of Fluid Type	45
3.1.1 Water Injection on joint Fracture Models.....	45
3.1.2 Polymer (Xanthan Gum) solution on Joint Fracture Models.....	47
3.2 Sheared Fractures: Water Injection in 5 mm Horizontally(Sheared) Displaced Models ...	48

3.3 Quantitative Analysis.....	49
3.3.1 Wetted Areas for Water Flow.....	49
3.3.2 Pressure Drop for Water Flow.....	50
3.3.3 Wetted Areas for Polymer Solution Flow.....	50
3.3.4 Pressure Drop for Water Polymer solution Flow.....	50
4. Conclusions and Remarks.....	51
References.....	54
CHAPTER 4: QUANTITATIVE AND VISUAL ANALYSIS OF PROPPANT TRANSPORT IN ROUGH FRACTURES AND APERTURE STABILITY.....	80
Preface.....	81
1. Introduction.....	82
2. Experimental Methodology.....	83
3. Results and Discussion.....	87
3.1 Effect of Fluid Type on Proppant Transportation Ability.....	87
3.2 Quantitative Analysis.....	93
3.3 Effect of Fracture Type(Joint and Horizontally Displaced – Sheared) on Proppant Transportation Ability.....	96
4. Conclusions and Remarks.....	105
References.....	106
CHAPTER 5: CONCLUSIONS AND RECOMMENDATIONS.....	109
Conclusions.....	110
Recommendations.....	111

List of Figures

CHAPTER 2: EFFECT OF FRACTURE ROUGHNESS, SHEAR DISPLACEMENT, FLUID TYPE AND PROPPANT ON THE PERMEABILITY OF A SINGLE FRACTURE: A VISUAL AND QUANTITATIVE ANALYSIS.....	8
Figure 1—Top and side views of fracture models.....	22
Figure 2—Side view of fractures Fr.5, Fr.6, Fr.8s sheared to 5 mm.....	22
Figure 3a—Schematic of experimental set-up.....	23
Figure 3b – Detailed model holder description.....	23
Figure 4 – Visualization of water flow in 7 –joint type- rough models +flat model. Blue areas correspond to air and yellow is dyed water.....	24
Figure 5a—Pressure drop in joint fractures while injecting water at 3.4 cc/min.....	26
Fig. 5b—Pressure drops across the fracture models versus injection rates.....	26
Figure 6 – Water injection at 5 mm sheared fracture models.....	27
Figure 7a—Pressure drop recorded during water injection (joint vs. sheared model).....	28
Figure 7b—Pressure difference between joint and sheared fracture models (the pressure difference between the joint and sheared models given in Fig. 7a after they are stabilized) against variogram, power spectral, triangular prism and ratio between total and planar area fractal dimensions (L-limestone; M-marble).....	30
Figure 8—Visualization of aqueous Xanthan Gum fluid flow on joint fracture models.....	30
Figure 9a—Comparison of Pressure Drops for XG solution vs. water while flowing through joint fractures.....	32
Figure 9b—Pressure drops in fracture models Fr.2, Fr.4s, Fr. 5 while injecting XG fluid and water.....	34
Figure 9c—Pressure difference between two fluid types injection on joint fractures (the pressure difference between the joint and sheared models given in Fig. 9a after they are stabilized) against variogram, power spectral, triangular prism and ratio between totaland planar area fractal dimensions (L-limestone; M-marble).....	34
Figure 10—Xanthan Gum+sand injection on 8 fracture models (blue parts are not saturated areas; green is Xanthan Gum; black is accumulated sand; red circles are transported sand	

indication). As seen, sands progress through channels and settle down eventually in the wider channels caused by tortuosity.....35

Figure 11a—Pressure Drop while proppants are transported through fracture models Fr.3, Fr.4s, Fr.5 using XG fluid and water at joint fractures.....37

Figure 11b—Pressure drop difference between Xanthan Gum and Xanthan Gum+sand injection on joint fractures (L-limestone; M-marble).....38

CHAPTER 3: FRACTAL ANALYSIS OF SINGLE-PHASE WATER AND POLYMER SOLUTION FLOW IN ROUGH FRACTURES.....39

Figure 1—Top and side views of fracture models (Raimbay et al. 2014). The thickness of the model varies slightly model by model.....58

Figure 2—Schematic of experimental set-up (Raimbay et al. 2014).....58

Figure 3—Planar view of water and polymer (Xanthan Gum) solution flow in the joint fracture models given in Table 1. Blue areas correspond to air and yellow is dyed water/polymer solution.....59

Figure 4—Wetted areas correlated to different roughness parameters (variogram analysis, power spectral density and triangular prism fractal dimensions, and ratio of total area to planar area) for seven fracture models. Fluid injected: Water. Fracture type: Joint. AGS: Average grain size.....61

Figure 5—Pressure drops (permeability) correlated to different roughness parameters (variogram analysis, power spectral density and triangular prism fractal dimensions, and ratio of total area to planar area) for seven fracture models. Fluid injected: Water. Fracture type: Joint. AGS: Average grain size.....62

Figure 6—Wetted areas correlated to different roughness parameters (variogram analysis, power spectral density and triangular prism fractal dimensions, and ratio of total area to planar area) for seven fracture models. Fluid injected: Polymer (Xanthan Gum) solution. Fracture type: Joint. AGS: Average grain size.....63

Figure 7—Pressure drop (permeability) correlated to different roughness parameters (variogram analysis, power spectral density and triangular prism fractal dimensions, and ratio of total area to planar area) for seven fracture models. Fluid injected: Polymer (Xanthan Gum) solution. Fracture type: Joint. AGS: Average grain size.....64

Figure 8—Planar view of water flow in 6 shear displaced rough models. Blue areas correspond to air and yellow is dyed water.....65

Figure 9—Wetted areas correlated to different roughness parameters (variogram analysis, power spectral density and triangular prism fractal dimensions, and ratio of total area to planar area) for six fracture models. Fluid injected: Water. Fracture type: Joint and horizontally displaced (sheared). L: Limestone, M: Marble.....66

Figure 10—Pressure drop (permeability) correlated to different roughness parameters (variogram analysis, power spectral density and triangular prism fractal dimensions, and ratio of total area to planar area) for seven fracture models. Fluid injected: water. Fracture type: Joint and horizontally displaced (sheared).....67

Figure A1—Testing different correlations between five variables and wetted areas for joint fracture cases for water.....68

Figure A2—Testing different correlations between five variables and wetted areas for sheared fracture cases for water.....69

Figure A3—Testing different correlations between five variables and pressure drop for joint fracture cases for water.....70

Figure A4—Testing different correlations between five variables and pressure drop for sheared fracture cases for water.....71

Figure A5—Testing different correlations between five variables and wetted area for joint fracture cases of polymer solution.....72

Figure A6—Testing different correlations between five variables and pressure drop for joint fracture cases of polymer solution.....73

CHAPTER 4: QUANTITATIVE AND VISUAL ANALYSIS OF PROPPANT TRANSPORT IN ROUGH FRACTURES AND APERTURE STABILITY.....80

Figure 1—Top and side views of fracture models.....85

Figure 2—Schematic of experimental set-up.....86

Figure 3—Images of embedded sand particles (black: sands - white: dry and injected fluid saturated areas); Xanthan Gum solution.....86

Figure 4—Planar view of water and polymer (Xanthan Gum) solution flow in joint-type (mating) fractured models given in Table 1. Blue areas correspond to air, yellow is dyed water/polymer solution, and black is embedded sand.....88

Figure 5—Pressure drop while proppants transported by water in the samples listed in Table 1 and a flat (smooth) fracture. Upper graph shows all these samples and the smooth samples case is excluded in the bottom graph for a better view of pressure drops in rough fractures...90

Figure 6—Pressure drop while proppants transported by Xanthan Gum solution in rough fracture models and a flat (smooth) model. Upper graph shows all the samples and the smooth samples case is excluded in the bottom graph for a better view of pressure drops in rough fractures.....92

Figure 7—Pressure drops (permeability) correlated to different roughness parameters (variogram analysis, power spectral density and triangular prism fractal dimensions, and ratio of total fracture surface area to planar area) for seven fracture models. Fluid injected: Water (left column) and XG solution (right column). Fracture type: Joint.....95

Figure 8—Wetted areas correlated to different roughness parameters (variogram analysis, power spectral density and triangular prism fractal dimensions, and ratio of total fracture surface area to planar area) for seven fracture models. Fluid injected: Water (left column) and Xanthan Gum solution (right column). Fracture type: Joint.....96

Figure 9—Planar view of water and polymer (Xanthan Gum) solution flow in horizontally displaced (sheared-unmating) fracture models. Blue areas correspond to air, yellow is dyed water/polymer solution, and black is embedded sand.....97

Figure 10—Pressure drop while proppants transported by water (left plots) and Xanthan Gum solution (right plots) on joint-type (mating) and sheared (horizontally displaced-unmating) fracture models. Only an initial value (indicated by a blue circle) of pressure was recorded for the polymer solution of the joint model of Fr. 6 due to mechanical failure.....99

Figure 11—Pressure drop (permeability) correlated to different roughness parameters (variogram analysis, power spectral density and triangular prism fractal dimensions, and ratio of total fracture surface area to planar area) for seven fracture models. Fluid injected: water (left column) and XG (right column). Fracture type: Joint and Sheared. M: Marble, L: Limestone, G: Granite, CL: Crystallized Limestone.....102

Figure 12—Wetted areas correlated to different roughness parameters (variogram analysis, power spectral density and triangular prism fractal dimensions, and ratio of total fracture surface area to planar area) for seven fracture models. Fluid injected: water (left column) and XG (right column). Fracture type: Joint and Sheared. M: Marble, L: Limestone, G: Granite, CL: Crystallized Limestone.....103

List of Tables

CHAPTER 2: EFFECT OF FRACTURE ROUGHNESS, SHEAR DISPLACEMENT, FLUID TYPE AND PROPPANT ON THE PERMEABILITY OF A SINGLE FRACTURE: A VISUAL AND QUANTITATIVE ANALYSIS.....8

Table 1—Lithological descriptions of the rock samples and the calculated roughness parameters of the model fracture surfaces.....21

CHAPTER 3: FRACTAL ANALYSIS OF SINGLE-PHASE WATER AND POLYMER SOLUTION FLOW IN ROUGH FRACTURES.....39

Table 1—Lithological descriptions of the rock samples and the calculated roughness parameters (Develi and Babadagli 2015).....57

Table 2—Wetted areas by water (%) in joint and sheared fractures when water is injected.....57

Table A1—Correlations obtained for wetted area - joint fracture cases for water.....74

Table A2—Correlations obtained for wetted area - sheared fracture cases for water.....75

Table A3—Correlations obtained for pressure drop - joint fracture cases for water.....76

Table A4—Correlations obtained for pressure drop - sheared fracture cases for water.....77

Table A5—Correlations obtained for wetted area - joint fracture cases with polymer solution...78

Table A6—Correlations obtained for pressure drop - joint fracture cases with polymer solution.....79

CHAPTER 4: QUANTITATIVE AND VISUAL ANALYSIS OF PROPPANT TRANSPORT IN ROUGH FRACTURES AND APERTURE STABILITY.....80

Table 1—Lithology of the rock samples and the roughness parameters for the surfaces of model fractures.....85

CHAPTER 1: INTRODUCTION

Overview

Enormous hydrocarbon reserves in tight reservoirs promoted hydraulic fracturing technique as one of the most common techniques of well stimulation. The concept of hydraulically fracturing a formation was first introduced by J.B. Clark in the late 1940s where the main purpose of the technique was to increase production from petroleum reservoirs (Howard and Fast, 1970). Since then, with further development of hydraulic fracturing technique and its successful application in the petroleum industry, other engineering disciplines such as Enhanced Geothermal Energy and hazardous waste isolation, etc., have also begun to apply this technology in their operations (Bunger, et al., 2013). Therefore, characterization and modeling of fluid flow in fractures and fracture systems have been widely studied. As a fundamental approach in understanding fluid flow in fracture systems, fluid flow in a single fracture and its behavior should be properly understood.

An ideal single fracture is defined as a region between two parallel smooth plates where the hydraulic aperture width is a constant (Gangi, 1978; Kranz, et al. 1979; Tsang and Whitherspoon, 1983). In this case, cubic law can define the relationship between fracture conductivity and fluid flow. However, this approach cannot describe the nature of channeling that takes place in natural rough fractures as fractures have variable apertures and asperities within the walls (Walsh, 1981; Tsang, 1984). Therefore, fluid flow and its interaction with fractured rock and proppants filling the fracture cannot be described without precise description of geometry of surface roughness. Consequently, all these factors influence our modeling approach of fluid flow between rough fracture walls. Previous work shows that with small surface roughness the flow is homogeneous, then the smooth (cubic law) model is probably sufficient to describe flow in these fractures (Brown, 1987). In contrast, flow in fractures with large roughness and heterogeneous distribution of aperture involving channeling of fluid with partial covering the fracture surface will not be described adequately by cubic law where roughness should be taken into consideration.

In addition to rough fracture walls, it should also be considered whether the fractures are of joint or shear type. Joints are breaks that form as a result of opening displacement while shear fractures are breaks with displacement parallel to the plane of the breakage (Atkinson, 1987).

Flow in joint fractures is controlled by aperture distribution with heterogeneous distribution of contacting asperities causing channeling in flow paths. Whereas, as a result of shear displacement of fractures, redistribution of asperities takes place and connectivity of apertures increases, which results in the creation of less tortuous flow paths in the perpendicular direction (Nemoto et al., 2009).

Alongside mechanical properties of fractures, selection of proper fluid type with the ability to carry propping agent to generate desired fracture height growth and to provide fluid loss control also plays an important role. Selection of a fracturing fluid is not only a technically critical part but also an economically critical part of the fracturing treatment design as fluid and proppants together may represent more than 50% of the total cost of the operation (Holditch, 1984). Viscosity of fracturing fluid plays an important role in generating desired net pressure to control the growth of fracture height and provide sufficient aperture to place proppants into the fracture. For instance, high viscosity fluids build wider fractures with better proppant transportation abilities but also generate high net pressure, which could lead to undesired vertical height growth (Meng and Brown, 1987). In contrast, low viscosity fluids are effective in controlling vertical height growth but, on the other hand, have poor transport ability of cuttings causing the occurrence of proppant deposition at the inlet of the fracture before closure of the crack (Barber and Themig, 1985). Therefore, in this study, the effects of fluid type, proppant size and rock type (fracture characteristics) on the transport and distribution of proppants within the fracture were investigated.

Statement of the Problem

In order to simulate fluid flow in fracture systems, flow of fluid in a single fracture has been commonly studied. Many experimental studies on the fluid flow in fractures have been conducted using two smooth and parallel planes separated by a constant hydraulic aperture. Yet, the geometry of fractures in nature has surface asperities and voids within their walls that causes fluid to take tortuous flow path (Brown, 1987). There are numerical and experimental studies focused on fluid flow in single rough fracture models suggesting closure in the formation results in well-defined channels, which do not cover the whole fracture surface (Watanabe, et al. 2008). In addition to studies focused on roughness effect on channeling of fluid flow, permeability of

fractures was measured and compared against each other in order to define roughness effect on permeability (Tsang, 1984). As natural fractures are complex structures with different degree of surface roughness and rock types, the modeling of fluid flow between fracture walls with variety of roughness characteristics in different rock types should be clarified. Previous experimental studies have shown the effect of roughness on fluid path and permeability without using fractal dimensions such as variogram analysis (D_{va}), power spectral density (D_{psd}), triangular prism method (D_{tp}), and the ratio of total and planar areas (A_t/A_p). The use of fractal dimensions to correlate the degree of roughness to permeability and fracture surface coverage by fluid is a new approach.

In addition to fluid flow, transportation and distribution of propping agents (which are injected using different fluid type) with their impact on permeability in rough fractures should be studied. In previous experimental studies, proppants were injected into a smooth model with water as a hydraulic fracturing fluid and banking of proppants was observed at inlet of fracture with only a small amount of them reaching the tip of most fractures (Babcock et al., 1967; Raymond and Binder, 1967; Novotny, 1970; Penny, 1987). The distribution of proppants in those models can also be seen in layers (either monolayer or multilayer). There have also been some studies of proppant effect on permeability of rough fractures where proppants were placed and variation of proppant distribution was considered (Kassis et al., 2010). However, placement of propping agent depends on transportation ability of fluid type and surface roughness of fractures, which should be explained.

There are two types of fractures: joint and sheared. According to Tsang and Witherspoon (1983), well-matched fractures have narrow and peaked aperture distribution while with mismatching of fracture walls the aperture distribution broadens. Another study reports that as a result of shear displacement, connectivity of apertures increases, which also results in decrease of path tortuosity and increase of permeability (Nemoto et al., 2009). However, no study exists on the effect of shear displacement on transportation and distribution of proppants and its effect on the fracture. Therefore, a study with wide range of rock types with original roughness characteristics are expected to be useful in understanding fluid flow and proppant transportation in different reservoirs with different roughness characteristics, and can be used for improved design of hydraulic fracturing treatment.

Objectives of the Study

This study aims to achieve the following objectives:

1. Design an experimental setup for different type of fluid (water and Xanthan Gum) and proppant injection into the 2-D joint and shear rough fracture models in order to visualize and measure pressure drop to define surface roughness effect on flow of different fluid type.
2. Correlate the effect of surface roughness that have been defined using different fractal dimension methodologies (variogram analysis, D_{va} ; triangular prism, D_{tp} ; power spectral density analysis, D_{psd} , and ratio between total to planar area) with following properties:
 - Area swept by different type of fluid
 - Pressure drop
 - Rock type
 - Grain size
3. Investigate proppant transport ability of different fluids type (i.e., water and polymer fluid) in different rock type with different degree of roughness in joint and shear fractures.

Structure of the Thesis

The thesis is paper-based and is comprised of five chapters. The main body (Chapters 2-4) is composed of 3 papers that were presented at conferences and/or submitted to peer-reviewed journals. Each of the chapters contains their own introduction, literature survey, results, conclusions and references.

Chapter 1

This chapter includes a brief overview and background information about hydraulic fracturing and introduces associated problems. It also provides the statement of the problem and discusses objectives of the study.

Chapter 2

Experimental setup was designed to visually and quantitatively investigate the hydraulic characteristics of rough fractures in the presence of proppants. Water and polymeric

solutions representing typical rheological properties of hydraulic fracturing fluids were injected through the models (joint and sheared fractures) with and without propping agents. Proppants were placed in fracture models.

Chapter 3

This chapter presents a quantitative analysis of single phase flow in rough fractures at high rates representing hydraulic fracturing conditions. The inlet pressure and percentage of planar flow wetted area by injected water and polymeric solution were correlated to three fractal methods and suggested one promising method of surface roughness quantification.

Chapter 4

A new experimental setup was designed for injection of propping agents with fracturing fluid. Fracturing fluid water and polymer solution with proppants was injected on joint and horizontally displaced fracture models. Existing closure areas controlled by roughness dictated proppant movement and permeability change significantly in both joint and displaced type fractures. To quantify this effect, fracture permeability and proppant distribution (area saturated with sands) were correlated to three fractal methods.

Chapter 5

The last chapter outlines major conclusions of this study and offers recommendations for further continuation of this work.

References

- Atkinson, B.K. 1987. Fracture Mechanics of Rocks. University College London, Academic Press, London
- Babcock, R.E., Prokop, C.L. and Kehle, R.O. 1967. Distribution of Propping Agents in Vertical Fractures. University of Arkansas.
- Barber, P.L. and Themig, D.J. 1985. The Use of Density Control Foam Fracturing for Selective Proppant Placement in the Bartlesville Formation. Paper SPE 13797 presented at the SPE Production Operations Symposium, Oklahoma City, Oklahoma, 10-12 March.
- Brown, S.R. 1987. Fluid Flow Through Joints: The Effect of Surface Roughness. *Journal of Geophysical Research* **92** (B2): 1337-1347.
- Bunger, A.P., McLennan, J and Jeffrey, R. 2013. Effective and Sustainable Hydraulic Fracturing. InTech, Rijeka, Croatia.
- Gangi, A.F. 1978. Variation of Whole and Fractured Porous Rock Permeability with Confining Pressure. *Int. J. Rock Mech. Min. Sci. & Geomech. Abstr.* **15** (5): 249-257.
- Holditch, S.A. 1984. Criteria for Propping Agent Selection. *Sovereign Engin. Intern.*, 2nd. ed., 165 pp.; 3rd ed., 221 pp., Norton-Alcoa Proppants, Dallas, Texas.

- Howard, G.C. and Fast, C.R. 1970. Hydraulic Fracturing. Society of Petroleum Engineers of AIME, New York and Dallas.
- Kassis, S. and Sondergeld, C.H. 2010. Fracture Permeability of Gas Shale: Effect of Roughness, Fracture Offset, Proppant, and Effective Stress. Paper SPE 131376 presented at the CPS/SPE International Oil & Gas Conference and Exhibition, Beijing, China, 8-10 June.
- Kranz, R.L., Frankel, A.D., Engelder, T., et al. 1979. The Permeability of Whole and Jointed Barre Granite. *Int. J. Rock Mech. Min. Sci. & Geomech. Abstr.* **16** (4): 225-234.
- Meng, H.Z. and Brown, K.E. 1987. Coupling of Production Forecasting, Fracture Geometry Requirements, and Treatment Scheduling in the Optimum Hydraulic Fracture Design. Paper SPE 16435 presented at the Low Permeability Reservoirs Symposium, Denver, Colorado, 18-19 May.
- Nemoto, K., Watanabe, N., Hirano, N., et al. 2009. Direct Measurement of Contact Area and Stress Dependence of Anisotropic Flow Through Rock Fracture with Heterogeneous Aperture Distribution. *Earth and Planetary Science Letters* **281** (1-2): 81-78. <http://doi:10.1016/j.epsl.2009.02.005>.
- Novotny, E.J. 1970. Proppant Transport. Presented at the 52nd Annual Fall Technical Conference and Exhibition, Denver, Colorado, 9-12 October. SPE-6813.
- Penny, G.S. 1987. An Evaluation of the Effects of Environmental Conditions and Fracturing Fluid upon the Long-Term Conductivity of Proppants. Paper SPE 16900 presented at 62nd Annual Technical Conference and Exhibition, Dallas, Texas, 27-30 September.
- Raymond, L.R. and Binder, G.G. 1967. Productivity of Wells in Vertically Fractured, Damaged Formations. *J Pet Tech* **19** (01): 120-130.
- Tsang, Y.W. and Witherspoon, P.A. 1983. The Dependence of Fracture Mechanical and Fluid Flow Properties on Fracture Roughness and Sample Size. *Journal of Geophysical Research* **88** (B3): 2359-2366.
- Tsang, Y.W. 1984. The Effect of Tortuosity on Fluid Flow through a Single Fracture. *Water Resources Research* **20** (9): 1209-1215.
- Walsh J.B. 1981. Effect of Pore Pressure and Confining Pressure on Fracture Permeability. *Int. J. Rock Mech. Min. Sci. & Geomech. Abstr.* **18** (4): 429-435.
- Watanabe, N., Hirano, N., and Tsuchiya, N. 2008. Diversity of Channeling Flow in heterogeneous Aperture Distribution inferred from Integrated Experimental – Numerical Analysis on Flow through Shear Fracture in Granite. *Journal of Geophysical Research* **114** (B4). <http://doi:10.1029/2008JB005959>.

CHAPTER 2: EFFECT OF FRACTURE ROUGHNESS, SHEAR DISPLACEMENT, FLUID TYPE AND PROPPANT ON THE PERMEABILITY OF A SINGLE FRACTURE: A VISUAL AND QUANTATIVE ANALYSIS

This paper is a modified and improved version of SPE 171577, which was presented at the SPE Unconventional Resources Conference held in Calgary, Alberta, Canada, 30 September – 2 October 2014. A version of this chapter has been submitted to the journal.

Preface

Proppants are one of the essential parameters in fracking design. They not only provide fracture permeability but also prevent “healing” of fractures. Hence, the quantification of proppant transport characteristics is highly critical in a sustainable production from hydraulically fractured wells. Previous attempts in this regard were limited to smooth (parallel) fracture surfaces to a great extent but the roughness of fractures may control the permeability of hydraulic fractures in the presences of proppants.

This paper focuses on experimental measurements to visually and quantitatively investigate the hydraulic characteristics of rough fractures in the presence of proppants. Transparent models of the fractures of different origin rocks (granite, marble, and limestone) were prepared. Water and polymeric solutions representing typical rheological properties of hydraulic fracturing fluids were injected through the models (joint and sheared fractures) with and without propping agents. The permeability changes due to proppant distribution caused by the roughness of fracture surfaces were quantified and correlated to different fractal characteristics of surface roughness. Qualitative and quantitative analyses were supported by images collected through the experiments.

Proppant behavior in joint and shear type fractures were observed to be different. In both cases, fracture closure areas existed, which controlled the proppant transportation and fracture permeability. The qualitative and quantitative data provided on the degree of permeability change in a single fracture (in the presence and absence of propping agents) are expected to be useful in accurate performance estimation of oil/gas production from fractured systems.

1. Introduction

The main goal of hydraulic fracturing is to provide permeable flow path for hydrocarbons in tight formations. The stability of this permeable flow path can be achieved by propping agents that are injected with treated water. Design of fracturing fluid treatment together with selecting proper proppant type critically impacts the hydrocarbon recovery from the formation (Coulter et al. 2004; Terracina et al. 2010; Kassis et al. 2010; Ribeiro and Sharma 2012, 2013). The mechanism of proppant transport in rough-walled fractures and its effect on permeability should be understood clearly in the assessment of recovery performance, as well. Proppant transport depends on the distribution of asperities, surface roughness, and contact area, which are all controlled by lithological properties of the rocks (Fredd et al. 2000). In addition, rough surface coupled with shear displacement causes closures of the fracture at some points and this eventually affects the proppant transport (van Dam and de Pater 1999).

Numerous studies were conducted on the fluid flow and proppant transport through a single rock fracture. Based on these studies, one of the assumptions is that the single fracture is a region between two parallel (smooth) plates, where fluid flow can be described by the cubic law (Gangi 1978; Kranz et al. 1979; Tsang and Whitherspoon 1983). Alongside fluid flow, parameters that affect the distribution of propping agents in the parallel plate model were studied (Babcock et al. 1967; Raymond and Binder 1967; Novotny 1977; Penny 1987). Although the parallel plate model can give a qualitative description, the real fracture surfaces are rough, which causes a tortuous fluid path and eventually a deviation from the cubic law (Brown 1987; Renshaw 1995). In addition, it was found that the value of flow rate predicted by the parallel plate model is several orders of magnitude higher than the flow rate in rough models (Tsang 1984).

The adjacent rough walls of the horizontally displaced (sheared) fractures contact each other at some local points throughout the fracture, and the number, size, and spatial distribution of these contacting zones together with the void spaces around them effect the transport properties of this kind of fractures (Yeo et al. 1998; Lee and Cho 2001; Auradou et al. 2006; Koyama et al. 2007; Nemoto et al. 2008; Watanabe et al. 2008). Moreover, applied vertical (normal) stress in rough walled models decreases permeability of fracture (Bernabe 1986; van Dam and de Pater, 1999; He et al. 2013). All of these studies focused on fluid and propping agent flow in flat and rough

models with effect to permeability in applied horizontal or/and vertical stresses with/without the presence of proppants. There are very limited studies on the effect of different rock types with different roughness characteristics on permeability in the presence of proppant agent.

The objective of this paper is to examine the fluid flow and proppant transport in rough fractures of different rock samples (e.g., granite, marble, and limestone). The quantitative and visual data of fluid flow and proppant transport were collected at joint and (horizontally displaced) sheared fractures by injecting water and polymer solution. Natural sand proppants at concentrations of 0, 2, and 3lbm/ft² were used and the inlet pressure was continuously monitored to measure fracture permeability. This paper studies to what degree the roughness of different fractal dimensions controls fluid and proppant transport, and what effect it has on permeability.

2. Experimental Methodology

Seven single fracture models from 20x20x20 cm granite, marble, and limestone block were fractured under indirect tensile tests (as similar to the Brazilian test). The surface replicas were molded by using silicone rubber and transparent plastic to prepare transparent models in the dimensions of 20x20x5 cm (**Fig. 1**). In order to visualize our experiments, the top part of the model was made of solid transparent plastic, while non-transparent silicone rubber was used for the bottom part. Two models (Fr.4s and Fr.8s) had both sides made of solid transparent plastic. The details of the preparation of model fractures can be found in Develi and Babadagli (2015). The model fractures used in this study had perfectly-matching adjacent walls and exemplified joint-type fractures. To observe the effect of unmating fracture surfaces (i.e., sheared fractures), the upper part of the model was slightly displaced, leading to “roughness” or uneven distribution of aperture and “touching” points yielding to closure. As an example of displaced fracture, three different fracture models are shown in **Figure 2**.

In order to quantify the fracture surface roughness, fractal dimensions obtained by variogram analysis (D_{VA}), power spectral density (D_{PSD}), and triangular prism method (D_{TP}), as well as the ratio between total surface area and planar surface area (A_t/A_p), were estimated. The measured values for seven different models are summarized in **Table 1**. Methodologies used to measure these properties are defined in Develi and Babadagli (1998, 2015).

The scheme of experimental set-up, which includes the model holder, syringe pump, pressure transducer, and a camera, is shown in **Figure 3a**. The model holder consists of a base where one of the single fractures is usually placed. The injection part has a 500 ml reservoir attached to the model and injected fluid is introduced into it uniformly to create a 2-D displacement. The reservoir is connected to the syringe pump and a pressure transducer, which measures the pressure change in the inlet part of the model. The pressure change is recorded continuously through a data acquisition system. Simultaneously, corresponding pictures are taken for the purpose of correlating pressure change and flow of injected fluid with and without proppant. A fluorescent dye is added into water in order to trace the fluid flow inside the model. A UV light source is used to make the dyed fluid visible.

2-D experiments were performed by injecting water, polymer solution (0.03wt% Xanthan Gum), and polymer solution with proppant at joint and sheared fractures located horizontally. 300–400 μm natural sand was used at concentration of 0, 2, 3 lbm/ft^2 . In all cases, fluid was injected at constant flow rate with measuring pressure drop across the length of the fracture. The pressure drops represent the conductivity of the fracture since all the models are assumed to have the same cross sectional area due to the same size spacers used (2mm in height located at the four corners of the joint and sheared type fracture models). Hence, any change in conductivity is due to roughness that differs model by model.

Sand was introduced to the fracture models by placing it in the inlet of fracture models in a width of 2.5 cm (**Fig. 3b**) at the same amount for all models. The fluid introduced through the reservoir shown in this figure carries the sand into the fracture model.

3. Results and Discussion

A series of experiments were conducted on all seven fracture models and a flat model to measure and compare conductivity. For specific experiments such as polymer and proppant injection, representative lithologies with a variety of roughness types based on the fractal dimension values (Table 1) were selected. Results were compared for joint and horizontally displaced (sheared) fractures for two types of injected (“fracking”) fluids with natural sands representing proppants. Experiments are divided into five groups:

- a. Water injection on joint fracture models (8 fracture and flat model)
- b. Water injection on 5 mm shear displaced models (7 fracture models)
- c. Xanthan Gum injection on joint fracture models (7 fracture models)
- d. Xanthan Gum + Proppant injection on joint fractures (8 fracture models)

3.1 Water injection on joint fracture models. The pressure drop across the joint fracture models were recorded continuously during the experiment and corresponding pictures of fluid flow in fracture models (**Fig. 4**) were taken in order to correlate them with changes in pressure drop across the fracture models. **Figure 5a** shows the pressure drop across fracture models. Fr.1 was not included due to failure in the pressure gauge. One may infer from these data and images that the tortuous path of fluid is controlled by roughness characteristics; i.e., different displacement patterns in Figure 4 and different pressure behavior with respect to rate in **Figure 5b** are indications of the effect of roughness. For example, models Fr.3 and Fr.8s yielded similar pressure drop values and, interestingly, possessed very close values of D_{VA} (Table 1). In addition, the fluid flow pattern through both fractures showed a similar progress (Fig. 4). In comparison with other fracture models, they showed the smallest swept area.

One may also observe that pressure drop systematically decreases with decreasing variogram fractal dimension for three limestone models (Fr.1, Fr.3, Fr.6). The exception is Fr.2, which was recrystallized limestone and the structure of the rock had been changed to non-porous structure. Interestingly, sample Fr.2 had the lowest fractal dimension (D_{VA}) among all samples. Due to the coarse grain size and non-porous structure, the marble fracture models (Fr.4s, Fr.7 and Fr.8s) showed higher wavelength of roughness (“long range”) (Babadagli et al. 2015a-b). In this case, increasing roughness (or D_{VA}) resulted in a decrease in pressure drop and higher permeability than the limestone models. Other samples tested were porous limestone (Fr.3) and finer grain marble (Fr.8s). They showed a different type of roughness (“short range” or shorter wavelength) after fracturing.

Rough-walls of models control not only the flow path and channeling but also the pressure drop, thereby hydraulic conductivity. It was observed that the pressure drop for the flat model was the highest among all the cases investigated. This is because as the fluid is introduced into the rough models, the fracture dilates and the fluid preferentially flows in the largest channel created by the

rough nature of the fracture surfaces. Therefore, the roughness controls fluid path and, eventually, pressure drop in models.

3.2 Water injection on 5 mm shear displaced models. The fluid flow in a 5 mm fracture displacement in 7 fracture models is shown in **Figure 6**. The swept area in sheared fracture cases is slightly higher (comparing images Figs. 4 and 6). Comparison of pressure drop data of joint and sheared fractures is displayed in **Figure 7a**. With a 5 mm displacement of limestone models (Fr.3 and Fr.6), the pressure drop was almost the same as in the joint fracture; i.e., no change in permeability. However, for other limestone models (Fr.1 and Fr.2), shear displacement not only decreased pressure drop significantly but also increased the area swept. In the marble models (Fr.7 and Fr.8s), displacement pressure drop decreased with 5mm displacement but for Fr.7, which had higher variogram fractal dimension, the difference between joint and sheared fractures was more significant than for Fr.8s.

On the other hand, with a 5 mm displacement of Fr.4s, the pressure drop increased significantly, eventually causing a reduction in permeability. This is a coarse “grain” marble sample and its roughness characteristics are different from finer “grain” marble (Fr.8s) and grainy-porous limestone. As the rock becomes more porous (or granular), roughness is characterized at “small scale;” i.e., the roughness of short wave length is exhibited in the rocks with high porosity (or more granular) and is made of grains (Babadagli et al. 2015a-b). In rock types like marble, the roughness is in the nature of higher wavelengths or “long range,” which yields more channeling as seen in the case of Fr.4s (Fig. 6). In other words, when compared to the marbles and granites, limestone samples are expected to be more porous, which is critical in fracturing process and this may result different roughness properties. For example, if the individual pore sizes (not overall or total porosity of the rock) are large, then we can expect roughness characterized by long wavelength and low frequency (or low wavenumber). As such, if individual pore sizes (not overall or total porosity of the rock) are small, we can then expect short wavelength and thus high frequency (or high wavenumber) roughness.

To test the observed pressure data against surface characteristics, three fractal and one statistical surface roughness parameters listed in Table 1 were plotted (**Fig. 7b**) against the pressure differences between sheared and joint fractures given in **Fig. 7a**. The pressure differences were

calculated using the pressure values recorded after stabilization. The purpose of this attempt was to find out which of those four parameters can be used in correlating the surface roughness characteristics to hydraulic behavior of fractures. In all four cases given in Fig. 7b, Fr.1 showed a distinct behavior, which possessed the highest values of the four parameters; i.e., the roughest sample. Two trends are obvious in the D_{VA} correlations. The left-most grouping contained the smallest fractal dimensions (Fr.2, Fr.3, Fr.6, and Fr.8s). Interestingly they were all limestone with fine grains (see Table 1 for the grain sizes), except Fr.8s. Note that the sample Fr.8s was marble but both sizes were solid so that it might yield different results, mainly due to less deformability. Fr.8s yielded very minimal difference in pressure change (or permeability change) after sheared (the last plot in Fig. 7a). Other two samples (Fr.7 and Fr.4s) with higher D_{VA} showed another trend, which was highly apart from the other four samples. They were both marble samples with considerably different fractal dimensions. The trends were similar in the cases of D_{Tp} and A_t/A_p but the samples were more grouped (except Fr.1) compared to the D_{VA} cases. No typical trends/correlations were observed when D_{psd} was used as a roughness parameter.

3.3 Polymer (Xanthan Gum) solution injection in joint fracture models. The linear gel-Xanthan Gum (XG) at concentration of 0.03% (W/W) was injected into joint fracture models to mimic polymer based hydraulic fracturing fluids (**Fig. 8**). Compared with water injection, the swept areas were remarkably larger in this case and also pressure drop was significantly higher (**Fig. 9a**). Pressure drop change is not only caused by the increasing viscosity of the injected fluid but also the roughness, as implied by **Figure 9b**. Fr.2 and Fr.5 showed nearly the same pressure drop at different flow rates (Fig. 9b) in comparison with Fr.4s. Note that Fr.2 ($D_{va}=1.263$) and Fr.5 ($D_{va}=1.299$) had close variogram fractal dimensions than Fr.4s ($D_{va}=1.39$). Once again, Fr.4s showed an exceptional case; i.e., lower pressure drop even though it had higher variogram fractal dimension than Fr.2 and Fr.5. This can be attributed to the lithology of the model. Coarse “grain” marble showed higher wavelength roughness compared to finer grain marbles or “porous” limestone. This type of “long range” roughness results in more channeling compared to “short range” roughness that is exhibited by finer grain (or porous) rock samples as discussed before.

As seen through the snapshots given in Figure 8, the area swept by XG solution was much larger than those of corresponding water cases (Fig. 4). Some contact areas existed in Fr.1, Fr.2, Fr.3 cases of XG injection, which were all limestones with small grain sizes. The Fr.8 case was an exception. The patterns given in Figs. 4 and 8 were quite similar and the same (roughness controlled) channeled flow was observed in both water (Fig. 4) and XG (Fig. 8) cases.

Similar plots to Figure 7b were generated for the pressure differences between water and XG cases and displayed in **Figure 9c**. Interestingly, the trends are similar to the water case (joint/sheared fracture differences) except the A_i/A_p case. D_{VA} showed a good trend (as well as D_{TP}) indicating that the pressure drop difference between two types of rocks followed a systematic pattern and four distinct group of points were marked by different color symbols (Fig. 9c, D_{VA} case). For all rock types, with an increase of D_{VA} and D_{TP} , the difference in pressure drop decreased. This is consistent with the water case (joint/sheared fracture differences) given in Fig. 7b. D_{PSD} did not yield any trends as similar to the case given in Fig. 7b.

Up to this point, the effect of roughness on the flow of water and polymer based fluid through single fractures was evaluated. In practice, hydraulic fracturing is performed with fluids containing proppants. The transport of proppant with these fluids on rough fractures is also a critical problem. The next two sets of experiments investigate the transport of proppants through rough fractures.

3.4 Xanthan Gum solution + Proppant injection on joint fractures. Aqueous XG solution with natural sands was injected and the transportation of sands was traced. **Fig. 10** shows patterns of sand transportation with polymer fluid. The proppants moved with XG solution through the high conductivity areas of the fracture (channels) while causing change in pressure drop (or permeability). The degree of permeability change and the transportation/settlement of sands during and after fracturing are critical issues and, as shown visually, it is controlled by the roughness of the fracture. For instance, in cases Fr.3 and in Fr.4s (**Fig. 10a**), sand was distributed all over the area of fracture model and settled, but in case Fr.5, a granite sample, it did not move far from the inlet.

Fr.3 and Fr.5 showed an increase in the pressure drop across fracture models during XG solution with sand injection (**Fig. 11a**). This means that the added proppants reduced permeability.

Although both models possess low D_{VA} values (meaning the lowest degree of roughness), they unexpectedly exhibited lower values of the permeability than those of the rougher models. This behavior may be attributed to the development of a high degree of channeling, like the situation for Fr.3. The biggest difference between the “with and without sand cases” was observed for Fr.5. Having large size grains and low D_{VA} , this sample exhibited relatively smoother surface and the sand was not transported throughout the model as desired (Fig. 10, Fr.5 image). The rest of the limestone models (Fr.1, Fr.2 and Fr.6) showed a similar degree of reduction in pressure with proppant addition to XG solution.

It can be observed that the amount of transported sand over the model in Fr.3 is higher and distributed more evenly than in Fr.1, Fr.2 and Fr.6. That is the main reason for the decrease in permeability and this phenomenon is controlled by the -type of- roughness. For Fr.4s, the pressure drop was the same as pressure drop in injection of XG fluid only, meaning that the sand distributed in such a way that it did not change the conductivity of fracture. Note that this sample is manufactured using solid materials for both sides of the fracture unlike the others. The other two marble cases (Fr.7 and Fr.8s) showed a similar behavior and addition of sand decreased the pressure drop (increased permeability).

In a final attempt, the pressure differences given in Figure 11a were plotted against the roughness parameters listed in Table 1 (**Fig. 11b**). Out of four analyses, the D_{VA} showed a trend for each rock group as similar to the previous two cases given in (Figs. 7b and 9c); i.e., increasing fractal dimension resulted in larger pressure drops.

4. Conclusions and remarks

Rough walls of fracture affect the transport of fracturing fluids of different kind (water or polymer based fluid) and, therefore, roughness controls the permeability of fractures. With increasing degree of roughness, the permeability of the limestone joint fractures decreases. For the marble models, however, permeability increases with increasing roughness, which can be attributed to the development of a high degree of channeling.

In the case of sheared fractures through which water is injected, different samples of rocks, namely limestone, granite, and marble, showed different transport characteristics controlled by

roughness type. For example, permeability increases for the sheared limestone models as opposed to the joint ones. This may be attributed to the development of “easier” flow through channels formed as a result of horizontal displacement compared to the joint type models, which typically present less channeling. For the sheared marble models, however, permeability decreases with an increase of surface roughness.

The placement of proppants (in polymeric solution) is controlled by surface roughness and considerably changes the permeability of fracture. In the presence of proppants, fracture permeability increases with some exceptions (Fr.3, Fr.4s, and Fr.5). Of these, Fr.3 is a grainy limestone (the smallest grain size among all samples) possessing low fractal dimensions (smoother surfaces). This caused well distributed sand throughout the model. Fr. 5, on the other hand, had much larger grain size (but low fractal dimensions), resulting in the accumulation of sands at the entrance rather than being distributed throughout the model. Both cases caused a reduction in permeability. The rest of the limestone models (Fr.1, Fr.2 and Fr.6) showed a similar degree of reduction in pressure with proppant addition to XG solution. Hence, one may state that roughness with high wavelengths causes bigger channels, and proppant transport through joint type fractures and settlement does not significantly affect the permeability change. Roughness with smaller wavelengths is observed in granular (porous)/finer-grain rock types, yielding more proppant settlement and eventually more reduction in permeability.

To account for the changes in hydraulic behavior (permeability) caused by shearing, fracturing fluid type (water against polymeric solution), and proppant addition quantitatively, different fractal (D_{VA} , D_{PSD} , and D_{TP}) and statistical parameters (A_t/A_p) were used. The plots of pressure drop -permeability- changes against these four roughness parameters indicated that D_{VA} can be used in quantification of the hydraulic behavior of rough fractures.

Acknowledgments

This research was conducted under the second author’s (TB) NSERC Industrial Research Chair in Unconventional Oil Recovery (industrial partners are CNRL, SUNCOR, Petrobank, Sherritt Oil, APEX Eng., PEMEX, Statoil, and Husky Energy), the Helmholtz Alberta Initiative (HAI) project funded by the Alberta Government. The first author is thankful to JCS “Center for

International Programs” funded by the government of the Republic of Kazakhstan for the MSc scholarship granted. The fourth author (KD) thanks the Scientific and Technological Research Council of Turkey (TÜBİTAK) for his postdoctoral scholarship through the BIDEF program. We gratefully acknowledge these supports.

References

- Auradou, H., Drazer, G., Boschan, A., et al. 2006. Flow Channeling in a Single Fracture Induced by Shear Displacement. *Geothermics* **35**: 579-588. <http://doi:10.1016/j.geothermics.2006.11.004>
- Babadagli, T., Ren, X. and Develi, K. 2015a. Effects of Fractal Surface Roughness and lithology on Single and Multiphase Flow in a Single Fracture: An Experimental Investigation. *Int. J. of Multiphase Flow* **68**: 40-58.
- Babadagli, T., Raza, S., Ren, X. and Develi, K. 2015b. Effect of Surface Roughness and Lithology on the Water-Gas and Water-Oil Relative Permeability Ratios of Oil-Wet Single Fractures. *Int. J. of Multiphase Flow* **75**:68-81.
- Babcock, R.E., Prokop, C.L. and Kehle, R.O. 1967. Distribution of Propping Agents in Vertical Fractures. University of Arkansas.
- Bernabe, Y. 1986. The Effective Pressure Law for Permeability in Chelmsford Granite and Barre Granite. *Int. J. Rock Mech. Min. Sci. & Geomech. Abstr.* **23** (3): 267-275.
- Brown, S.R. 1987. Fluid Flow Through Joints: The effect of Surface Roughness. *Journal of Geophysical Research* **92** (B2): 1337-1347.
- Coulter, G.R., Benton, E.G, and Thomson, C.L. 2004. Water Fracs and Sand Quantity: A Barnett Shale Example. Paper SPE 90891 presented at the SPE Annual Technical Conference and Exhibition, Houston, Texas, September 26-29.
- Develi, K. and Babadagli, T. 1998. Quantification of Natural Fracture Surfaces using Fractal Geometry. *Math. Geol.* **30** (8): 971-998.
- Develi, K. and Babadagli, T. 2015. Experimental and Visual Analysis of Single-Phase Flow through Rough Fracture Replicas. *Int. J. of Rock Mech. and Min. Sci.* **73**:139-155.
- Fredd, C.N., McConnell, S.B., Boney, C.L., et al. 2000. Experimental Study of Hydraulic Fracture Conductivity Demonstrates the Benefits of Using Proppants. Presented at the SPE Rocky Mountain Regional/Low permeability Reservoirs Symposium, Denver, Colorado, 12-15 March. SPE-60326.
- Gangi, A.F. 1978. Variation of Whole and Fractured Porous Rock Permeability with Confining Pressure. *Int. J. Rock Mech. Min. Sci. & Geomech. Abstr.* **15** (5): 249-257.
- He, J., Ling, K., Pie, P., et al. 2013. A Correlation to Evaluate the Fracture Permeability Changes as Reservoir is Depleted. Paper SPE 165709 presented at the SPE Eastern Regional Meeting, Pittsburgh, Pennsylvania, 20-22 August.
- Kassis, S. and Sondergeld, C.H. 2010. Fracture Permeability of Gas Shale: Effect of Roughness, Fracture Offset, Proppant, and Effective Stress. Paper SPE 131376 presented at the CPS/SPE International Oil & Gas Conference and Exhibition, Beijing, China, 8-10 June.
- Kranz, R.L., Frankel, A.D., Engelder, T., et al. 1979. The Permeability of Whole and Jointed Barre Granite. *Int. J. Rock Mech. Min. Sci. & Geomech. Abstr.* **16** (4): 225-234.
- Koyama, T., Neretnieks, I., and Jing, L. 2007. A Numerical Study on Differences in using Navier-Stokes and Reynold Equations for Modeling the Fluid Flow and Particle Transport in Single Rock Fractures with Shear. *International Journal of Rock Mechanics & Mining Sciences* **45** (7): 1082-1101
- Lee, H.S. and Cho, T.F. 2002. Hydraulic Characteristics of Rough Fractures in Linear Flow under Normal and Shear Load. *Rock Mechanics and Rock Engineering* **35** (4): 299-318. <http://doi:10.1007/s00603-002-0028-y>.

- Nemoto, K., Watanabe, N., Hirano, N., et al. 2008. Direct Measurement of Contact Area and Stress Dependence of Anisotropic Flow Through Rock Fracture with Heterogeneous Aperture Distribution. *Earth and Planetary Science Letters* **281** (1-2): 81-78. <http://doi:10.1016/j.epsl.2009.02.005>.
- Novotny, E.J. 1977. Proppant Transport. Presented at the 52nd Annual Fall Technical Conference and Exhibition, Denver, Colorado, 9-12 October. SPE-6813.
- Penny, G.S. 1987. An Evaluation of the Effects of Environmental Conditions and Fracturing Fluid upon the Long-Term Conductivity of Proppants. Paper SPE 16900 presented at 62nd Annual Technical Conference and Exhibition, Dallas, Texas, 27-30 September.
- Pope, D.S., Leung L.K., Gulbis J., et al. 1994. Effects of Viscous Fingering on Fracture Conductivity. Presented at the SPE Annual Technical Conference and Exhibition, New Orleans, 25-28 September. SPE-28511.
- Raymond, L.R. and Binder, G.G. 1967. Productivity of Wells in Vertically Fractured, Damaged Formations. *J Pet Tech* **19** (01): 120-130.
- Renshaw, C.E. 1995. On the Relationship between Mechanical and Hydraulic Apertures in Rough-Walled Fractures. *Journal of Geophysical Research* **100** (B12): 629-636.
- Ribeiro, L.H. and Sharma, M.M. 2012. A New Three-Dimensional, Compositional, Model for Hydraulic Fracturing with Energized Fluids. Presented at the SPE Annual Technical Conference and Exhibition, San Antonio, Texas, 8-10 October. SPE-159812.
- Ribeiro, L.H. and Sharma, M.M. 2013. Fluid Selection for Energized Fracture Treatments. Presented at the SPE Hydraulic fracturing Technology Conference, Woodland, Texas, 4-6 February. SPE-163867.
- Terracina, J.M., Turner, J.M., Collins, D.H., et al. 2010. Proppant Selection and its Effect on the Results of Fracturing Treatments Performed in Shale Formations. Presented at the SPE Annual Technical Conference and Exhibition, Florence, Italy, 19-22 September. SPE-135502.
- Tsang, Y.W. and Witherspoon, P.A. 1983. The Dependence of Fracture Mechanical and Fluid Flow Properties on Fracture Roughness and Sample Size. *Journal of Geophysical Research* **88** (B3): 2359-2366.
- Tsang, Y.W. 1984. The Effect of Tortuosity on Fluid Flow through a Single Fracture. *Water Resources Research* **20** (9): 1209-1215.
- Van Dam, D.B. and de Pater, C.J. 1999. Roughness of Hydraulic Fractures: The importance of in – situ Stress and Tip. Presented at SPE Annual Technical Conference and Exhibition, Houston, Texas, 3-6 October. SPE-56596.
- Watanabe, N., Hirano, N., and Tsuchiya, N. 2008. Diversity of Channeling Flow in heterogeneous Aperture Distribution inferred from Integrated Experimental – Numerical Analysis on Flow through Shear Fracture in Granite. *Journal of Geophysical Research* **114** (B4) <http://doi:10.1029/2008JB005959>.
- Qingzhi, W., Xiaochun, J., Shah, S.N., and Li, Y. 2013. Experimental Investigation of Propped Fracture Network Conductivity in Naturally Fractured Shale Reservoirs. Presented at the SPE Annual Technical Conference and Exhibition, New Orleans, Louisiana, 30 September – 2 October. SPE-166474.
- Mei, Y., Economides, M.J., Chenji, W., et al. 2013. Hydraulic Fracture Design Flaws – Proppant Selection. Presented at the SPE Annual Technical Conference and Exhibition, New Orleans, Louisiana, 30 September – 2 October. SPE-166299.
- Yeo, I.W., De Freitas, M.H., and Zimmerman, R.W. 1998. Effect of Shear Displacement on the Aperture and Permeability of a Rock Fracture. *Int. J. Rock Mech. Min. Sci. & Geomech. Abstr.* **35** (8): 1051-1070.

Fracture model	Rock type					Average grain size
		D_{va}	D_{psd}	D_{tp}	A_t/A_p	(mm)
FR. 1	Beige limestone with abundant and coarse fossil shells	1.373	2.277	2.012	1.145	N/A
FR. 2	Semi re-crystallized micritic pink limestone	1.263	2.558	2.007	1.079	0.4
FR. 3	Micro-fossiliferous, micritic sparry calcite cemented pisolitic beige limestone	1.303	2.266	2.007	1.061	0.3
FR. 4s	Coarse grained white marble	1.39	2.418	2.009	1.098	3
FR. 5	Holocrystalline amphibole granite	1.299	2.335	2.008	1.083	2
FR. 6	Micritic cemented, fissured beige limestone with abundant fossils	1.29	2.3	2.010	1.115	0.8
FR. 7	Medium-coarse white grained marble	1.326	2.321	2.006	1.072	1.5
FR. 8s	Finer – coarse grained marble	1.302	N/A	N/A	N/A	N/A
Flat		1	2	2	-	-

Table 1—Lithological descriptions of the rock samples and the calculated roughness parameters of the model fracture surfaces.

D: fractal dimension; Subscripts – va: variogram analysis; psd: power spectral density, tp: triangular prism, A_t/A_p : ratio between total surface area (A_t) and planar surface area (A_p). Both sides of models Fr .4s and Fr .8s are made of solid transparent plastic (data from Develi and Babadagli, 2015 and Babadagli et al. 2015a-b).

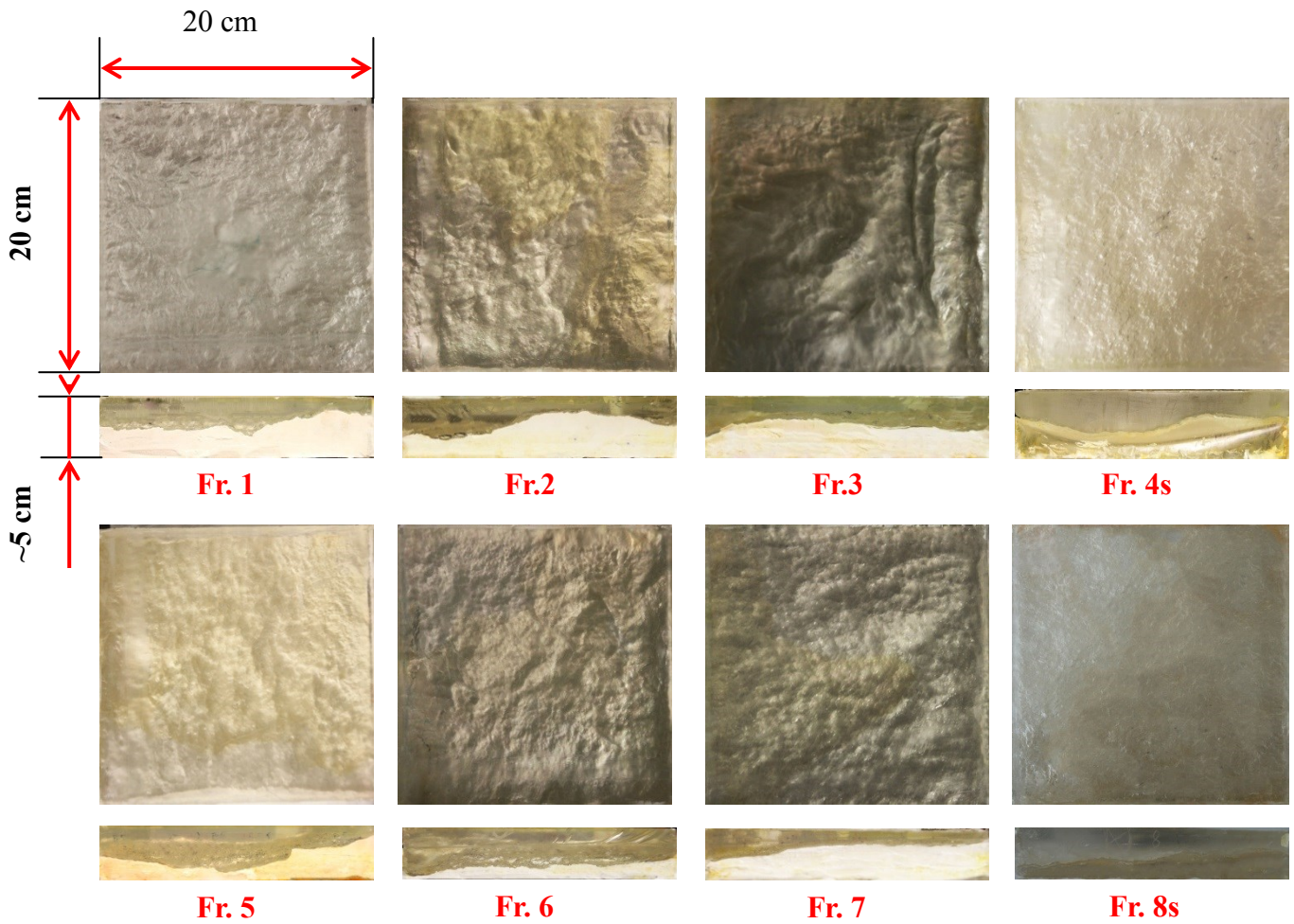


Figure 1—Top and side views of fracture models.

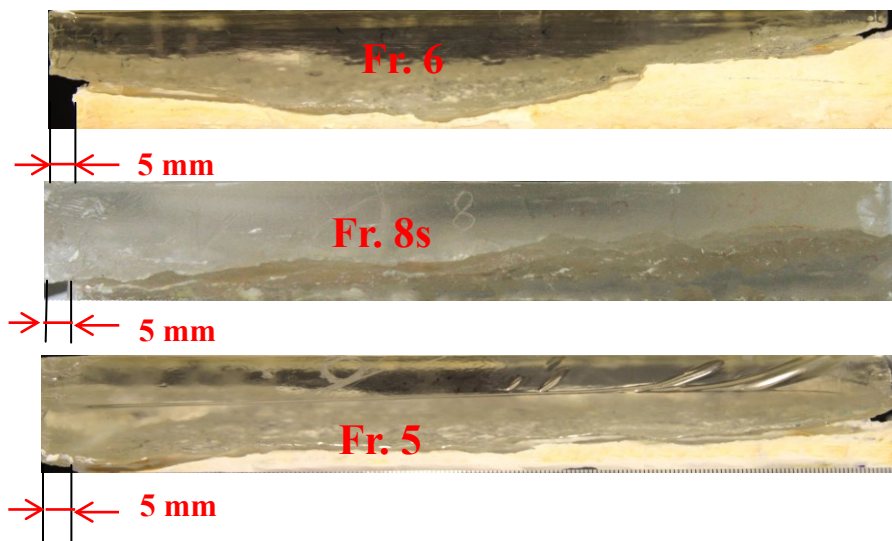


Figure 2—Side view of fractures Fr.5, Fr.6, Fr.8s sheared to 5 mm.

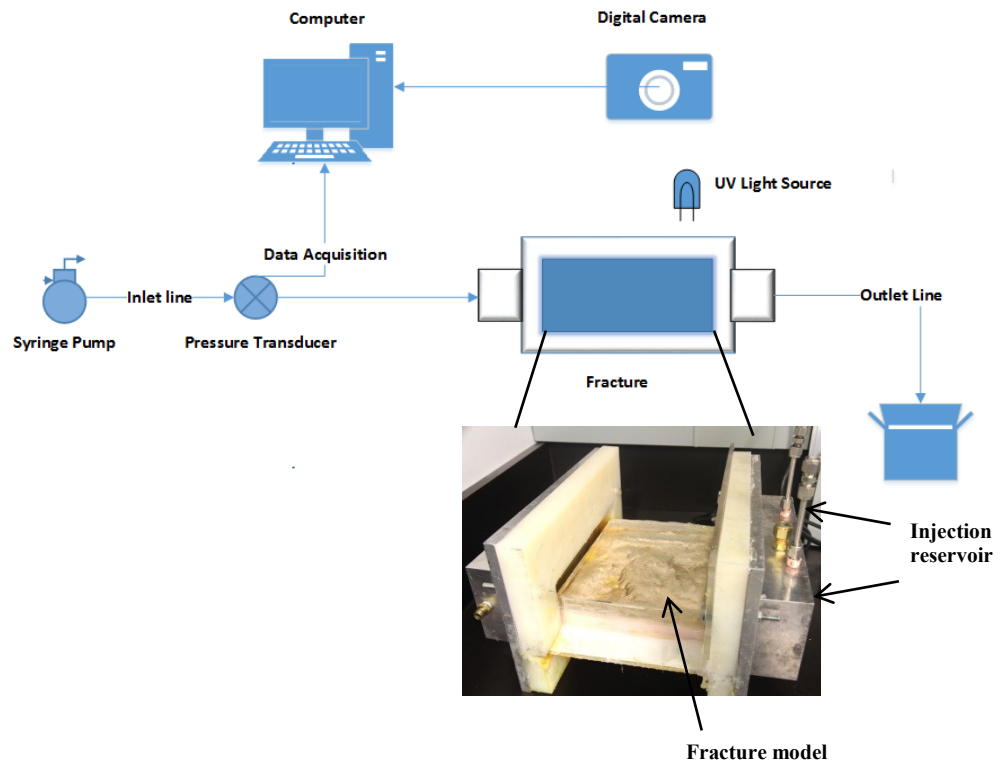


Figure 3a—Schematic of experimental set-up.

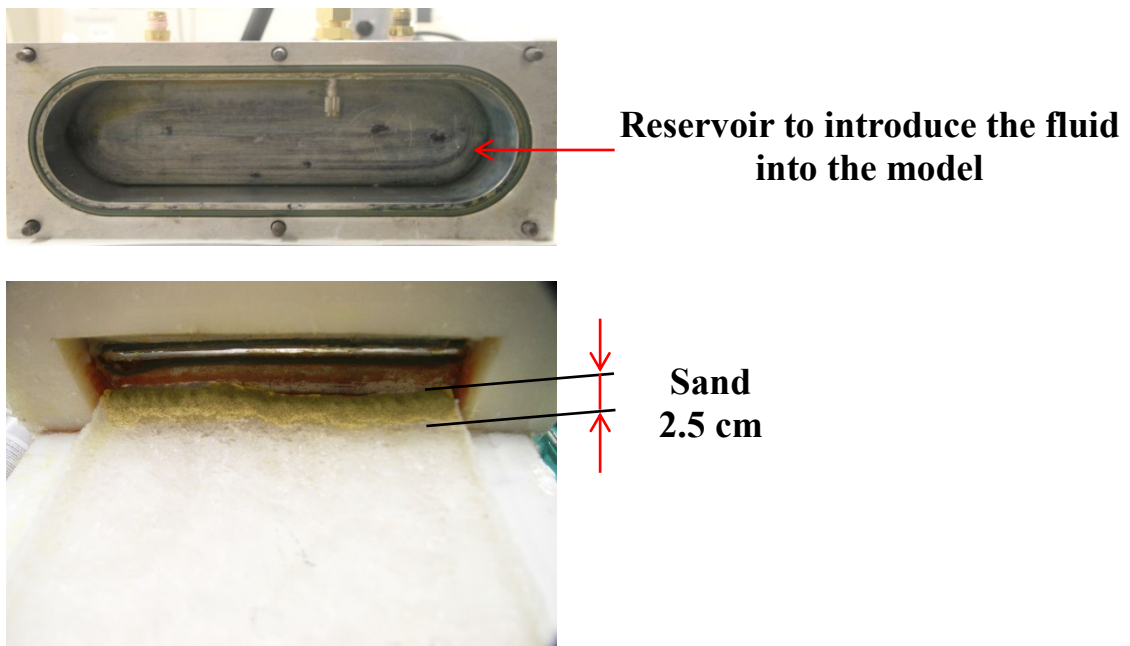
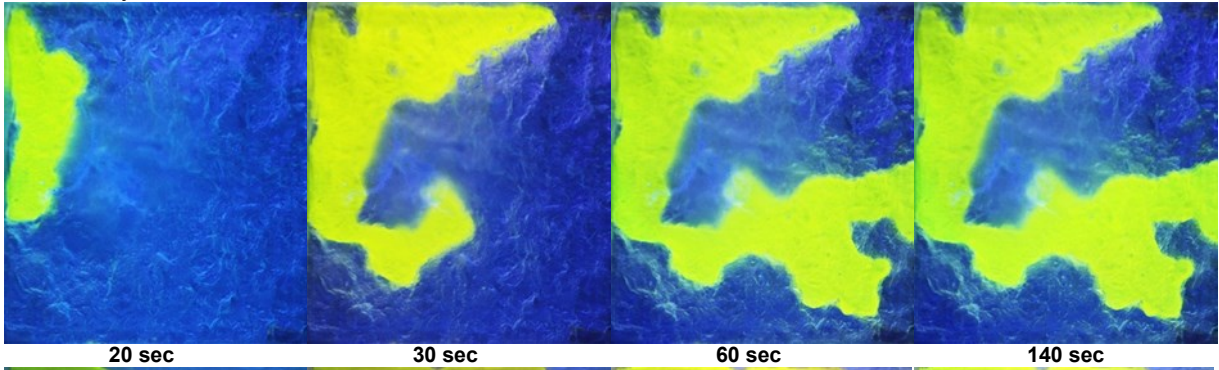


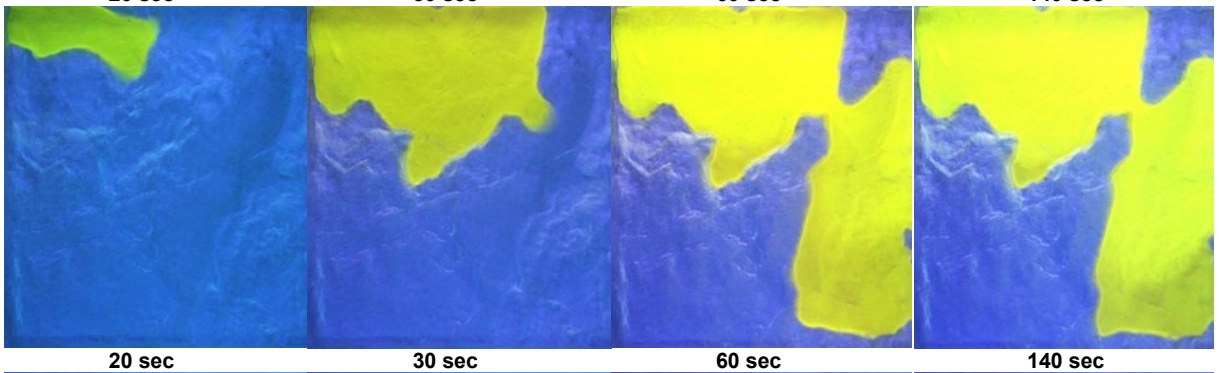
Figure 3b—Detailed model holder description.

Flow direction
→

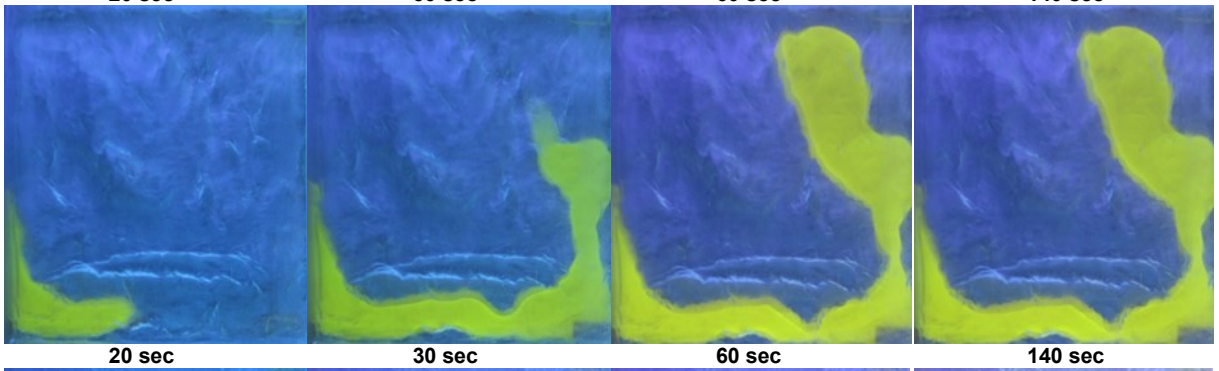
Fr. 1



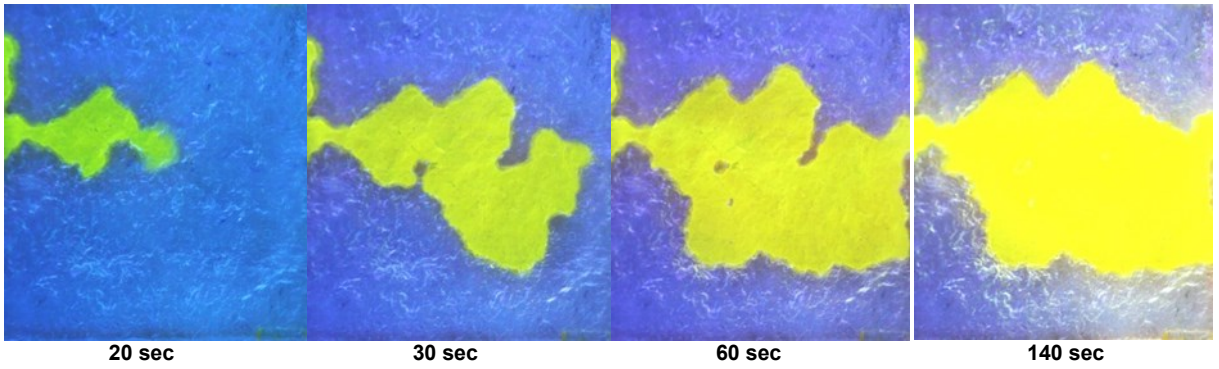
Fr. 2



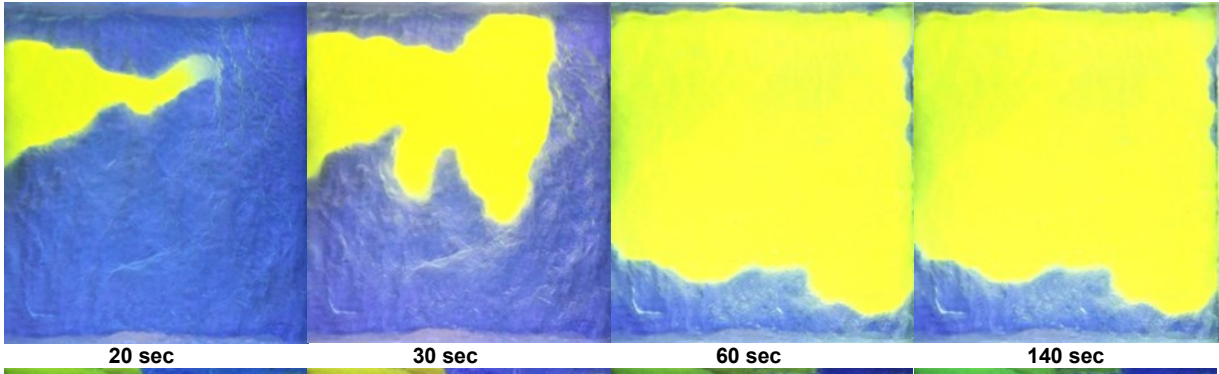
Fr. 3



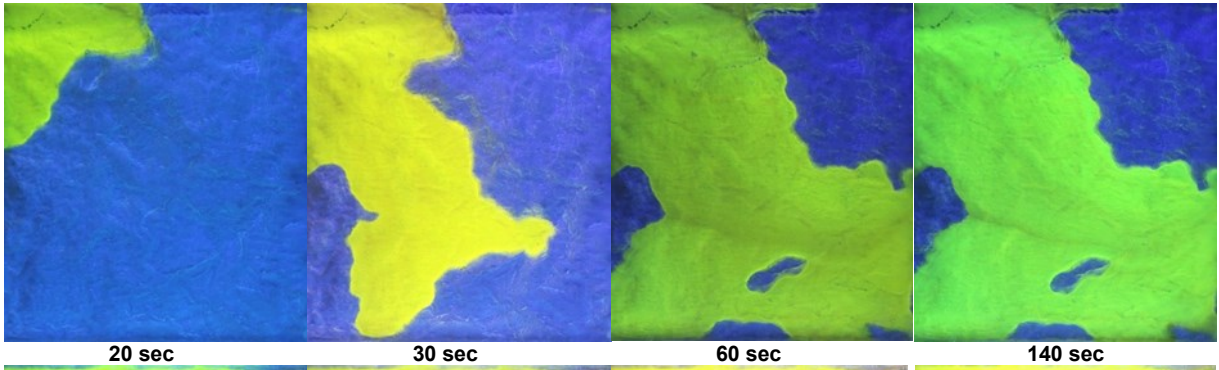
Fr. 4s



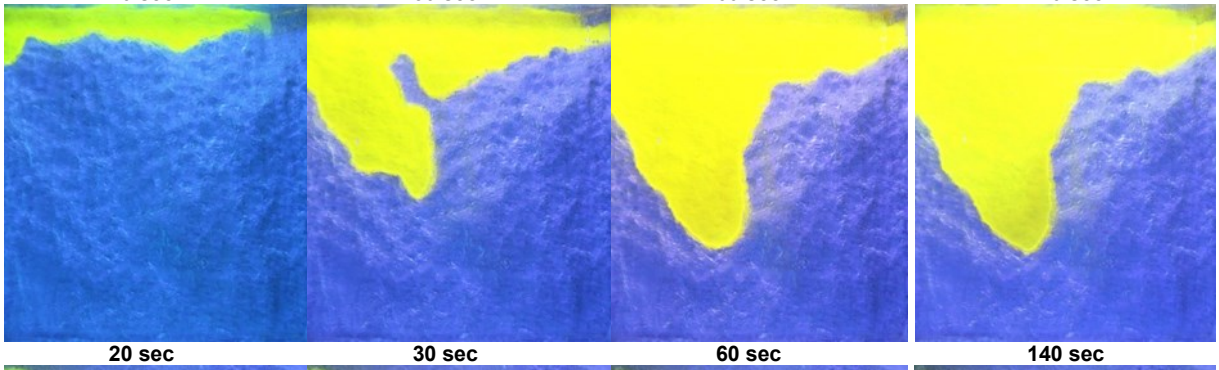
Fr. 5



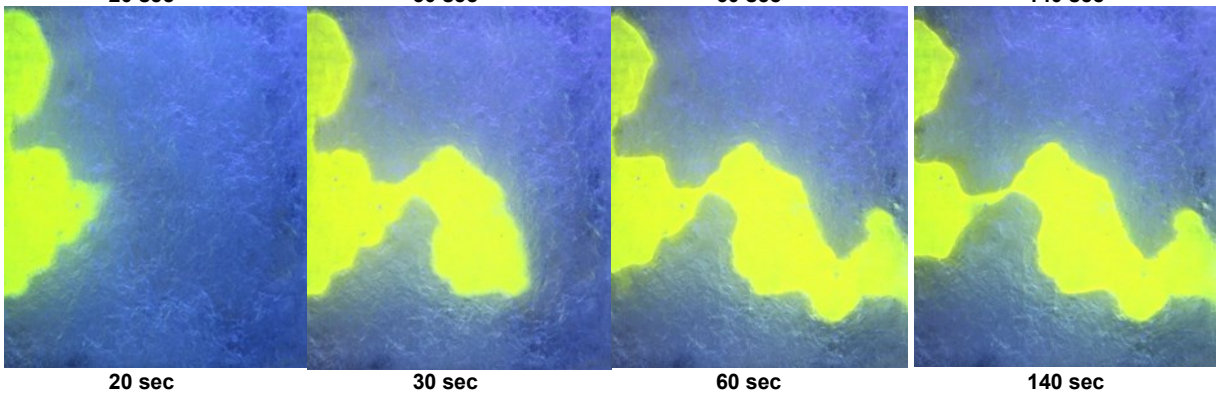
Fr. 6



Fr. 7



Fr. 8



Flat

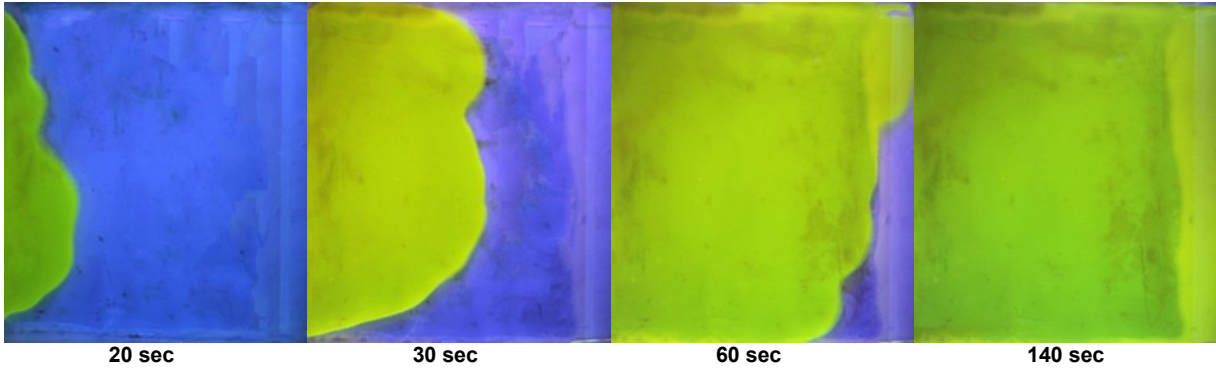


Figure 4—Visualization of water flow in 7-joint type- rough models + flat model. Blue areas correspond to air and yellow is dyed water.

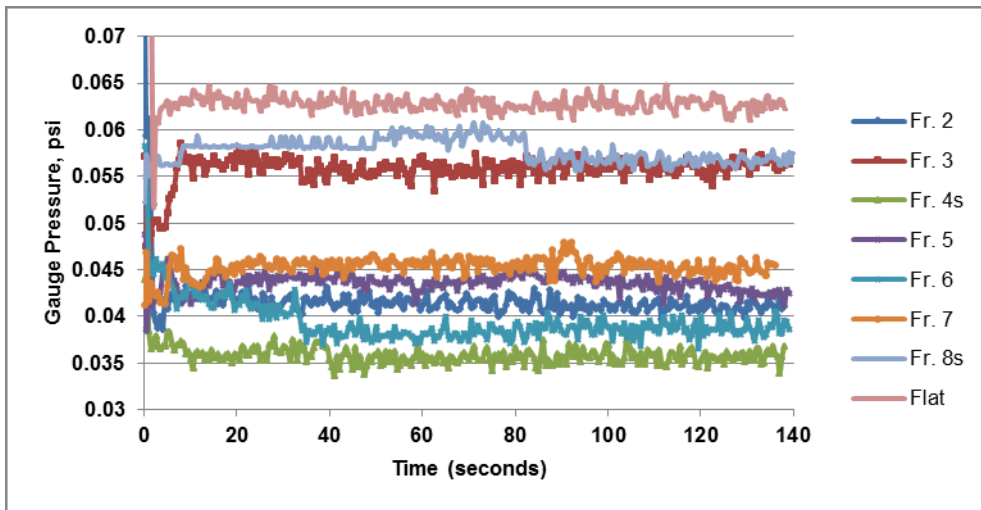


Figure 5a—Pressure drop in joint fractures while injecting water at 3.4 cc/min.

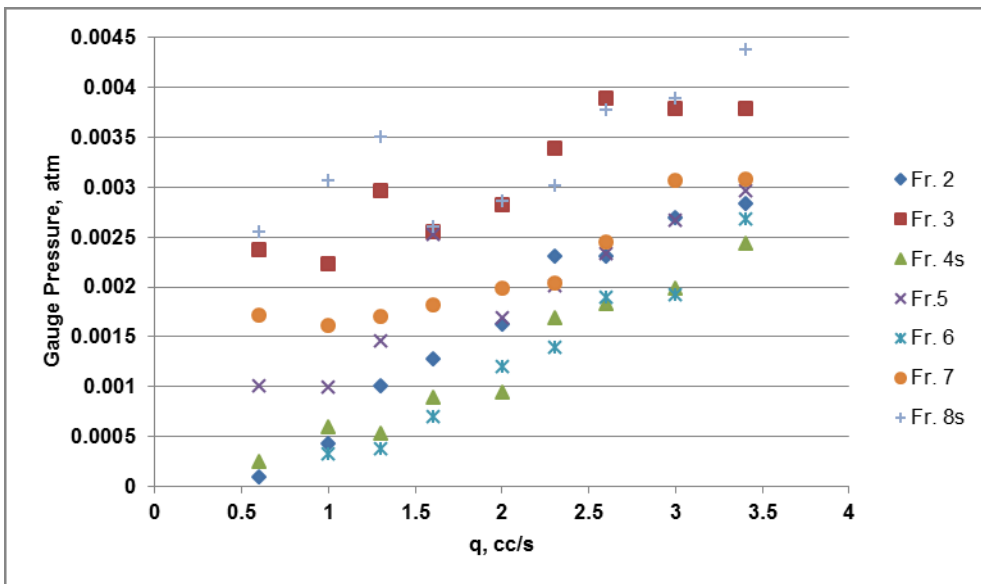
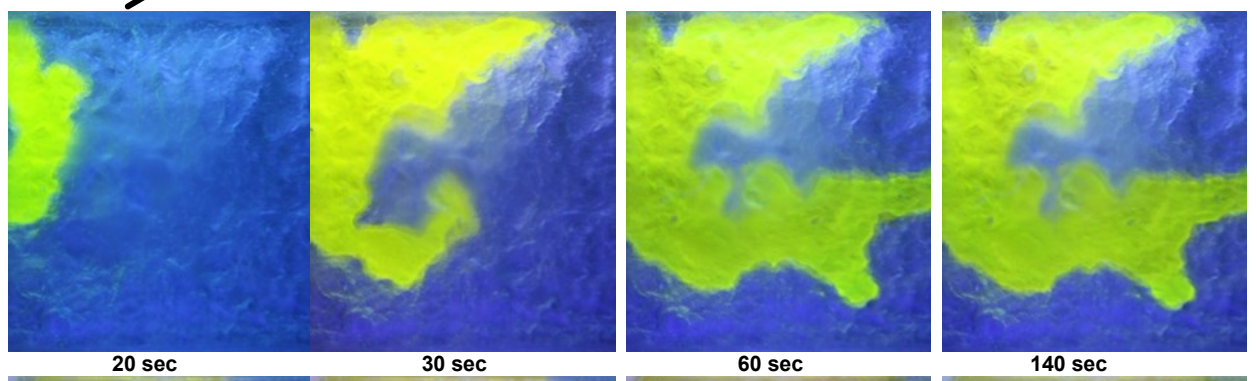


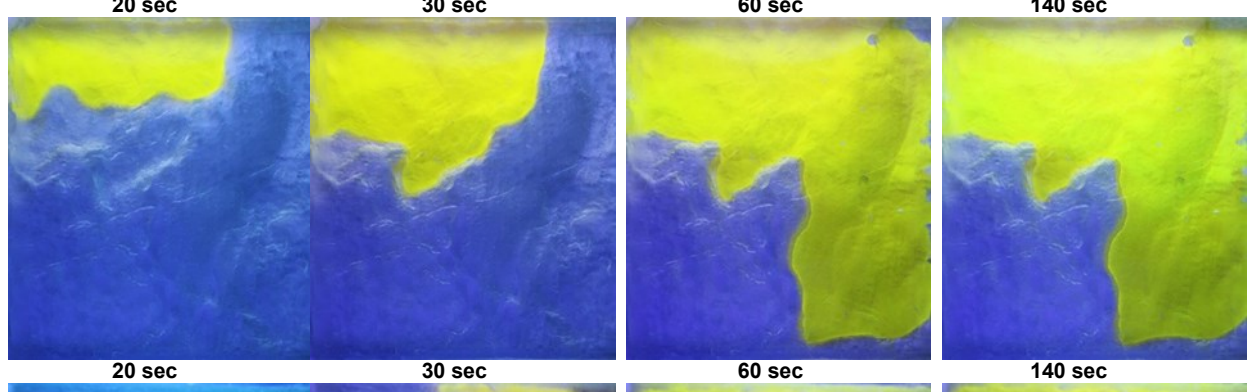
Figure 5b—Pressure drops across the fracture models versus injection rates.

Flow direction
→

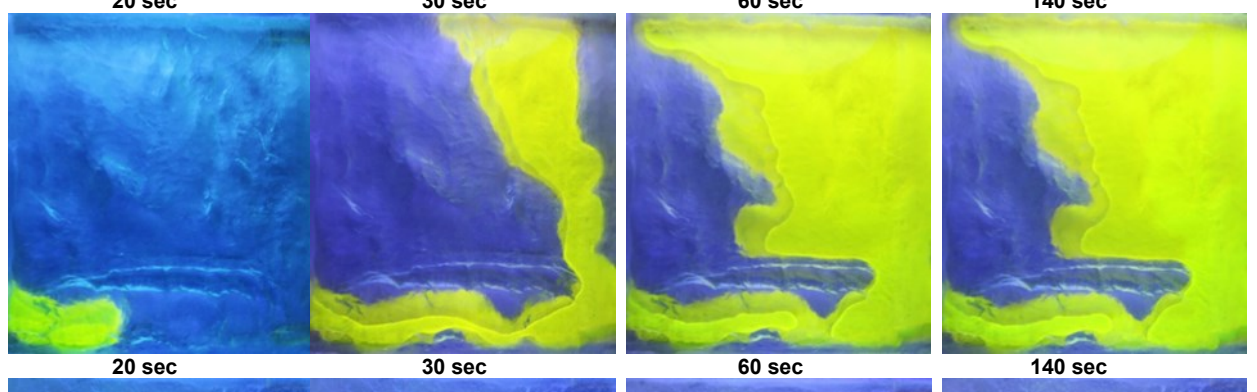
Fr. 1



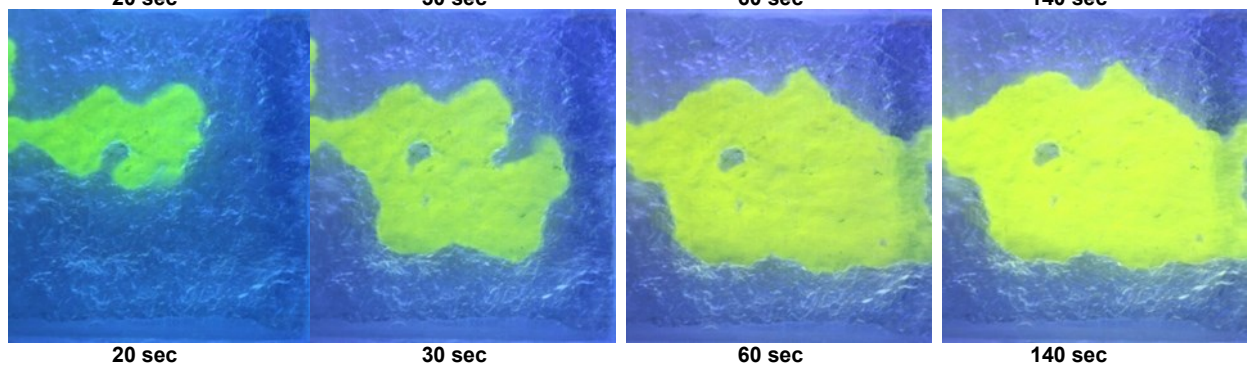
Fr. 2



Fr. 3



Fr. 4s



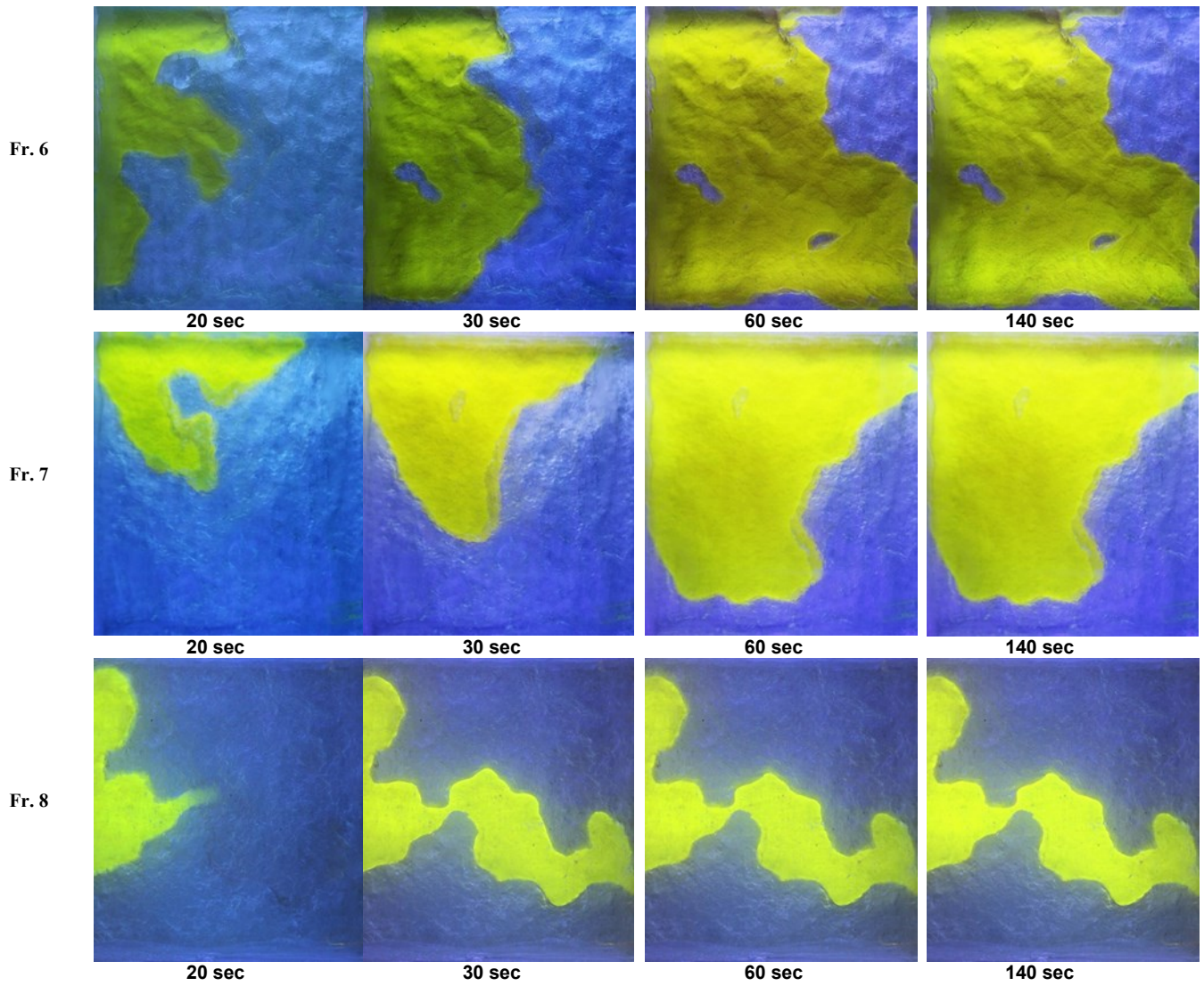
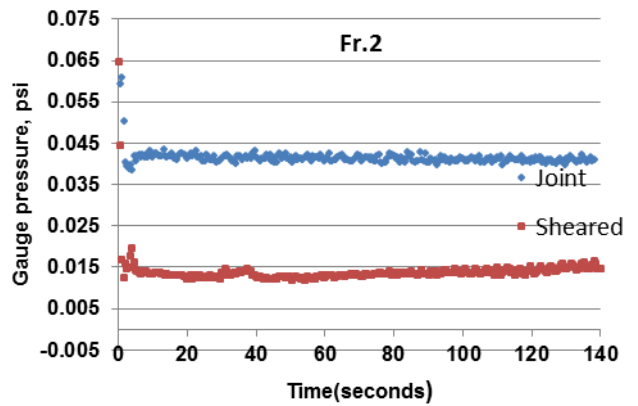
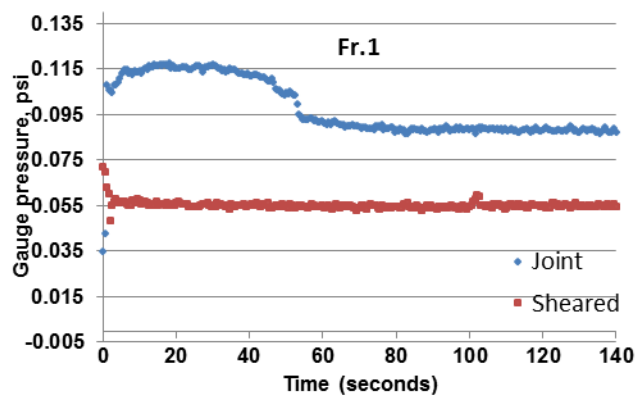


Figure 6—Water injection at 5 mm sheared fracture models.



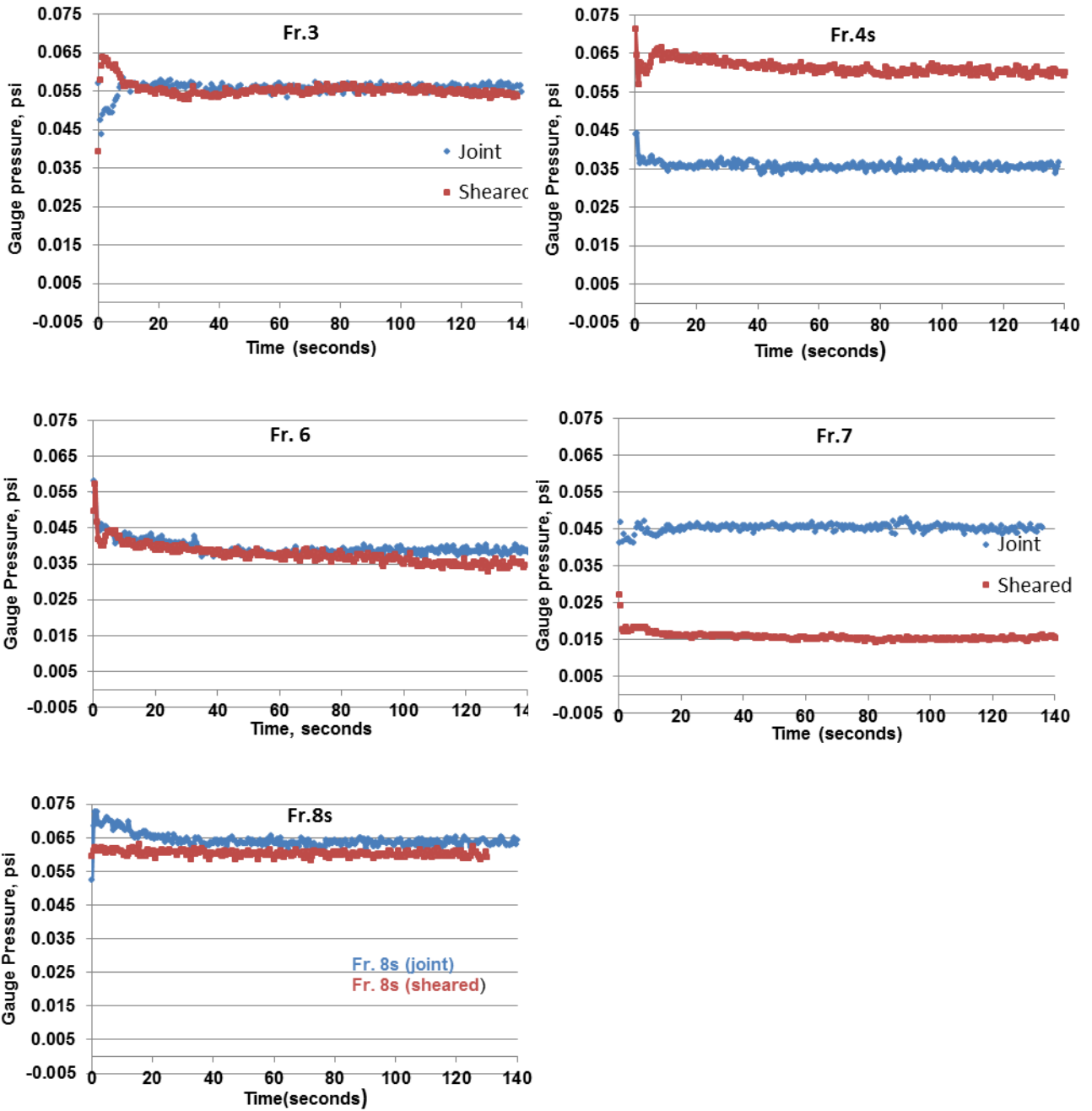


Figure 7a—Pressure drop recorded during water injection (joint vs. sheared model).

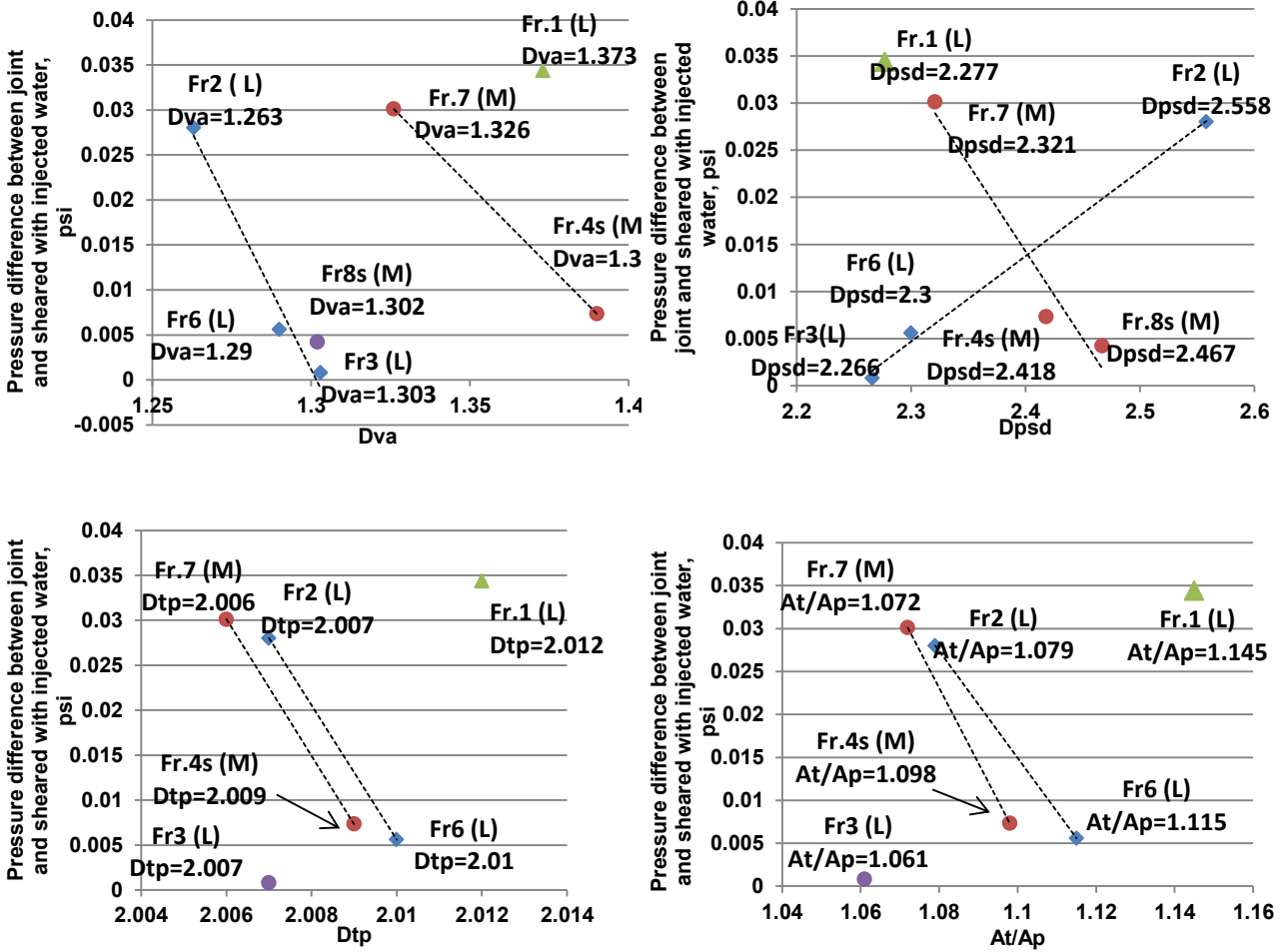
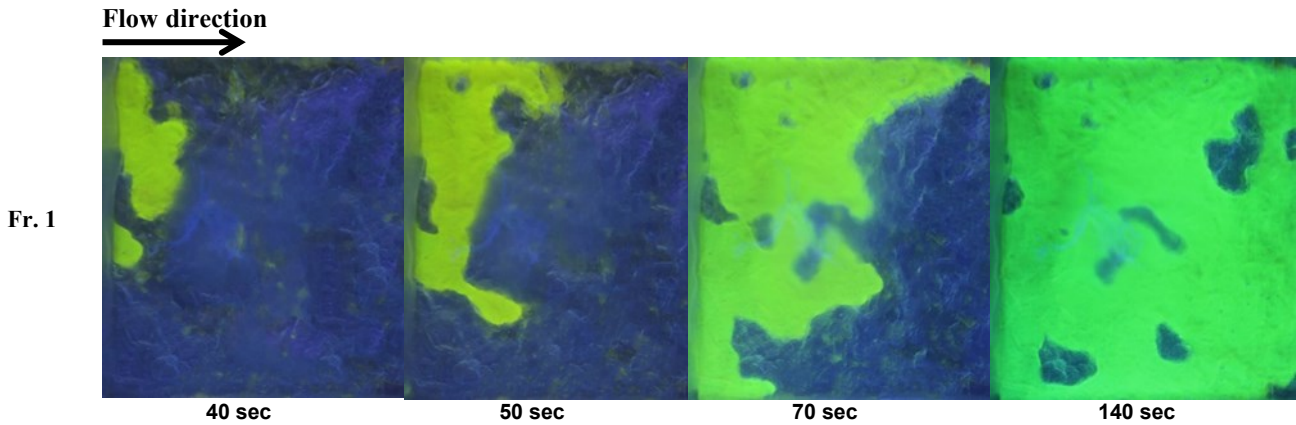
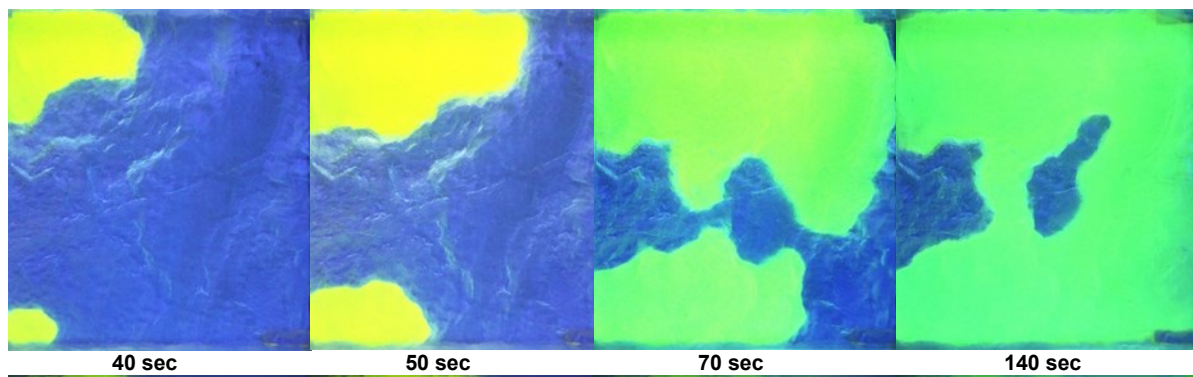


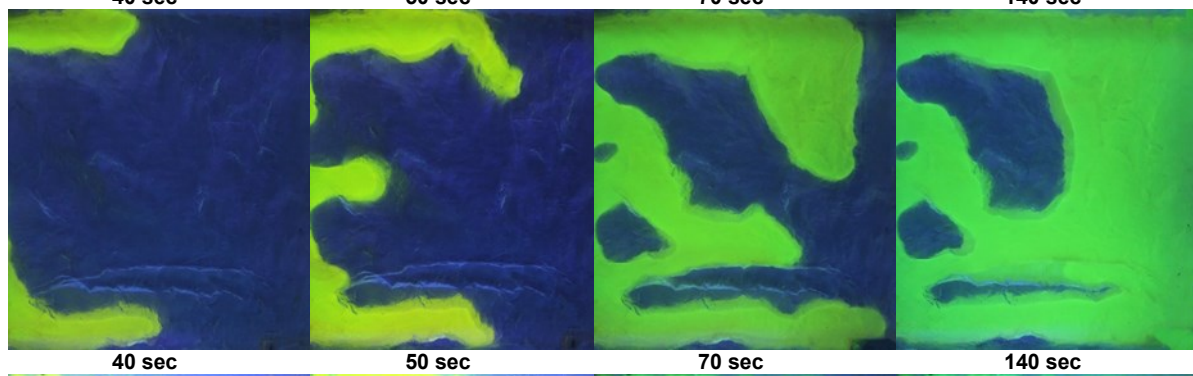
Figure 7b—Pressure difference between joint and sheared fracture models (the pressure difference between the joint and sheared models given in Fig. 7a after they are stabilized) against variogram, power spectral, triangular prism and ratio between total and planar area fractal dimensions (L-limestone; M-marble).



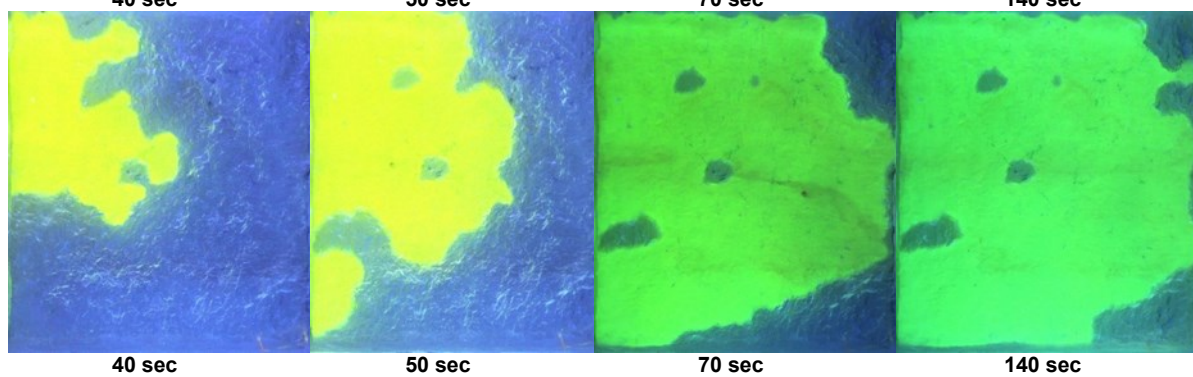
Fr. 2



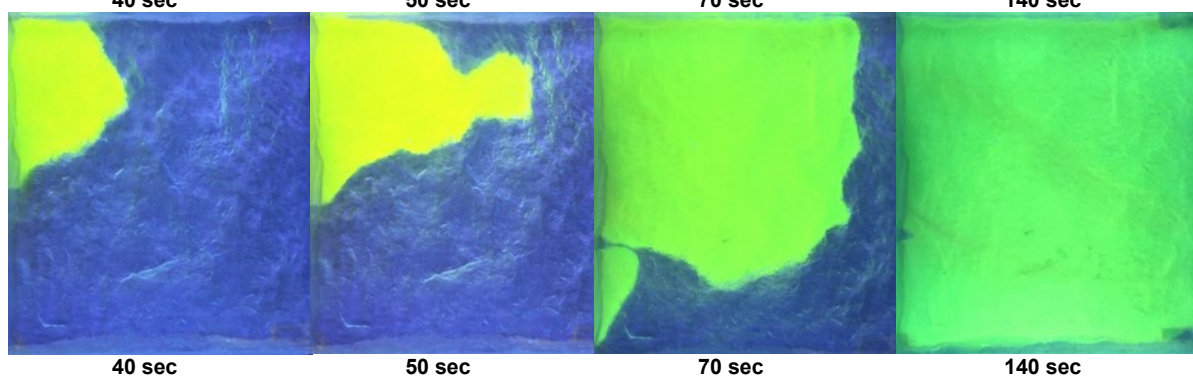
Fr. 3



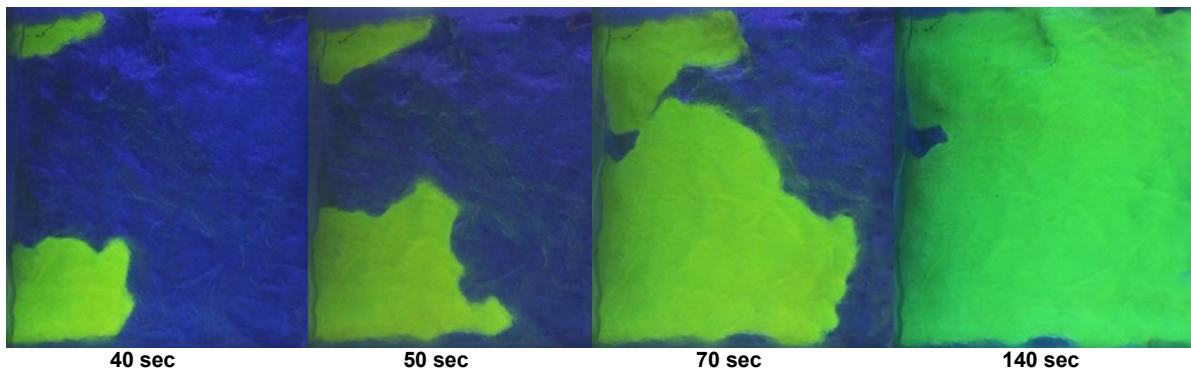
Fr. 4s



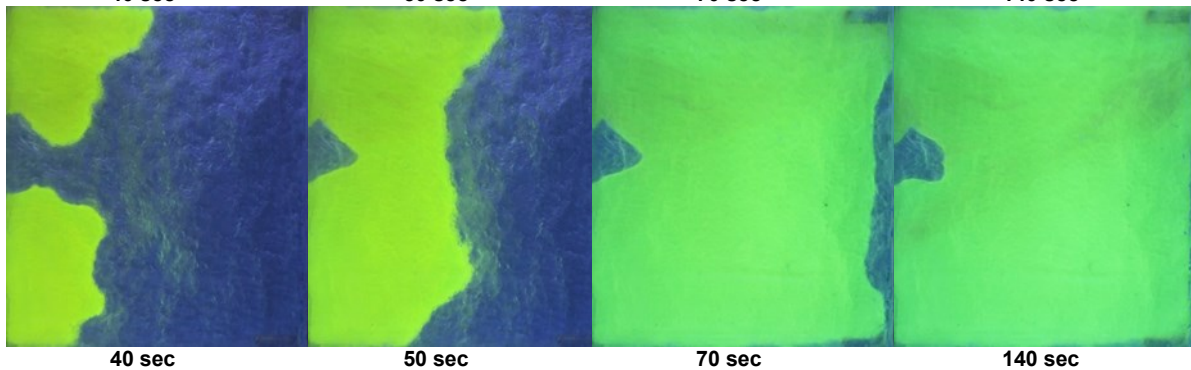
Fr. 5



Fr. 6



Fr. 7



Fr. 8

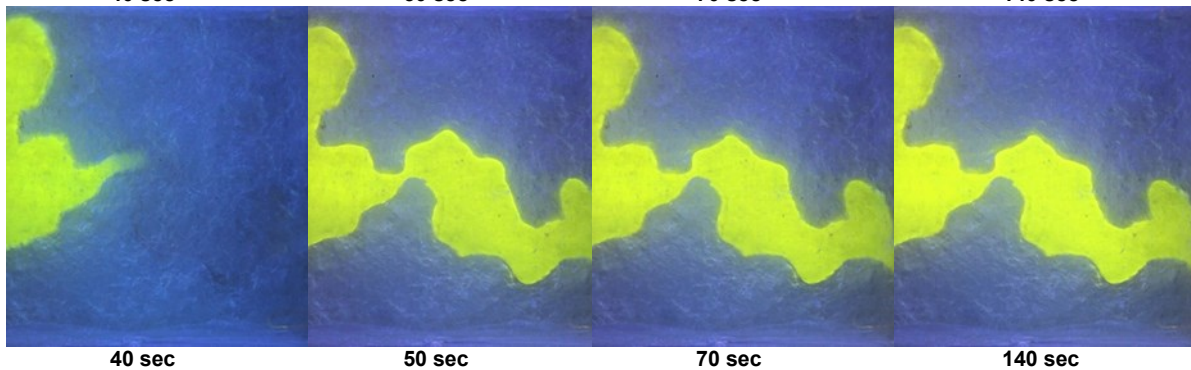
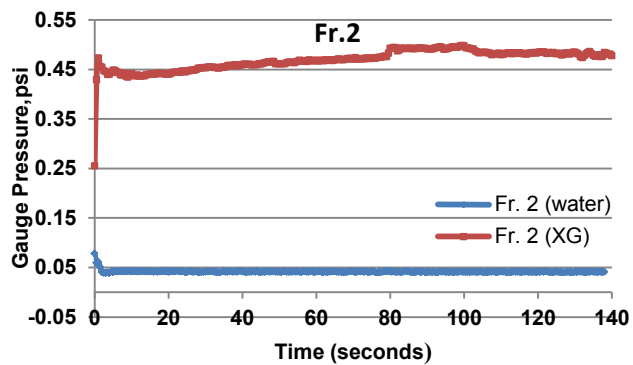
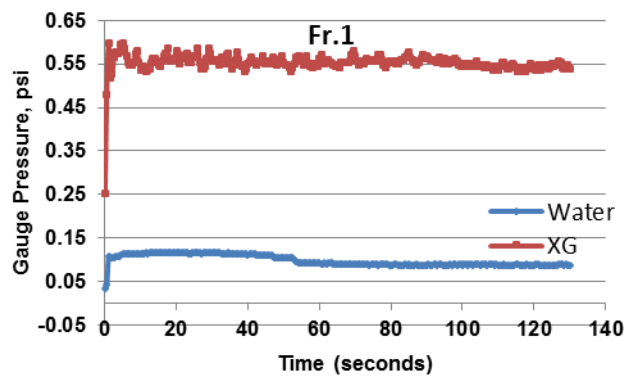


Figure 8—Visualization of aqueous Xanthan Gum fluid flow on joint fracture models.



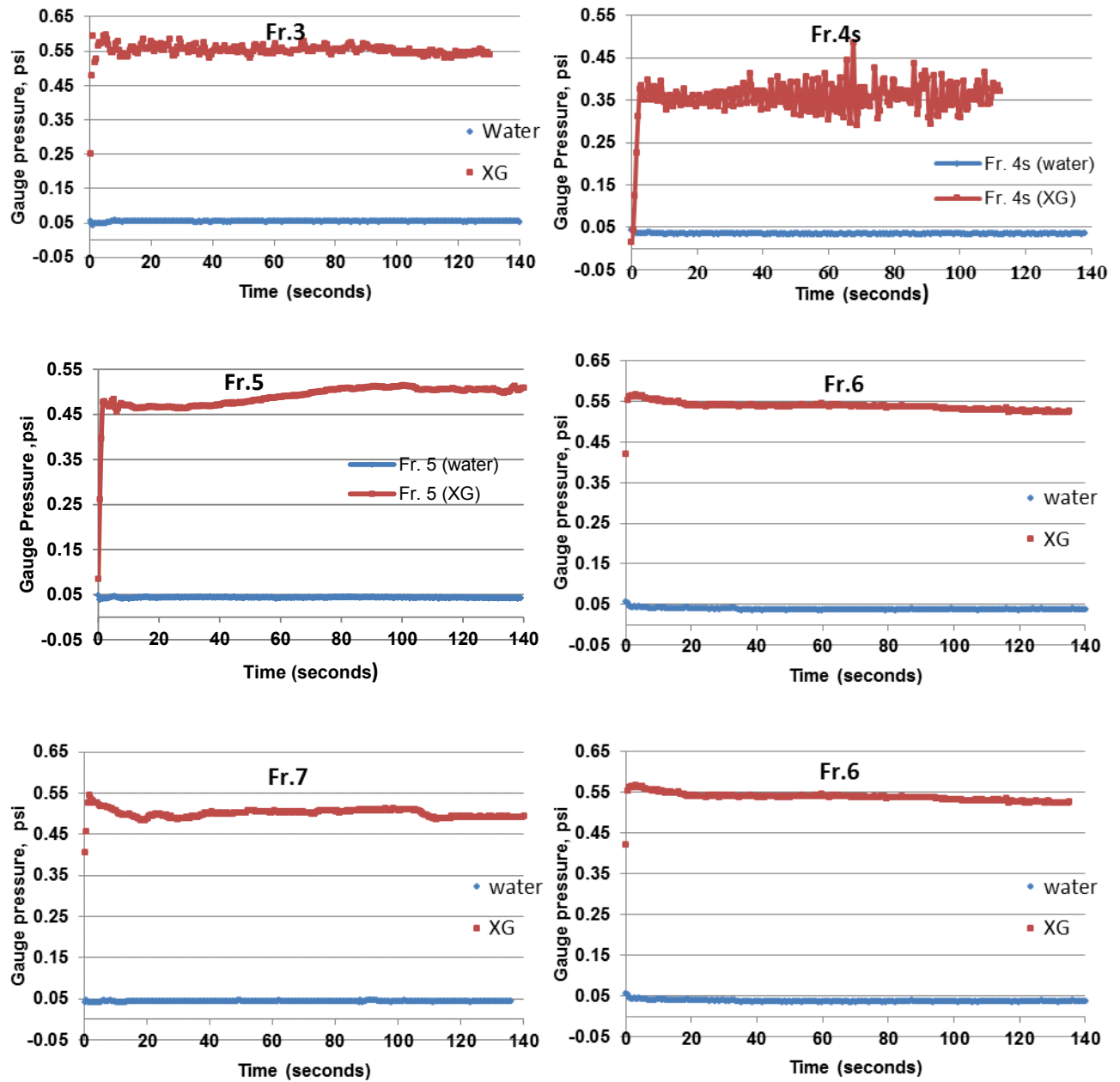


Figure 9a—Comparison of Pressure Drops for XG solution vs. water while flowing through joint fractures.

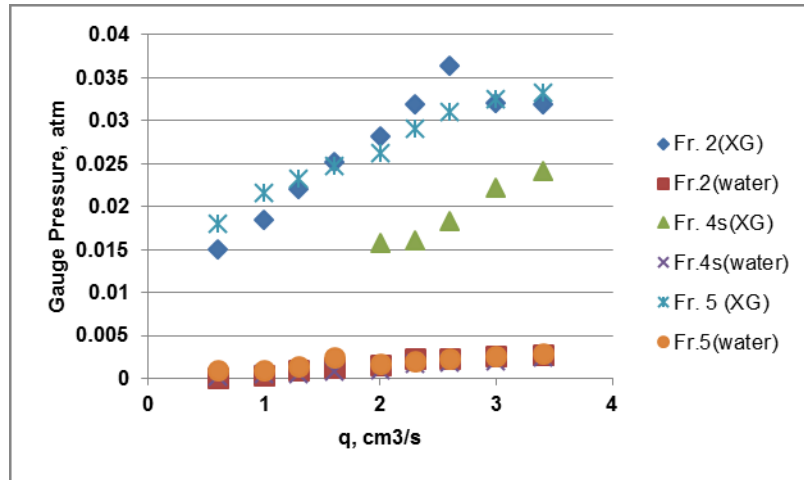


Figure 9b—Pressure drops in fracture models Fr.2, Fr.4s, Fr. 5 while injecting XG fluid and water.

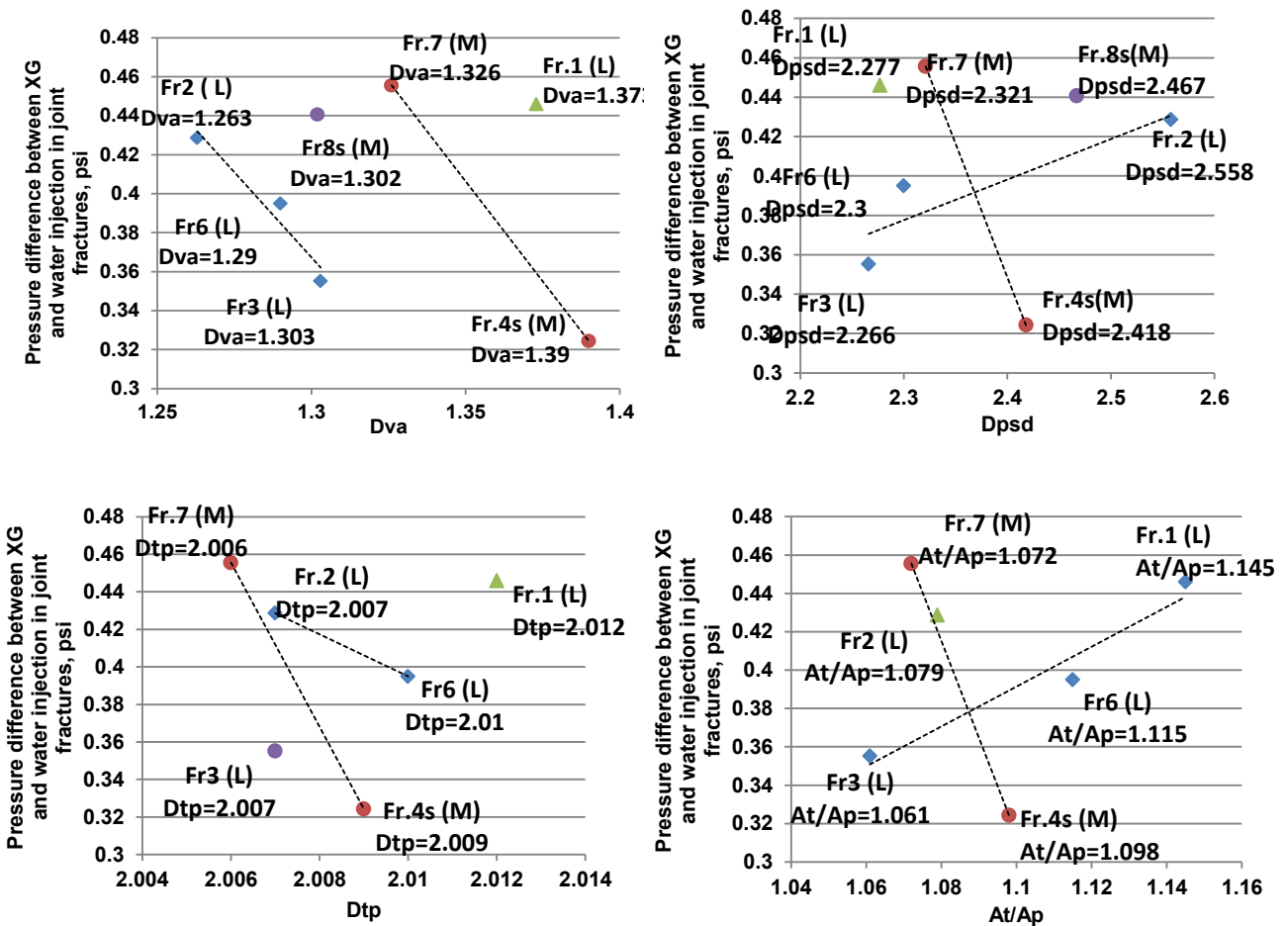


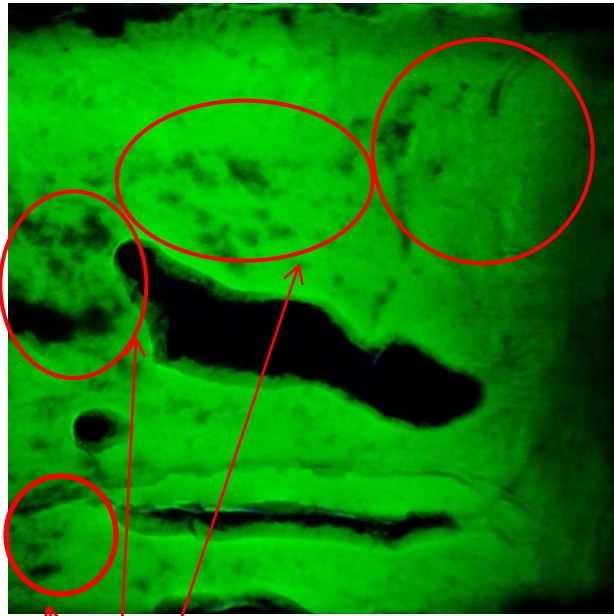
Figure 9c—Pressure difference between two fluid types injection on joint fractures (the pressure difference between the joint and sheared models given in Fig. 9a after they are stabilized) against variogram, power spectral, triangular prism and ratio between total and planar area fractal dimensions (L-limestone; M-marble).



**Fr. 1
limestone**

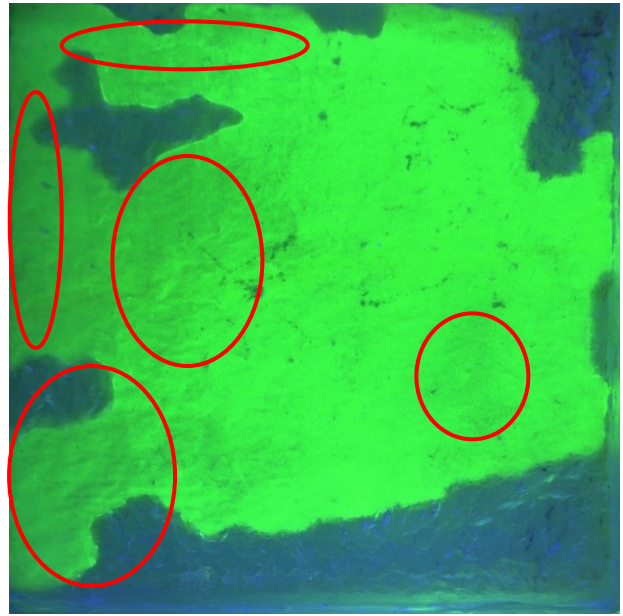


**Fr.2
Micritic limestone**

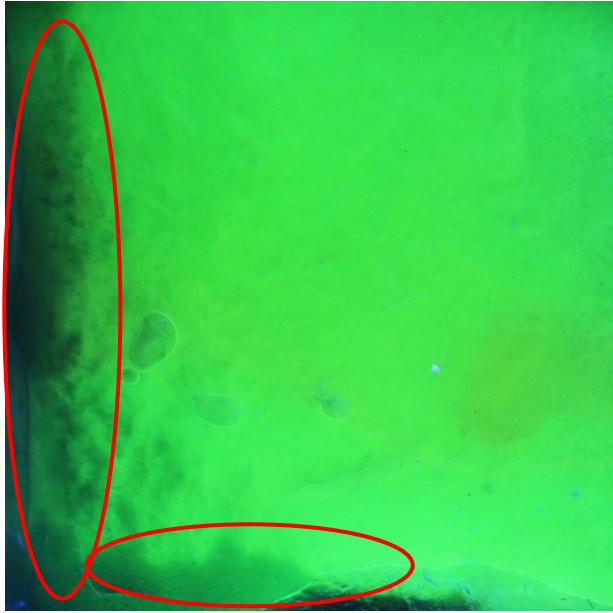


**Fr.3
limestone**

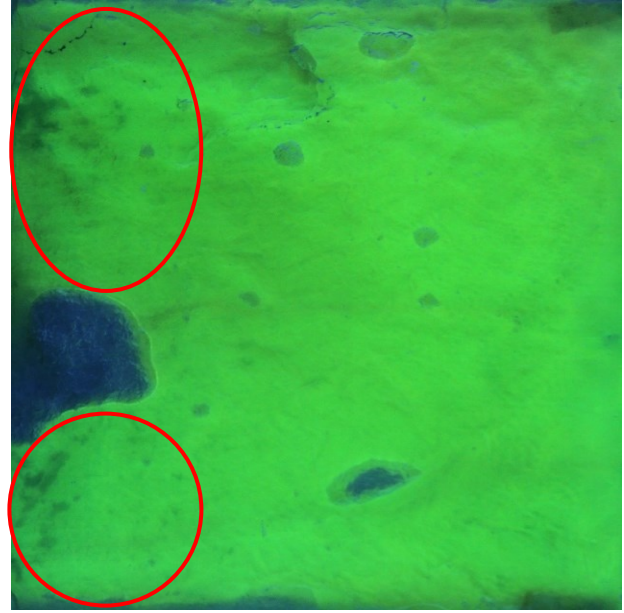
**Dark areas are
progressing sand**



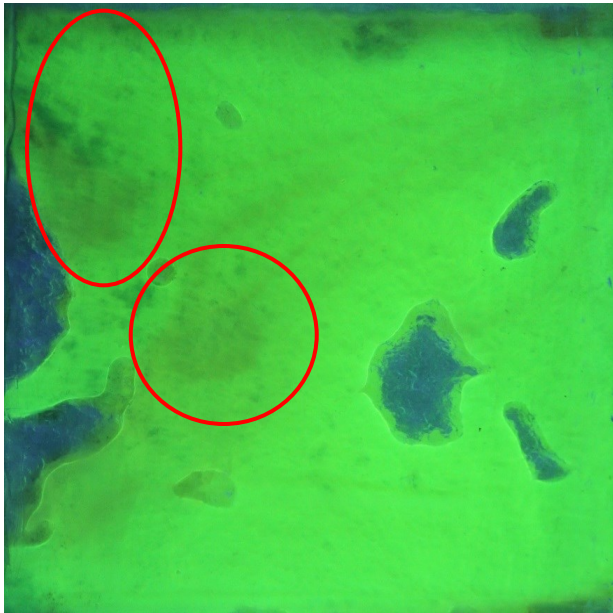
**Fr. 4s
Crystalline marble**



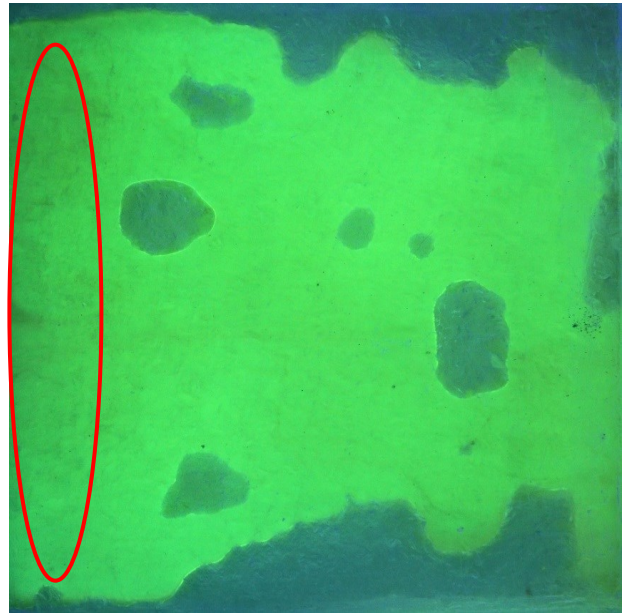
**Fr.5
Granite**



**Fr. 6
Micritic limestone**



**Fr.7
Coarse crystalline marble**



**Fr.8s
Crystalline marble**

Figure 10—Xanthan Gum+sand injection on 8 fracture models (blue parts are not saturated areas; green is Xanthan Gum; black is accumulated sand; red circles are transported sand indication). As seen, sands progress through channels and settle down eventually in the wider channels caused by tortuosity.

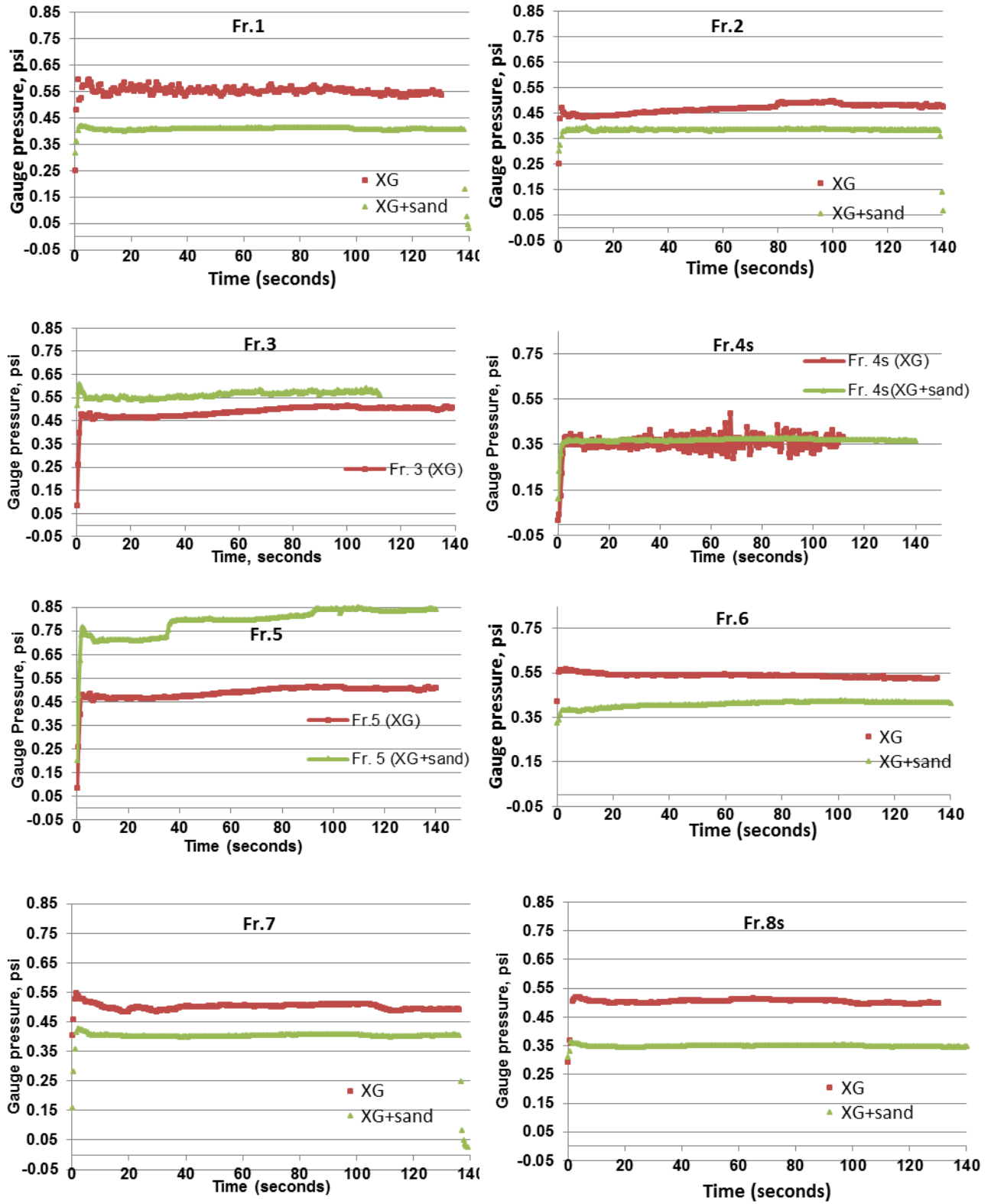


Figure 11a—Pressure Drop while proppants are transported through fracture models Fr.3, Fr.4s, Fr.5 using XG fluid and water at joint fractures.

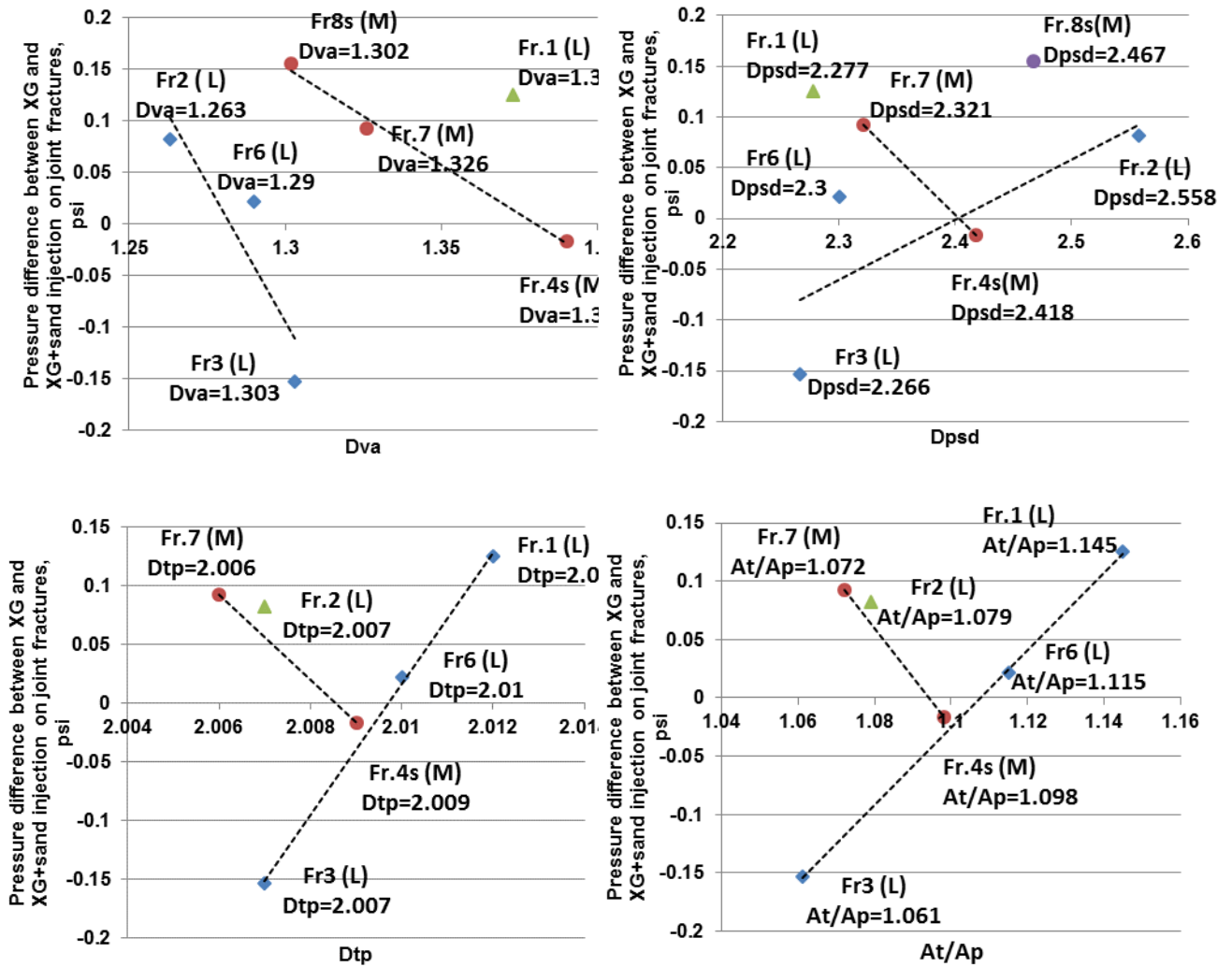


Figure 11b–Pressure drop difference between Xanthan Gum and Xanthan Gum+sand injection on joint fractures (L–limestone; M–marble).

CHAPTER 3: FRACTAL ANALYSIS OF SINGLE-PHASE WATER AND POLYMER SOLUTION FLOW AT HIGH RATES IN OPEN AND HORIZONTALLY DISPLACED ROUGH FRACTURES

A version of this chapter has been submitted to the journal for publication.

Preface

A study on the quantitative analysis of single phase flow in rough fractures at high rates representing hydraulic fracturing conditions was presented in this paper. 2-D transparent models of original fractures obtained from different rock types (granite, marble and limestone) were reproduced by molding. To represent typical hydraulic fracturing fluids, water and polymeric solutions were injected at a constant flow rate. The inlet pressure was continuously monitored to correlate the permeability changes due to surface roughness of fractures. The fluids distributions were also mapped using the images acquired through the experiments. The surface roughness was quantified using three fractal methods (variogram, power spectral density, and triangular prism) and the ratio of total and planar areas, and these parameters were correlated to the percent wetted areas and pressure drop (i.e., permeability). This exercise was performed on joint type and horizontally displaced (sheared) model fractures.

The percentage of planar flow wetted area and pressure drop changed remarkably with rock types. Both parameters were controlled by grain size and the surface roughness of fractures. Increasing degree of the roughness caused a decrease in permeability and area wetted by fluid. Models generated from bigger grain size rocks showed more channeling and a lower percentage of fluid wetted areas as well as lower pressure drop (higher permeability). The variogram fractal dimension showed better agreements among other methods for both fluid (water and polymeric solution) and fracture types (joint and horizontally displaced).

1. Introduction

Flow of Newtonian and non-Newtonian fluids in fractures is commonly encountered in different industrial applications including hydraulic fracturing. The distribution of these fluids carrying proppants is critically important to create and maintain the conductivity of the fractures. The common approach followed by practitioners in estimating the conductivity capacity is the assumption of two parallel smooth plates (smooth surfaces) to represent the fracture and applying the Darcy's law (cubic law):

$$Q = -\frac{\Delta P k A}{L \mu} \quad (1)$$

where Q is the flow rate, L is the length of fracture, ΔP is the pressure drop through the length of the fracture, A is the cross sectional area, and μ is the fluid viscosity.

If the fracture surface is considered as a smooth planar area, the permeability of fracture (k_f) is defined as follows (Gangi 1978):

$$k_f = \frac{b^2}{12} \quad (2)$$

where b is the aperture of the fracture; i.e., the distance between two plates.

Since the relation of flow rate with pressure drop in a length of fracture is given by the Darcy's law:

$$Q = -\frac{k_f * A * \Delta P}{\mu * L} \quad (3)$$

Then flow through fracture with fracture permeability in a cross-sectional area of $A=W*b$ is defined as:

$$Q = -\frac{\Delta P * W * b^3}{12 * L * \mu} \quad (4)$$

where b and W are the average aperture and the width of the fracture.

Flat plate model is inadequate for predicting permeability in fractures as the change of the aperture width results in inconsistent values of permeability (Kranz 1979). With a decrease in the wavelength of the fracture wall due to roughness the overall aperture decreases, which yields a decrease in the permeability of fracture (Tsang and Witherspoon 1983; Briggs et al. 2014). Brown (1987) showed that with the assumption of smooth fracture surfaces, the flow rate predicted by cubic law can be 70-90% higher than realistic (rough) representation of surface fractures. In fact, when fluid flows in smooth fractures, the velocity profiles are ideally parabolic, which is not the case in the presence of surface roughness. Therefore, flow in a rough surface fractures cannot sufficiently be characterized by the cubic law (Eq. 4). Additional physical and theoretical parameters such as distribution of asperities should be incorporated into the cubic law (Koyama et al. 2007).

The resistance of fluid to flow through variable openings caused by surface roughness leads to diverted flow around asperities in contact and to take a tortuous or channeling flow path (Walsh 1981). Tortuous fluid path is controlled by the hydraulic aperture, which decreases with increasing surface roughness and, eventually, affects the permeability of fracture (Tsang 1984; Renshaw 1995). Variation of surface roughness depends on rock type and its material grain size (van Dam and Pater 1999; Develi and Babadagli 2015). Meanwhile, mismatching of two surfaces is formed as a result of shear displacement, which leads to redistribution of asperities (variable aperture structure) and increase in heterogeneity (Yeo et al. 1998; Lee and Cho 2002; Auradou et al. 2006; Watanabe 2008). Then, aperture distribution broadens with increasing mismatching and this results in a more challenging type flow and thereby an increase in fracture connectivity (Tsang and Witherspoon 1983; Nemoto et al. 2008). These observations were also supported by visualization studies (Rasmuson and Neretnieks 1986; Crawford 2003; Develi and Babadagli 2015; Babadagli et al. 2015a-b). These studies verify that surface roughness is a significant parameter and can lead to a considerable difference from the parallel smooth plate model. The main problem is to quantify these effects for a wide range of rock, fracture and fluid types to eventually incorporate the roughness effect into the flow equations.

In our earlier studies, the roughness effect was qualitatively and quantitatively analyzed for single phase flow in deformable (dilating) fractures (Develi and Babadagli 2015) and multiphase flow (Babadagli et al. 2015a-b). These studies were conducted at the flow conditions applicable

to natural flow or water-gas injection to enhance oil/gas recovery. Therefore, the injection rates were relatively low. The objective of this paper is to examine the flow of Newtonian and non-Newtonian fluids at much higher rates that are applicable to hydraulic fracturing conditions. This type of high rate application is particularly important for distributing the proppant injected throughout the fracture as uniformly as possible to maintain hydraulic conductivity during the production stage. Experiments were carried out in joint type and horizontally displaced (sheared) fractures representing different roughness characteristics (granite, marble, and limestone) and quantitative analyses were performed using fractal properties of fracture surfaces. The quantitative and visual data of fluid flow were collected from the experiments performed on the joint and horizontally displaced (sheared) fractures by injecting water and polymer solution. The degree of roughness was described by several fractal methods (variogram analysis, power spectral density analysis, and triangular prism surface area method) and using the ratio between total and planar areas of the surfaces. Then, correlations between the roughness parameters and wetted areas and fracture permeability were sought for Newtonian and non-Newtonian fluids flowing in joint and horizontally displaced (sheared) fractures.

2. Experimental Methodology

Seven rock samples of different kinds (granite, marble, and limestone) with dimensions 20x20x20 cm were fractured under tension (modified Brazilian test). Then, single fracture models square in shape with a side length of 20 cm were produced by a series molding and casting processes of the created rock fractures (**Fig. 1**). To visualize the experiments, the upper part was made of transparent plastic while the lower part was manufactured using a non-transparent rubber. One model's (Fr.4s) both sides were made of solid transparent plastic as an exception. The details of the procedure followed to prepare fracture models are provided in Develi and Babadagli (2015).

The surface roughness of fracture models were first scanned through a fully computer-controlled surface scanner and then quantified by using variogram analysis, power spectral density, triangular prism, and ratio between total and planar areas methods. The values of estimated fractal dimension for seven fracture models are summarized in **Table 1**. The detailed

information about the surface scanner used and the methods for roughness quantification can be found in Develi and Babadagli (1998, 2015) and Babadagli et al. (2015b).

The experimental set-up consists of a model holder, syringe pump, pressure transducer, and camera as described by Raimbay et al. (2014, 2015) (**Fig. 2**). A 500 ml reservoir, fed continuously with a pump, was attached to introduce the injected fluid into the model uniformly. This created a 2-D (planar) displacement. The pressure in the injection end was continuously recorded and images were acquired periodically. To create clear boundaries of the displacement front for further image processing, a fluorescent dye was added into water and photos were taken in a dark room condition under UV black light source to make the dyed fluid visible. Details on the experimental set-up can be found in (Raimbay et al. 2014).

2-D experiments were performed by injecting water and polymer solution (0.03 weight% Xanthan Gum) in joint and horizontally displaced (sheared) fractures located horizontally at a flow rate of 204 ml/min. At zero shear stress, the -apparent- viscosity of Xanthan Gum (XG) was 364 cp. In all cases, fluids were injected at a constant flow rate while measuring pressure drop across the length of the fracture continuously. As all the models were identical in dimensions and the same spacers (2 mm) were used (fixed aperture in all models), the differential pressure measured was directly proportional to permeability. Thereby, any change in the pressure (and permeability) was due to roughness, which differed sample by sample.

As mentioned above, in the images taken during the experiments, the area wetted can be distinguished from dry area by adding fluorescent dye into the injected fluids and using UV light source. All images were scaled to have the same number of pixels and then flow wetted surface area was measured using ImageJ program (Rasband 1997-2005). The percentage area wetted by water and XG solutions was calculated using:

$$FWA(\%) = \frac{\textit{Flow wetted area}}{\textit{Total area}} \times 100 \quad (5)$$

3. Results and Discussion

The results were presented for two types of fluids (water and polymer solution) and fractures (joint and horizontally displaced). For each case, the pressure drop (permeability) and wetted

areas were correlated to three fractal dimensions representing self-affine (variogram, D_{va} , and power spectral density analysis, D_{psd}) and self-similar (triangular prism, D_{tp}) nature of the surfaces as well as the ratio between total and planar areas of the surfaces (A_t/A_p). The analyses were performed considering three parameters, namely rock type, roughness (quantified by different fractal dimensions and A_T/A_p ratio), and average grain size.

3.1 Effect of Fluid Type

3.1.1 Water injection on joint fracture models. The images at two different times (beginning and at the end of experiments) for water and polymer solution are shown in **Fig. 3**. Expectedly, polymer solution sweep was much more successful and less affected by the roughness. Channeling was obvious in the case of water (Fr.1, Fr.2, Fr.3, Fr.4s, and Fr.7). Polymer solution area coverage (wetted area) was affected by local roughness and unwetted areas were formed in the form of “pockets” of small (Fr.1, Fr.4s) and larger (Fr.2, Fr.3) sizes. Note that these are typically limestone, having small grain sizes, except Fr.4s. Other samples (Fr.5, Fr.6, Fr.7) showed almost perfect sweep (or wetting) with the polymer solution at the end of the experiment. When compared to the water flow, higher pressure drop occurred during the polymer flow as a result of its lower mobility due to higher viscosity, which caused spatially more homogenous sweeping of the larger areas without any considerable tortuous flow channeling. But, in the case of water, the flow path preferentially followed the channels through, where releasing the energy is much easier for a fluid with lower viscosity and thus higher mobility.

For a quantitative analysis, the wetted areas by water were plotted against D_{va} , D_{psd} , D_{tp} , and (A_t/A_p) in **Fig. 4**. The trends are indicated using dashed lines. Two distinct correlations were observed in all four cases and all based on the fractal dimensions. Lower and higher fractal dimensions showed two different -linear- trends regardless the grain size and rock type. The only exception is Fr.1, which yielded the highest D_{va} , D_{tp} and (A_t/A_p). Although it obeyed the trend in the case of D_{va} (red circles in Fig. 4a), this particular samples (Fr.1) did not fall into any other two correlations in the cases of D_{tp} and (A_t/A_p). Higher variogram dimension means more “wiggly,” rough, or less correlated systems. This type of porous rocks results in fracture roughness with shorter wavelength. Babadagli et al. (2015b) conducted multiphase flow (displacement) experiments on Fr.1 sample and, in accordance with our observations, observed

residual water saturation development as small pockets due to “small scale” roughness (not a strong “wetting” nature). This is the characteristic of this type of limestone rock that presents roughness at the grain scale due to small grain size and porous structure (short wavelength type roughness). In fact, Fr.1 showed the highest number of “isles” for the polymer solution case and severe channeling for the water case (Fig. 3).

The area wetted by water was higher in the models with lower variogram dimensions (e.g., $D_{va} < 1.3$), indicating that the degrees of roughness were lower and, as the grain size increased, more area was wetted. The same behavior is observed for the higher fractal dimensions (e.g., $D_{va} > 1.3$), but the change in the wetted area was not as sensitive to the fractal dimension and grain size as in the case of $D_{va} < 1.3$. Sensitivity to the grain size was not systematically observed for the other three roughness parameters D_{psd} , D_{tp} and (A_t/A_p) , even though a similar trend to the case of D_{va} were captured.

Similar observations were reported in the literature. Schmittbuhl et al. (2008) showed that coarse grain size of fracture increases the wavelength of fracture opening and hence, increases conductivity as well as the area wetted by the injected fluid. Develi and Babadagli (2015) reported a similar behavior; i.e., $D_{va} \approx 1.3$ is a threshold that separates the distinct behaviors with different slopes. Note that their injection rates were in the acceptable ranges to represent single phase flow in subsurface reservoirs while our injection rate was much higher to represent hydraulic fracture (high pressure injection) conditions. For their injection rate conditions (nearly 10 times smaller than our injection rates), they observed a decreasing trend in wetted areas with increasing D_{VA} and (A_t/A_p) . It should also be emphasized that although we used the same model fractures in this study as in Develi and Babadagli (2015), we kept them open by using 2 mm spacer to represent hydraulic fracture opening under high pressure and stress while their -joint-fracture models were tightly closed.

Interestingly, the trends are similar in terms of the grain size and fractal dimension and rock type in the cases of D_{tp} and (A_t/A_p) . Although the latter is not a fractal characteristic, these two roughness parameters represent the self-similar nature of the fracture surface; i.e., spatial distribution of the futures (roughness). Hence, they can be used alternately to cover this type of characteristics of the roughness.

A similar exercise was done for the pressure drop to account for the effect of roughness on the hydraulic conductivity of rough fractures (**Fig. 5**). Distinguishable trends also exist and are indicated by the dashed lines in Fig. 5. Fr.1, as similar to the previous wetted area analysis, is off-trend in all cases given in Fig. 5. Other than this sample, the variogram plot (Fig. 5a) showed that increasing fractal dimension and grain size resulted in decreasing pressure drop regardless of the rock type. Two characteristic behaviors (trends) are clearly seen and $D_{va} = \sim 1.3$ is a threshold that separates these two distinct behaviors. Although a similar declining trend was captured in the case of D_{psd} , there was no specific trend in terms of grain size or fractal dimension (Fig. 5b).

The two trends were identical for D_{tp} and (A_t/A_p) (Figs. 5c-d). As the D_{tp} and (A_t/A_p) decreases pressure drop decreases and more pressure drop is observed for the high D_{tp} and (A_t/A_p) values and smaller grain sizes, which correspond to the limestone cases (Fr.3, Fr.6, and Fr.1).

Similar to the wetted area cases discussed above, we observed an opposite trend to the work of Develi and Babadagli (2015). Fig. 5 shows a systematic decrease in pressure drop (or increase in permeability) with increasing D_{VA} , D_{psd} , D_{tp} and (A_t/A_p) . Using the same models but with much lower injection rates (10 times), Develi and Babadagli (2015) observed a decreasing trend of permeability with increasing D_{VA} (they did not provide any analysis using other three roughness parameters). These observations imply that the flow rate (and the stress created by fracturing process) critically alters the hydraulic behavior and amplifies the effect of roughness. Therefore, one should be careful in selecting proper model (or correlation) representing the physics of the process in simulating the hydraulic behavior of fractures. In any event, the four parameters tested in the present paper (extremely high injection rate for hydraulic fracturing cases) and Develi and Babadagli (2015) (low injection rate representing natural flow) can be used in correlations to incorporate the roughness.

3.1.2 Polymer (Xanthan Gum) solution injection on joint fracture models. Although the swept (wetted) areas were remarkably larger in this case compared to those of water injection (**Fig. 3**), the trends were similar when the wetted area was plotted against D_{va} (**Fig. 6a**). As the fractal dimension and grain sizes increased, the wetted areas increased linearly and two distinct trends were observed. Fr.2, Fr.5, and Fr.6 representing lower fractal dimensions showed a trend as similar to the water case. In both trends, increasing grain size resulted in a larger wetted area.

When the wetted area was plotted against D_{psd} , for the rock samples of Fr.1, Fr.3, and Fr.6, the trend was the same trend as in the water case. However, high fractal dimension and larger grains size samples showed a different behavior (Fig. 6b). D_{tp} and (A_t/A_p) plots showed identical trends as similar to the water case, but it was difficult to capture a correlation with respect to the fractal dimension and grain sizes (Fig. 6c-d).

Viscous nature of polymer solution not only increased the planar area wetted with the fluid but also affected the pressure drop (it is ten times higher than water injection case). However, the trends were similar as in water case (Fig. 7) when the pressure drop was plotted against D_{va} and D_{psd} . On the other hand, no distinct trends were obtained when D_{tp} and (A_t/A_p) were correlated to the area wetted (Fig. 7c-d) unlike the water case given in Fig. 5c-d.

3.2 Sheared Fractures: Water Injection in 5 mm Horizontally (Sheared) Displaced Models.

The images captured at the beginning and at the end of the experiments on six horizontally displaced (5mm) models are shown in Fig. 8. The wetted area in the sheared fracture cases is systematically higher than in the joint type fracture cases (Fig. 3) but the displacement patterns are visually identical. Table 2 shows the comparison of the wetted areas for the joint type and horizontally displaced fractures. The change in the wetted area is at the same ratio for the four cases (Fr.2, Fr.6, Fr.1, Fr.4s) but Fr.3 and Fr.7 yielded much larger wetted areas in the sheared case (Fig. 9). These two models were limestone and marble but possessed D_{va} corresponding to the threshold values mentioned before (~ 1.3). In this case, a linear trend of decreasing wetted areas with increasing D_{va} (Fig. 9a) instead of a bi-linear trend observed for the joint case (Fig. 4a). On the other hand, Fr.3 and Fr.7 had low D_{psd} , D_{tp} and (A_t/A_p) values. Note that these two samples had the largest (Fr.7) and smallest (Fr.3) grain sizes.

As similar to the joint case (Fig. 4b), the bi-linear trend can be pronounced when D_{psd} was used as the roughness parameter (Fig. 9b). No correlation was observed with the D_{tp} and A_t/A_p unlike the joint type fracture samples. All these indicate that D_{va} can still be used as the roughness parameters in the case of sheared fractures.

With a 5 mm horizontally displaced model, a degree of pressure reduction (permeability increase) was observed (**Fig. 10**). This reduction is very minimal in the cases of Fr.3, Fr.4s and Fr.6, which corresponded to two limestone samples with D_{va} values near the threshold value (~ 1.3) (Fr.3 and Fr.4). Note that the Fr.4s model had marble on both sides but possessed the highest fractal dimension. A bi-linear trend can be pronounced in Fig. 10a for the horizontally displaced case.

Although no systematic correlation was obtained, a similar trend to the joint case (Fig. 5b) was observed when D_{psd} was used as the roughness parameter. Interestingly, D_{tp} and A_t/A_p yielded linear correlations (identical to each other) and increasing values of these parameters resulted in an increase in pressure (permeability reduction) (Fig. 10c-d), which is opposite to the joint fracture cases (Fig. 5c-d).

3.3 Quantitative Analysis

Based on the results obtained from the qualitative analysis of the experimental data, a quantitative study was carried out where wetted area and pressure drop were correlated to the five variables (D_{va} , D_{psd} , D_{tp} , A_t/A_p , and average grain size –AGS) using multi variable regression method. We begin with correlating these variables to the wetted areas and pressure drops individually. The plots are given in Appendix (**Figs. A1 through A4**). Five different correlation types (linear, logarithmic, exponential, inverse linear, and inverse logarithmic) were tested and the ones yielding the highest regression coefficient were selected for multivariable regression analysis.

Next, the correlations with different number of variables were generated. The outcome of this exercise is summarized below.

3.3.1 *Wetted Areas for Water Flow*

Six correlations were tested for joint and sheared fractures. As shown in the tables given in Appendix (**Tables A1 and A2**), the strongest correlations were obtained for both cases when all five parameters were included. When D_{psd} was excluded, a significant reduction in the regression coefficient (R^2) was observed (second equation with four variables in Tables A1 and

A2). Further removal of parameters (D_{tp} , A_t/A_p) did not change the R^2 (third and fourth equations with three and two variables, respectively, in Tables A1 and A2).

Based on the systematic trends observed for D_{va} and AGS in Figs. 4a and 6a, these two parameters were correlated to wetted area individually. Interestingly, D_{va} and AGS showed much stronger correlations ($R^2 = 0.69$ and 0.3 , respectively) with the wetted area (WA) for the sheared models (Table A2) compared to the joint ones ($R^2 = 0.08$ and 0.07 , respectively) (Table A1). In fact, D_{va} and AGS yielded the strongest correlation among all parameters for both cases (Figures A1 and A2) but was much higher for the sheared model ($R^2 = 0.82$ and 0.87 for the exponential correlation, respectively) compared to the joint model ($R^2 = 0.28$ [logarithmic correlation] and 0.40 [inverse linear correlation], respectively).

3.3.2 Pressure Drop for Water Flow

Pressure drop correlations followed a similar trend for the joint (Table A3) and sheared (Table A4) models. The highest R^2 was obtained when all five variables were included. What is interesting is that the average grain size (AGS) yielded the strongest correlation when used as the only variable, being much stronger for the joint case, whereas D_{va} showed the weakest correlation with pressure drop (the last row in both tables).

3.3.3 Wetted Areas for Polymer Solution Flow

The same multiple regression analysis procedure was followed for the joint fracture cases of polymer solution flow. AGS yielded better correlations than other roughness parameters (except the exponential one) (Fig. A5). When all five parameters are considered, a correlation with a relatively low R^2 was obtained (0.76) (Table A5). When D_{tp} was excluded as the parameter showing the least strong correlation (Fig. A5), the R^2 was improved slightly (0.78).

3.3.4 Pressure Drop for Water Polymer Solution Flow

Fig. A6 showed that three fractal dimensions are very weakly correlated. In addition to AGS, A_t/A_p also yielded a better correlation. Interestingly, the low R^2 (0.50) obtained for the correlation with five variable, improved significantly (0.66) when the parameter showing the least strong correlation (D_{psd}) was excluded (Table A6).

The lower correlation coefficients obtained with polymer on the joint fractures compared to the water cases indicate that the mobility ratio should be considered in addition to the roughness parameters in the correlations. One may infer from the lower R^2 values obtained for the polymer case (0.78 and 0.66 for the wetted area and pressure drop, respectively) compared to the water ones (0.99 and 0.91 for the wetted area and pressure drop, respectively), fluid rheological characteristic (mainly viscosity) is almost equally important as the roughness parameters especially on conductivity (pressure drop).

4. Conclusions and Remarks

Single phase flow experiments were performed on the transparent replicas of fractures (developed from seven different rock types under tension) using water and polymeric solution. The tests were performed for joint type and horizontally displaced (sheared) fractures. The images acquired and pressure recorded were used to generate the plots of wetted area and pressure drop (i.e., permeability) against four different roughness parameters (fractal dimensions obtained by variogram analysis, D_{va} , power spectral density, D_{psd} and triangular prism method, D_{tp} , and the ratio of total and planar areas, A_t/A_p). In this analysis, the grain size effect was also included. The following conclusions can be drawn and remarks can be made from the observations.

Joint Type Fractures

1. No clear single trend was obtained for all rock types for either the wetted areas or pressure drop. Instead, two distinct trends were typically observed for all four roughness parameters when water flowed in a single fracture. Increasing D_{va} , D_{psd} , D_{tp} , A_t/A_p values and grain sizes resulted in more wetted areas regardless of the rock type (i.e., limestone, granite, marble). Threshold values of D_{va} , D_{psd} , D_{tp} , A_t/A_p separating the two distinct trends were found as 1.3, 2.3, 2.007, and 1.083, respectively. A similar behavior was observed for the polymeric solution case when D_{va} was used as the correlating parameter. D_{psd} also showed similar trends for both water and polymeric cases below this threshold value. Above it, the trend of wetted area change with D_{psd} was the opposite (increasing

fractal dimension yielded smaller wetted area). No typical trend was obtained for the polymeric solution when D_{tp} and A_t/A_p were used as the correlating parameter.

2. Pressure drop followed a similar trend to the wetted area case when plotted against D_{va} , i.e., two distinct trends separated by a threshold value of $D_{va} \sim 1.3$ were observed for both water and polymer solution cases. Increasing grain sizes resulted in a decrease in pressure drop. In the D_{psd} cases, water and polymer showed similar trends but no correlation was observed. Although D_{tp} and A_t/A_p showed good correlations with the pressure drop in the water case (decreasing pressure drop with increasing values, except the highest fractal dimension case –Fr.1), no typical trends were observed with these roughness parameters for the polymeric solution case. Hence, they can be used as alternative to each other to represent the self-similar nature of fracture roughness.
3. The results showed that D_{va} can be used as roughness parameters in modeling fracture flow regardless of the fluid type. It cannot, however, capture all the characteristics of roughness and can be considered together with D_{tp} and A_t/A_p in modeling single phase flow in rough fractures. In all cases, D_{tp} and A_t/A_p showed identical trends. Hence, they can be used as alternative to each other to represent the self-similar nature of fracture roughness. In modeling polymer flow, D_{psd} could be incorporated if the fractal dimension of the surface was (typically) less than 2.3.
4. D_{va} , D_{tp} , D_{psd} and A_t/A_p represents different roughness characteristics of the surfaces and, ideally, they should be combined when the roughness effect is to be incorporated in modeling single phase flow in single fractures.
5. Grain size and fractal dimension are critical parameters in correlating fracture roughness to the hydraulic behavior of single fractures.

Horizontally Displaced Fractures

6. The wetted area in the horizontally displaced fracture cases was systematically higher than in the joint type fracture cases (Fig. 3). However, the displacement patterns were

visually identical. The change in the wetted area was similar for the four cases (Fr.2, Fr.6, Fr.1, Fr.4s). Fr.3 and Fr.7, on the other hand, showed much larger wetted areas in the sheared case. A linear trend was observed for the sheared case when D_{va} was used as the roughness parameter but the bilinear behavior was maintained for the D_{psd} case. No correlation was observed with the D_{tp} and A_t/A_p unlike the joint samples.

7. A bi-linear trend was observed when D_{va} was used as the roughness parameter for the horizontally displaced case. Although no systematic correlation was obtained, a similar trend to the joint case (Fig. 5b) was observed when D_{psd} was used as the roughness parameter for the horizontally displaced case. D_{tp} and A_t/A_p yielded linear correlations (increasing values of those parameters resulted in an increase in pressure), which was opposite to the joint cases (Fig. 5c-d).
8. Similar to the joint case, D_{va} can be used as a roughness parameter to correlate the hydraulic behavior of single fractures. Although no trends were observed for the wetted areas, D_{tp} and A_t/A_p showed strong correlations with pressure drop. Hence, their combination with D_{va} can be considered in incorporating the roughness effect into flow modeling.

Quantitative Analysis

9. A quantitative study was carried out to correlate wetted area and pressured drop with five variables (D_{va} , D_{psd} , D_{tp} , A_t/A_p , and average grain size–AGS) using multi variable regression method. The strongest correlations were obtained for both cases when all five parameters were included.
10. The most interesting observation was the correlations obtained with D_{va} and AGS individually. They showed much stronger correlation with the wetted area (WA) on the sheared models (Table A2) compared to the joint ones (Table A1).

11. When considered as a single variable, the AGS yielded the strongest correlation, being much stronger for the joint case, whereas D_{va} showed the weakest correlation with pressure drop.
12. The lower correlation coefficients obtained with polymer compared to the water cases indicate that the viscosity term (mobility ratio) should be considered in addition to the roughness parameters. Flow behavior characteristic (mainly viscosity) is almost equally important as roughness on fluid distribution (wetted area) and especially conductivity (pressure drop).

Acknowledgments

This research was conducted under the second author's (TB) NSERC Industrial Research Chair in Unconventional Oil Recovery (industrial partners are CNRL, SUNCOR, Touchstone Exp., Sherritt Oil, APEX Eng., PEMEX, Saudi Aramco and Husky Energy), the Helmholtz Alberta Initiative (HAI) project funded by the Alberta Government. The first author gratefully acknowledges MSc scholarship support of JCS "Center for International Programs" funded by the government of the Republic of Kazakhstan and thanks Ms. Yu Wang for her help in the regression analysis part of the study. The fourth author (KD) is thankful to the Scientific and Technological Research Council of Turkey (TÜBİTAK) for his postdoctoral scholarship through the BİDEP program.

References

- Auradou, H., Drazer, G., Boschan, A., et al. 2006. Flow Channeling in a Single Fracture Induced by Shear Displacement. *Geothermics* **35**: 579-588. <http://doi:10.1016/j.geothermics.2006.11.004>.
- Babadagli, T., Ren, X., and Develi, K. 2015a. Effects of Fractal Surface Roughness and Lithology on Single and Multiphase Flow in a Single Fracture: An Experimental Investigation. *Int. J. of Multiphase Flow* **68**: 40-58.
- Babadagli, T., Raza, S., Ren, X. et al. 2015b. Effect of Surface Roughness and Lithology on the Water-Gas and Water-Oil Relative Permeability Ratios of Oil-Wet Single Fractures. *Int. J. of Multiphase Flow* **75**: 68-81.
- Briggs K., Hill A.D., and Zhu D. 2014. The Relationship between Rock Properties and Fracture Conductivity in the Fayetteville Shale. Presented at SPE Annual Technical Conference and Exhibition, Amsterdam, The Netherlands, 27-29 October. SPE-170790.

- Brown, S.R. 1987. Fluid Flow Through Joints: The effect of Surface Roughness. *Journal of Geophysical Research* **92** (B2): 1337-1347.
- Crawford J., Moreno, L., and Neretnieks, I. 2003. Determination of the flow-wetted surface in fractured media. *J. Contam. Hydrol* **61**: 361-369.
- Develi, K. and Babadagli, T. 1998. Quantification of Natural Fracture Surfaces using Fractal Geometry. *Math. Geol.* **30** (8): 971-998.
- Develi, K. and Babadagli, T. 2015. Experimental and Visual Analysis of Single-Phase Flow through Rough Fracture Replicas. *Int. J. of Rock Mech. and Min. Sci.* **73**: 139-155.
- Gangi, A.F. 1978. Variation of Whole and Fractured Porous Rock Permeability with Confining Pressure. *Int. J. Rock Mech. Min. Sci. & Geomech. Abstr.* **15** (5): 249-257.
- Kranz, R.L., Frankel, A.D., Engelder, T. et al. 1979. The Permeability of Whole and Jointed Barre Granite. *Int. J. Rock Mech. Min. Sci. & Geomech. Abstr.* **16** (4): 225-234.
- Koyama, T., Neretnieks, I., and Jing, L. 2007. A Numerical Study on Differences in using Navier-Stokes and Reynold Equations for Modeling the Fluid Flow and Particle Transport in Single Rock Fractures with Shear. *International Journal of Rock Mechanics & Mining Sciences* **45** (7): 1082-1101.
- Lee, H.S. and Cho, T.F. 2002. Hydraulic Characteristics of Rough Fractures in Linear Flow under Normal and Shear Load. *Rock Mechanics and Rock Engineering* **35** (4): 299-318. <http://doi:10.1007/s00603-002-0028-y>.
- Nemoto, K., Watanabe, N., Hirano, N. et al. 2008. Direct Measurement of Contact Area and Stress Dependence of Anisotropic Flow Through Rock Fracture with Heterogeneous Aperture Distribution. *Earth and Planetary Science Letters* **281** (1-2): 81-78. <http://doi:10.1016/j.epsl.2009.02.005>.
- Raimbay, A., Babadagli, T., Kuru, E. et al. 2014. Effect of Fracture Surface Roughness and Shear Displacement on Permeability and Proppant Transportation in a Single Fracture. Presented at the 2014 SPE Unconventional Res. Conf., Calgary, AB, Canada, 30 Sept.-2 Oct. SPE-171577.
- Raimbay, A., Babadagli, T., Kuru, E. et al. 2015. Quantitative and Visual Analysis of Proppant Transport in Rough Fractures and Aperture Stability. Presented at the 2015 SPE Hydraulic Fracturing Technology Conf., The Woodlands, TX, USA, 3-5 Feb. SPE-173385.
- Rasband, W.S., ImageJ, U. S. National Institutes of Health, Bethesda, Maryland, USA, 1997-2005, <http://rsbweb.nih.gov/ij/docs/user-guide.pdf>.
- Rasmuson, A. and Nereitneiks, I. 1986. Radionuclide transport in fast channels in crystalline rock. *Water Resour. Res.* **22** (8): 1247-1256.
- Renshaw, C.E. 1995. On the Relationship between Mechanical and Hydraulic Apertures in Rough-Walled Fractures. *Journal of Geophysical Research* **100** (B12): 629-636.
- Schmittbuhl, J., Steyer, A., Jouniaux, L. et al. (2008). Fracture Morphology and Viscous Transport. *Int J Rock Mech Min Sci* **45**: 422-430.
- Tsang, Y.W. and Witherspoon, P.A. 1983. The Dependence of Fracture Mechanical and Fluid Flow Properties on Fracture Roughness and Sample Size. *Journal of Geophysical Research* **88** (B3): 2359-2366.
- Tsang, Y.W. 1984. The Effect of Tortuosity on Fluid Flow through a Single Fracture. *Water Resources Research* **20** (9): 1209-1215.
- Van Dam, D.B. and de Pater, C.J. 1999. Roughness of Hydraulic Fractures: The importance of in-situ Stress and Tip. Presented at SPE Annual Technical Conference and Exhibition, Houston, Texas, 3-6 October. SPE-56596.

- Walsh J.B. 1981. Effect of Pore Pressure and Confining Pressure on Fracture Permeability. *Int. J. Rock Mech. Min. Sci. & Geomech. Abstr.* **18** (4): 429-435.
- Watanabe, N., Hirano, N., and Tsuchiya, N. 2008. Diversity of Channeling Flow in heterogeneous Aperture Distribution inferred from Integrated Experimental – Numerical Analysis on Flow through Shear Fracture in Granite. *Journal of Geophysical Research* **114** (B4). <http://doi:10.1029/2008JB005959>.
- Yeo, I.W., De Freitas, M.H., and Zimmerman, R.W. 1998. Effect of Shear Displacement on the Aperture and Permeability of a Rock Fracture. *Int. J. Rock Mech. Min. Sci. & Geomech. Abstr.* **35** (8): 1051-1070.

Fracture model	Rock type	D _{va}	D _{psd}	D _{tp}	A _t /A _p	Average grain size (AGS), mm
FR.1	Beige limestone with abundant coarse fossil shells	1.373	2.277	2.012	1.145	Not measurable
FR.2	Semi re-crystalized micritic pink limestone	1.263	2.558	2.007	1.079	0.4
FR.3	Micro- fossiliferous pisolitic beige limestone	1.303	2.266	2.007	1.061	0.3
FR.4s	Coarse grained white marble	1.39	2.418	2.009	1.098	3
FR.5	Holocrystalline amphibole granite	1.299	2.335	2.008	1.083	2
FR.6	Micritic cemented, fissured beige limestone with abundant amount of fossils	1.29	2.3	2.010	1.115	0.8
FR.7	Medium-coarse grained white marble	1.326	2.321	2.006	1.072	1.5
Flat	-	1	2	2	1	-

Table 1—Lithological descriptions of the rock samples and the calculated roughness parameters (Develi and Babadagli 2015).

D: fractal dimension; A_t/A_p: ratio between total surface area (A_t) and planar surface area (A_p),

Subscripts – va: variogram analysis; psd: power spectral density; tp: triangular prism.

Boths sides of model Fr.4s is made of solid transparent plastic.

Sample	Joint (% Water)	Horizontally displaced (sheared) (% Water)
fr.1	38.64	54.55
fr.2	45.90	69.06
fr.3	26.47	71.41
fr.4s	37.00	53.64
fr.6	62.48	81.45
fr.7	33.79	71.82

Table 2—Wetted areas by water (%) in joint and sheared fractures when water is injected.

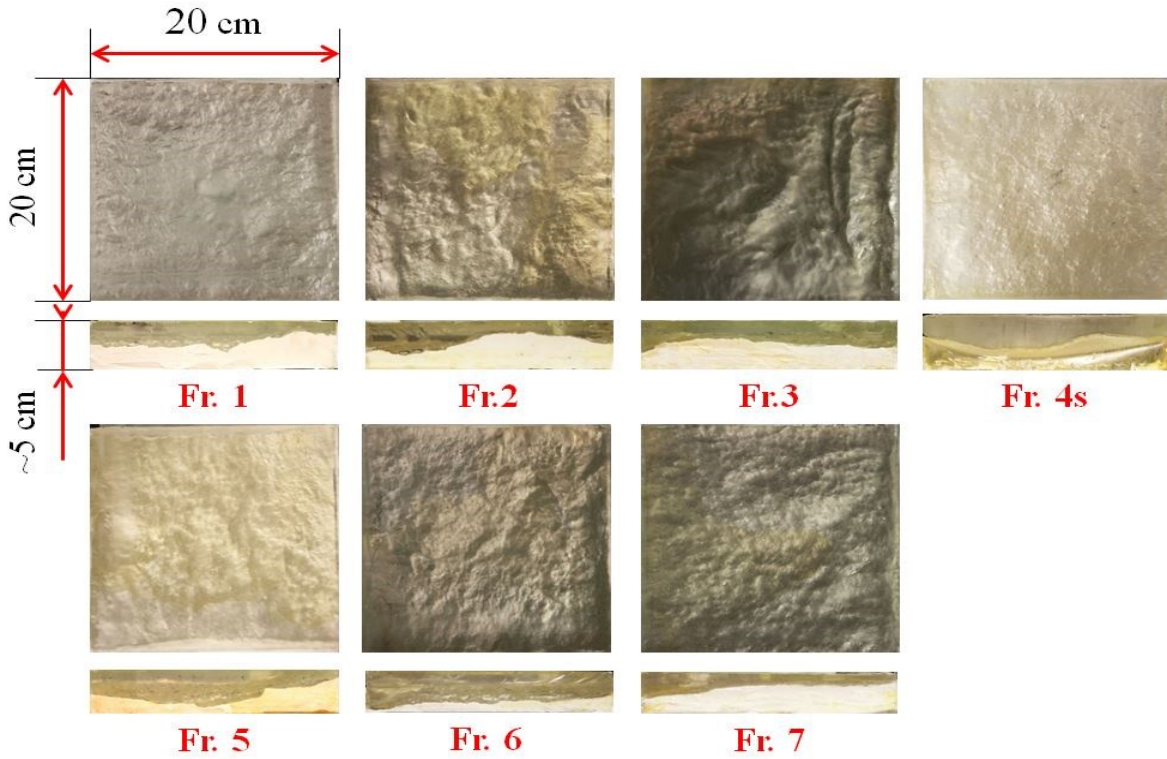


Figure 1—Top and side views of fracture models (Raimbay et al. 2014). The thickness of the model varies slightly model by model.

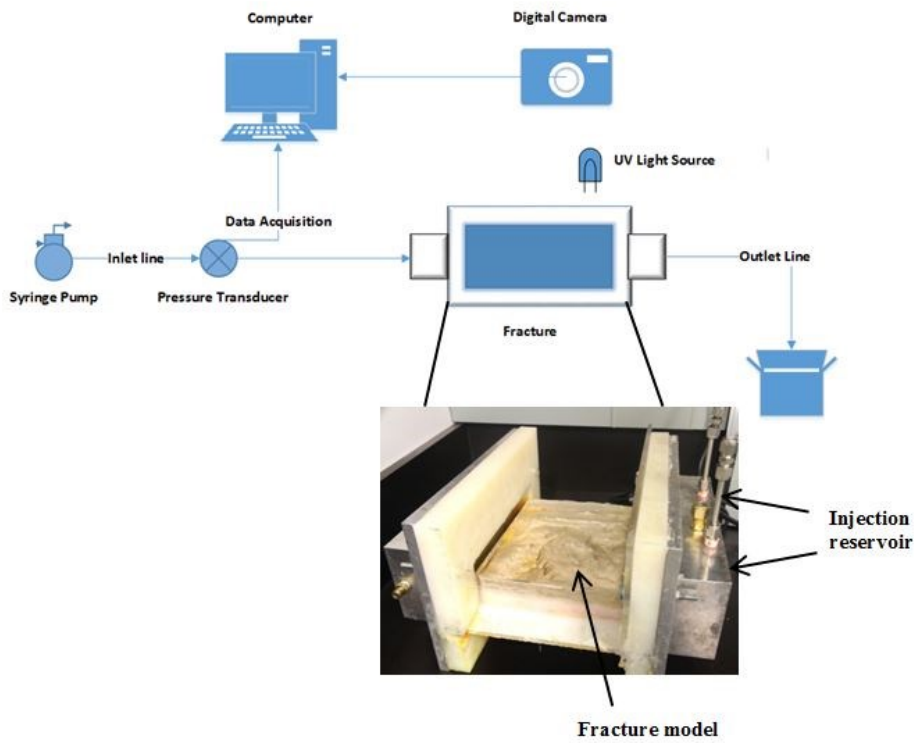
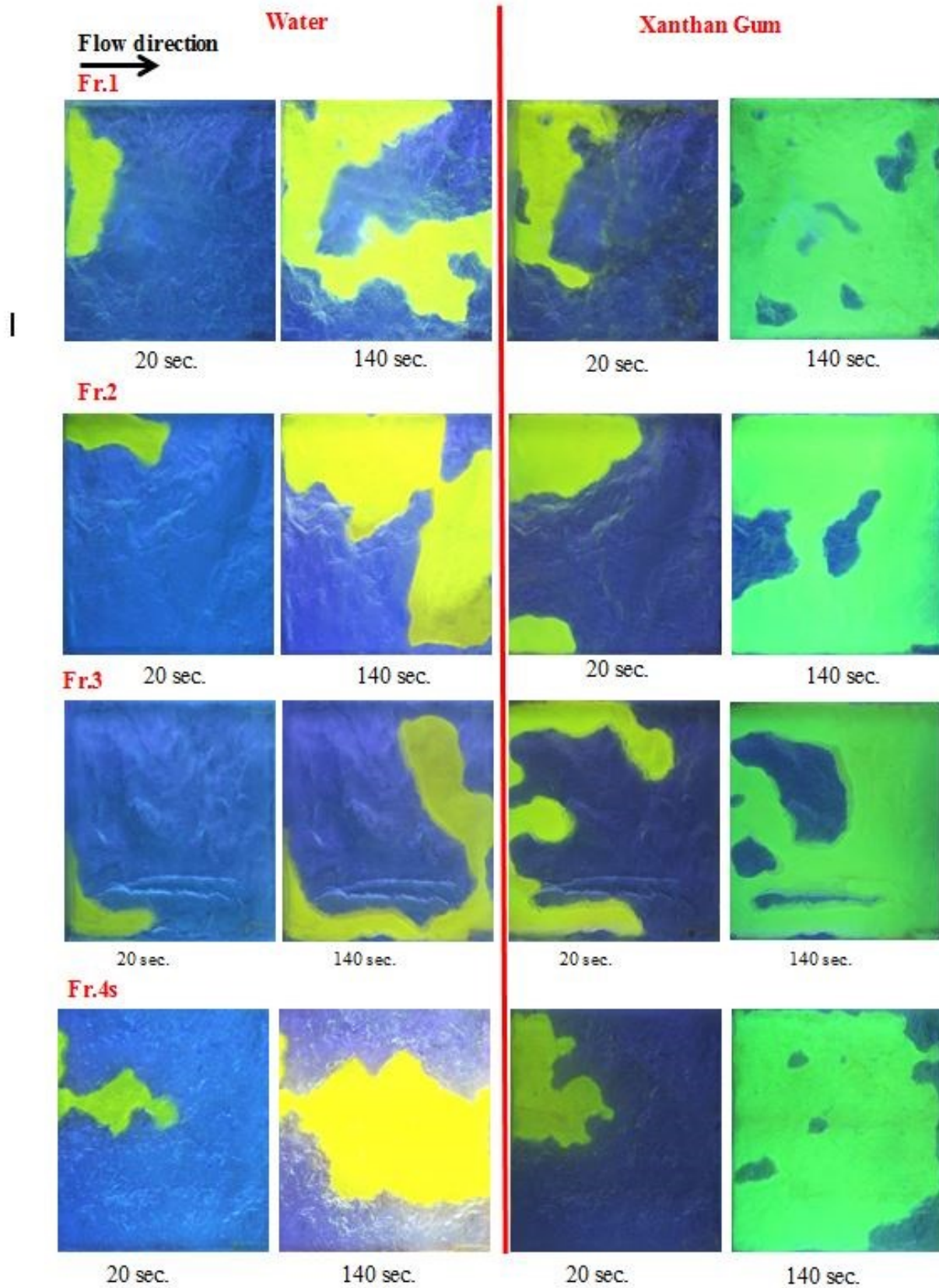


Figure 2—Schematic of experimental set-up (Raimbay et al. 2014).



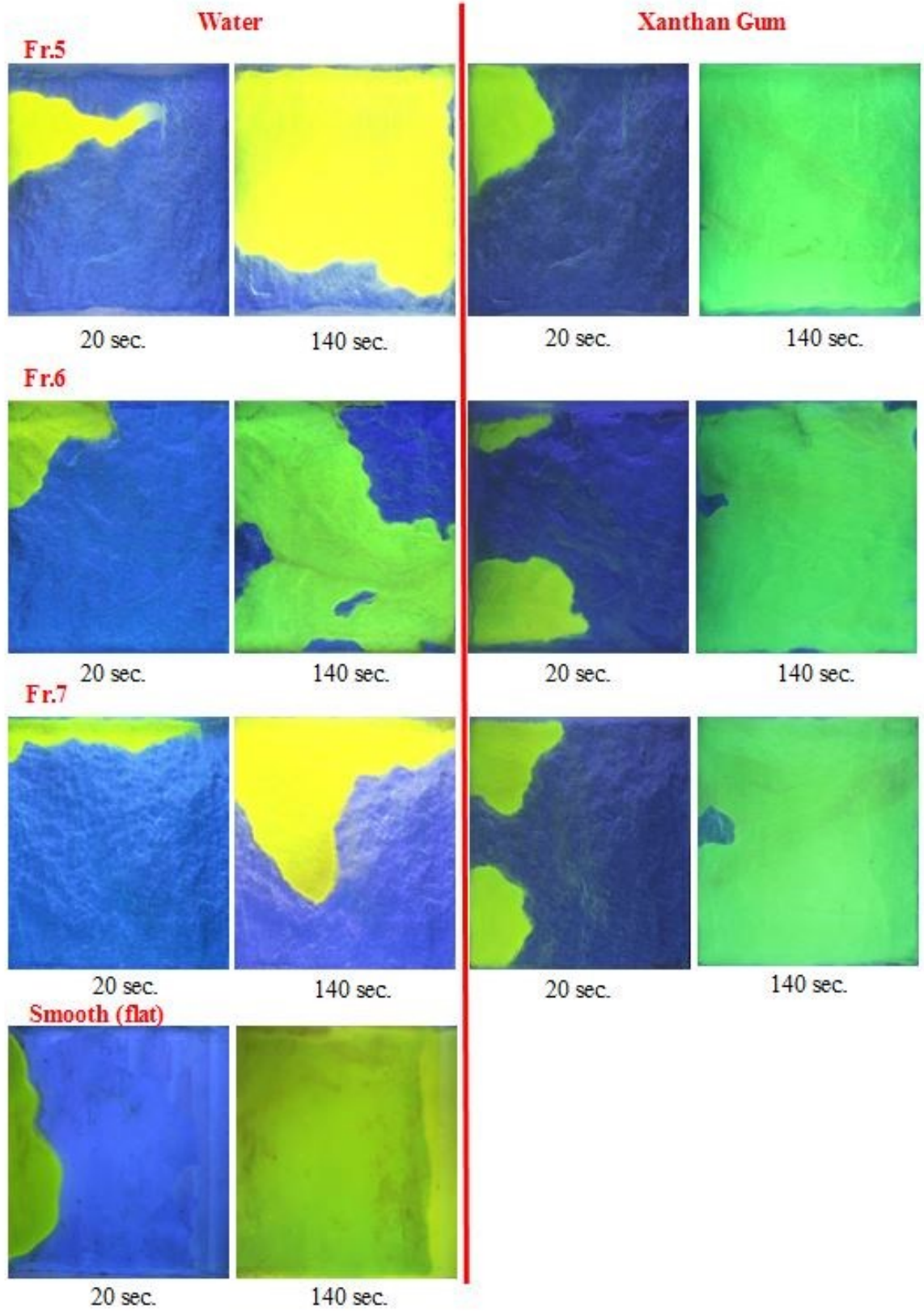
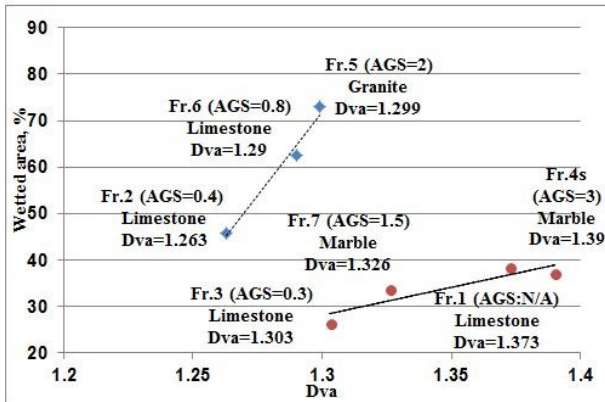
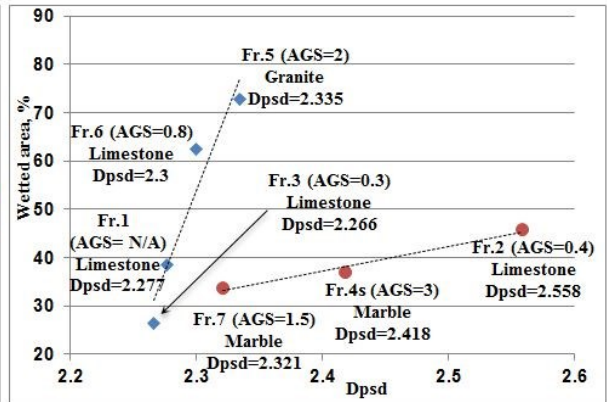


Figure 3—Planar view of water and polymer (Xanthan Gum) solution flow in the joint fracture models given in Table 1. Blue areas correspond to air and yellow is dyed water/polymer solution.

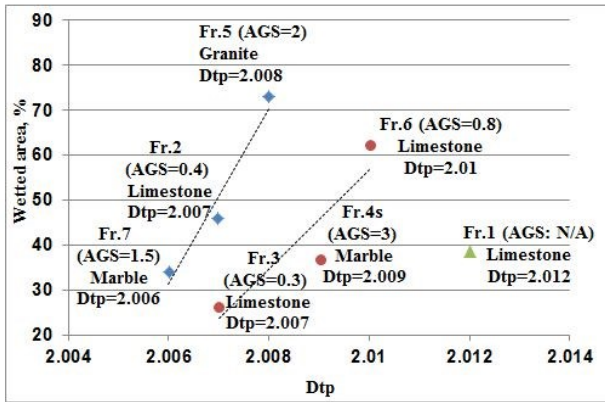
a



b



c



d

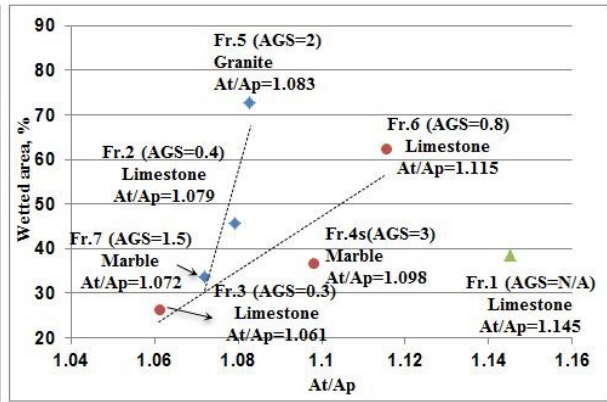


Figure 4—Wetted areas correlated to different roughness parameters (variogram analysis, power spectral density and triangular prism fractal dimensions, and ratio of total area to planar area) for seven fracture models. Fluid injected: Water. Fracture type: Joint. AGS: Average grain size.

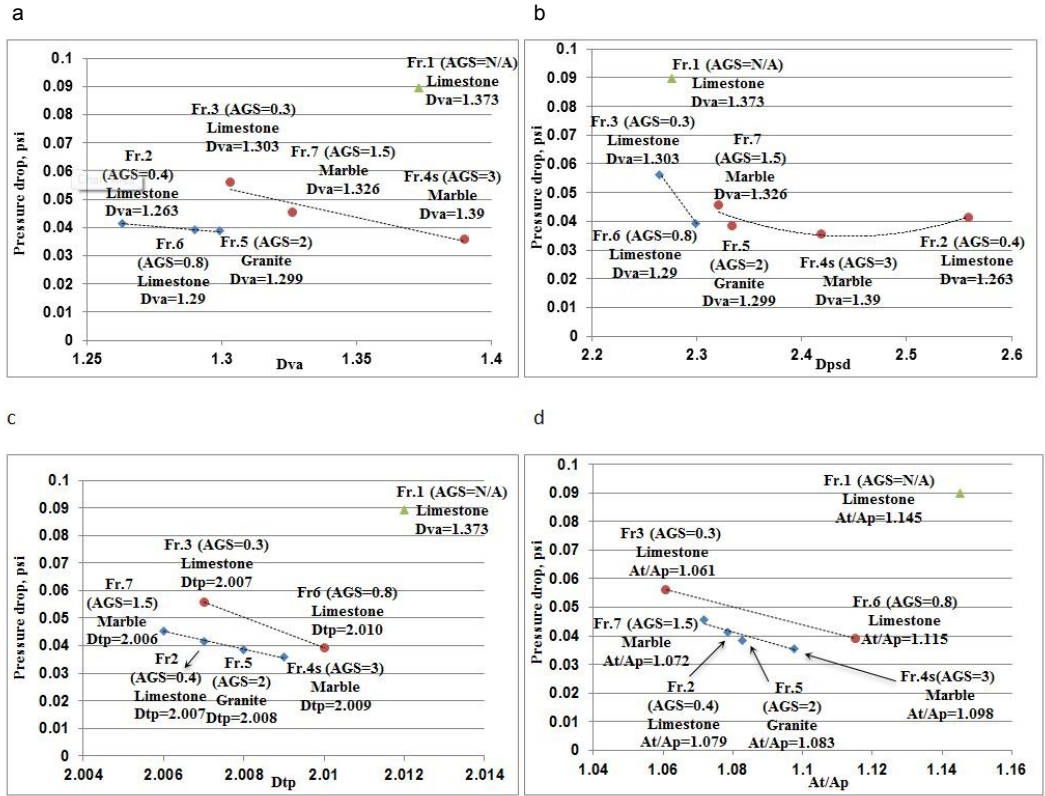


Figure 5—Pressure drops (permeability) correlated to different roughness parameters (variogram analysis, power spectral density and triangular prism fractal dimensions, and ratio of total area to planar area) for seven fracture models. Fluid injected: Water. Fracture type: Joint. AGS: Average grain size.

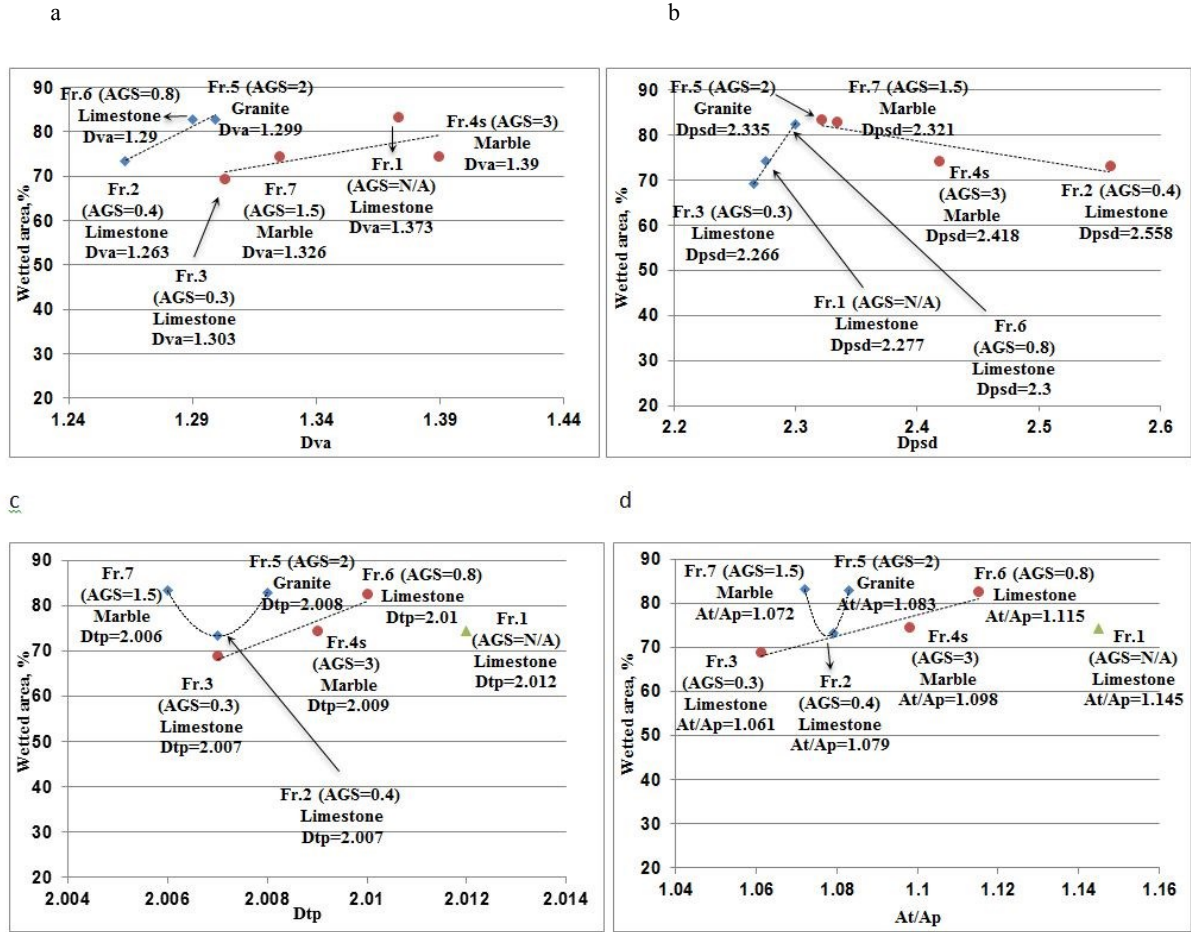
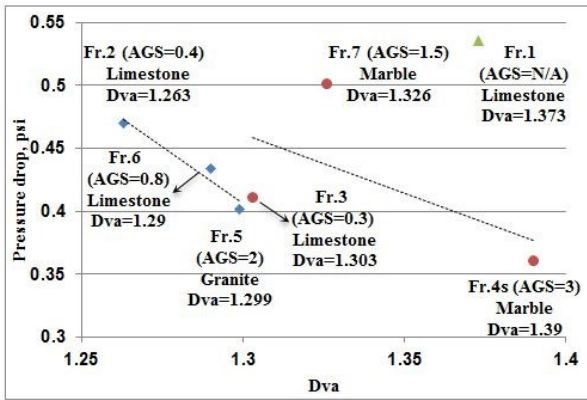
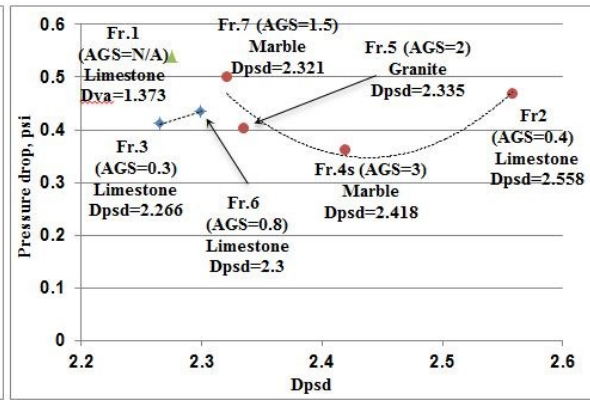


Figure 6—Wetted areas correlated to different roughness parameters (variogram analysis, power spectral density and triangular prism fractal dimensions, and ratio of total area to planar area) for seven fracture models. Fluid injected: Polymer (Xanthan Gum) solution. Fracture type: Joint. AGS: Average grain size.

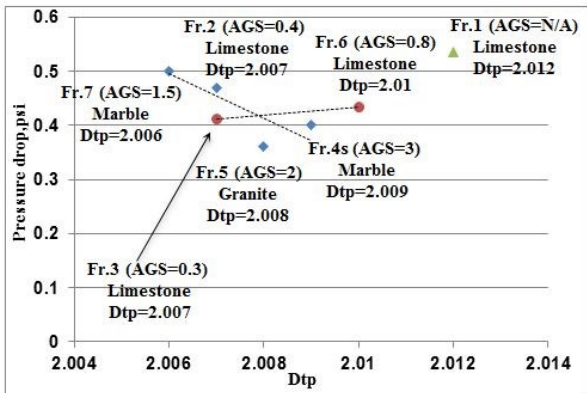
a



b



c



d

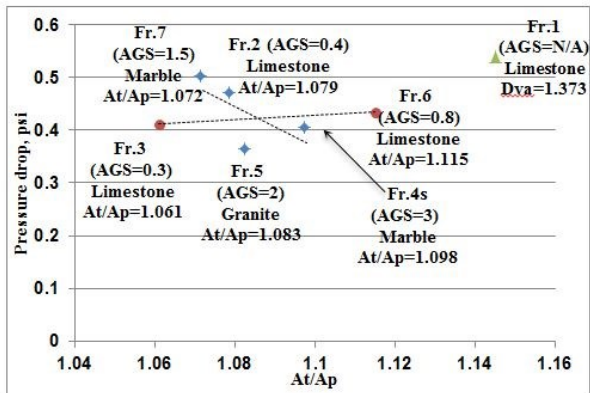


Figure 7—Pressure drop (permeability) correlated to different roughness parameters (variogram analysis, power spectral density and triangular prism fractal dimensions, and ratio of total area to planar area) for seven fracture models. Fluid injected: Polymer (Xanthan Gum) solution. Fracture type: Joint. AGS: Average grain size.

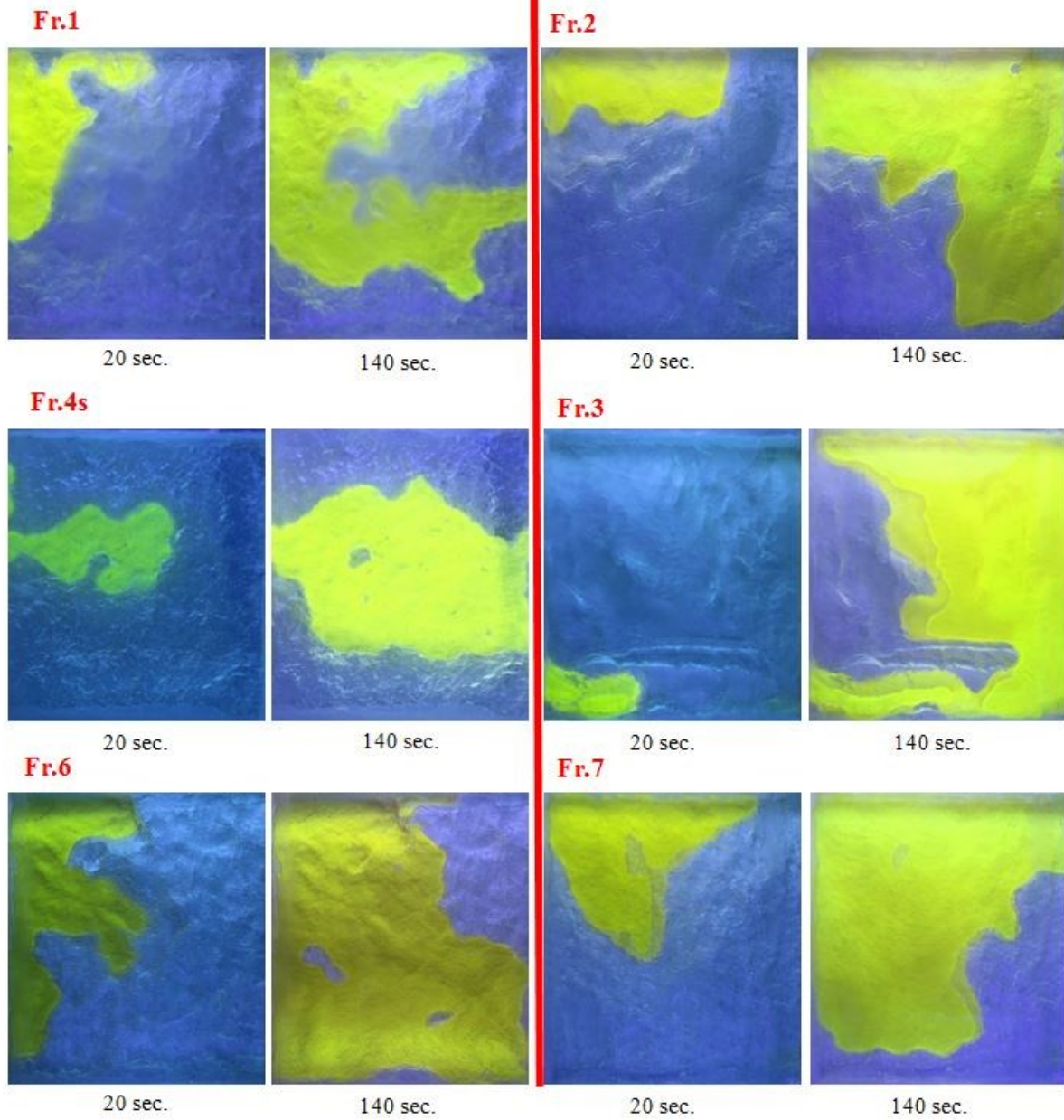


Figure 8—Planar view of water flow in 6 shear displaced rough models. Blue areas correspond to air and yellow is dyed water.

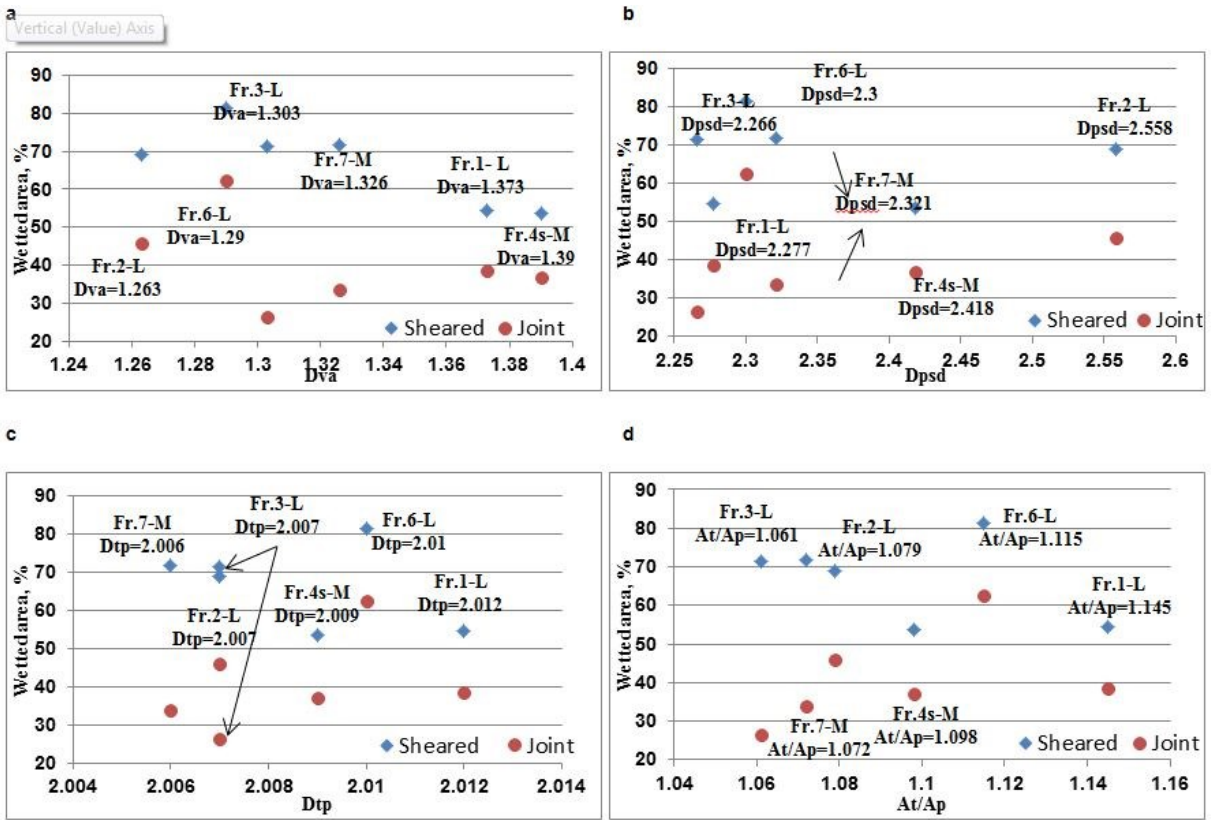


Figure 9—Wetted areas correlated to different roughness parameters (variogram analysis, power spectral density and triangular prism fractal dimensions, and ratio of total area to planar area) for six fracture models. Fluid injected: Water. Fracture type: Joint and horizontally displaced (sheared). L: Limestone, M: Marble.

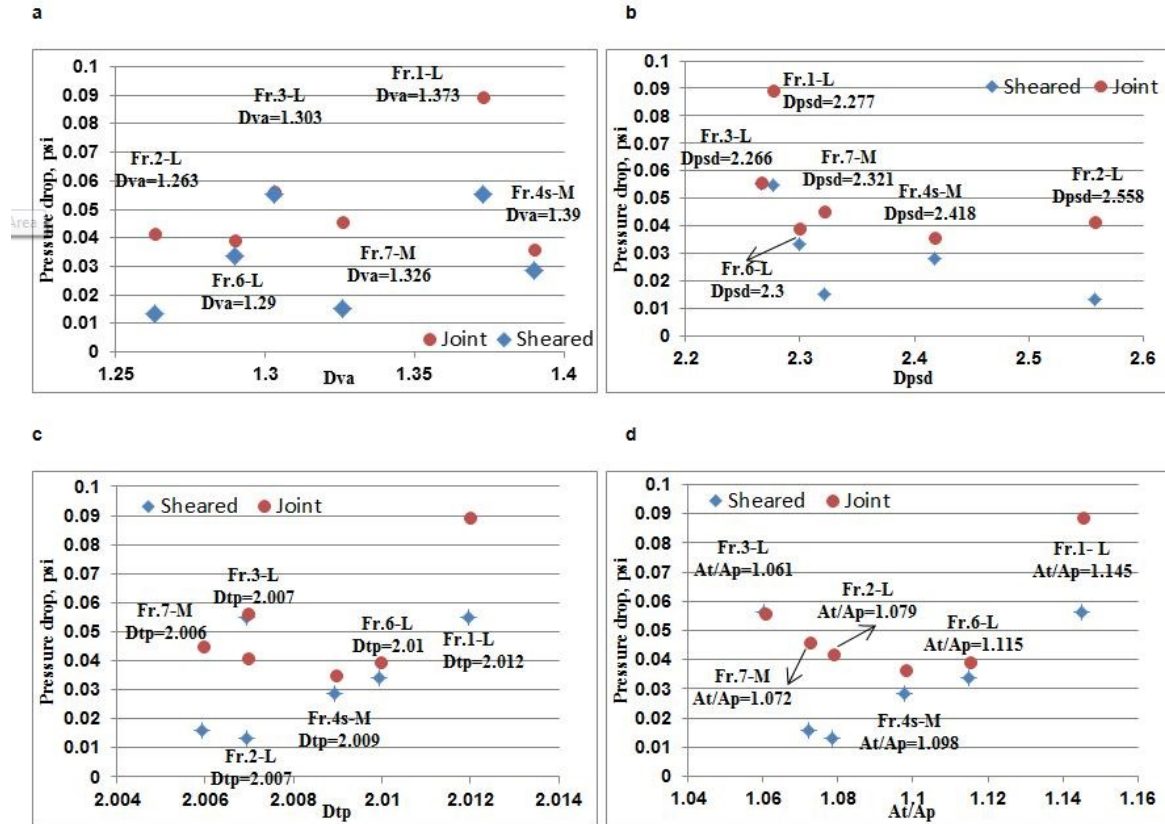


Figure 10—Pressure drop (permeability) correlated to different roughness parameters (variogram analysis, power spectral density and triangular prism fractal dimensions, and ratio of total area to planar area) for seven fracture models. Fluid injected: water. Fluid injected: water. Fracture type: Joint and horizontally displaced (sheared).

APPENDIX: Multivariable regression analysis results

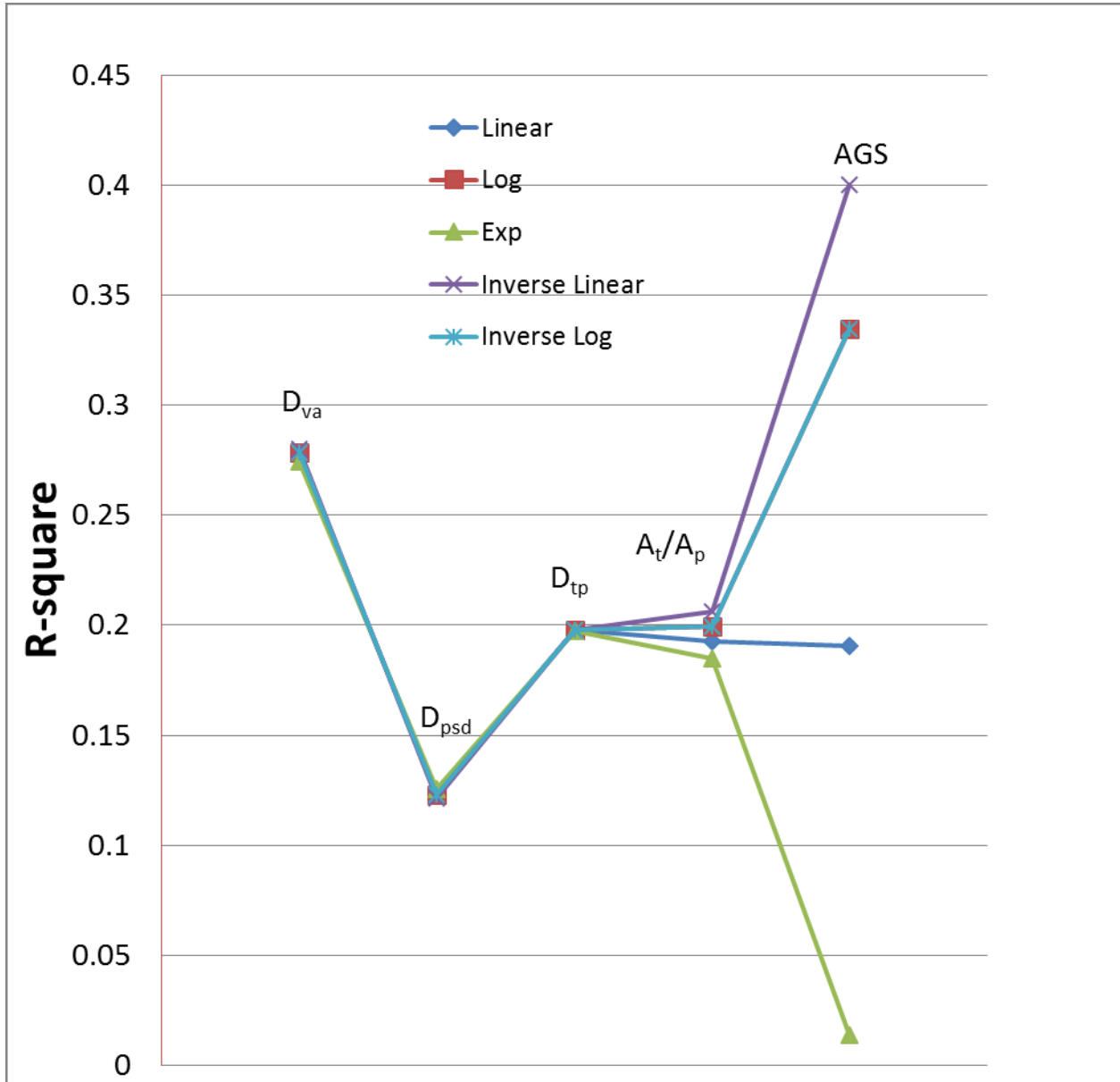


Figure A1—Testing different correlations between five variables and wetted areas for joint fracture cases for water.

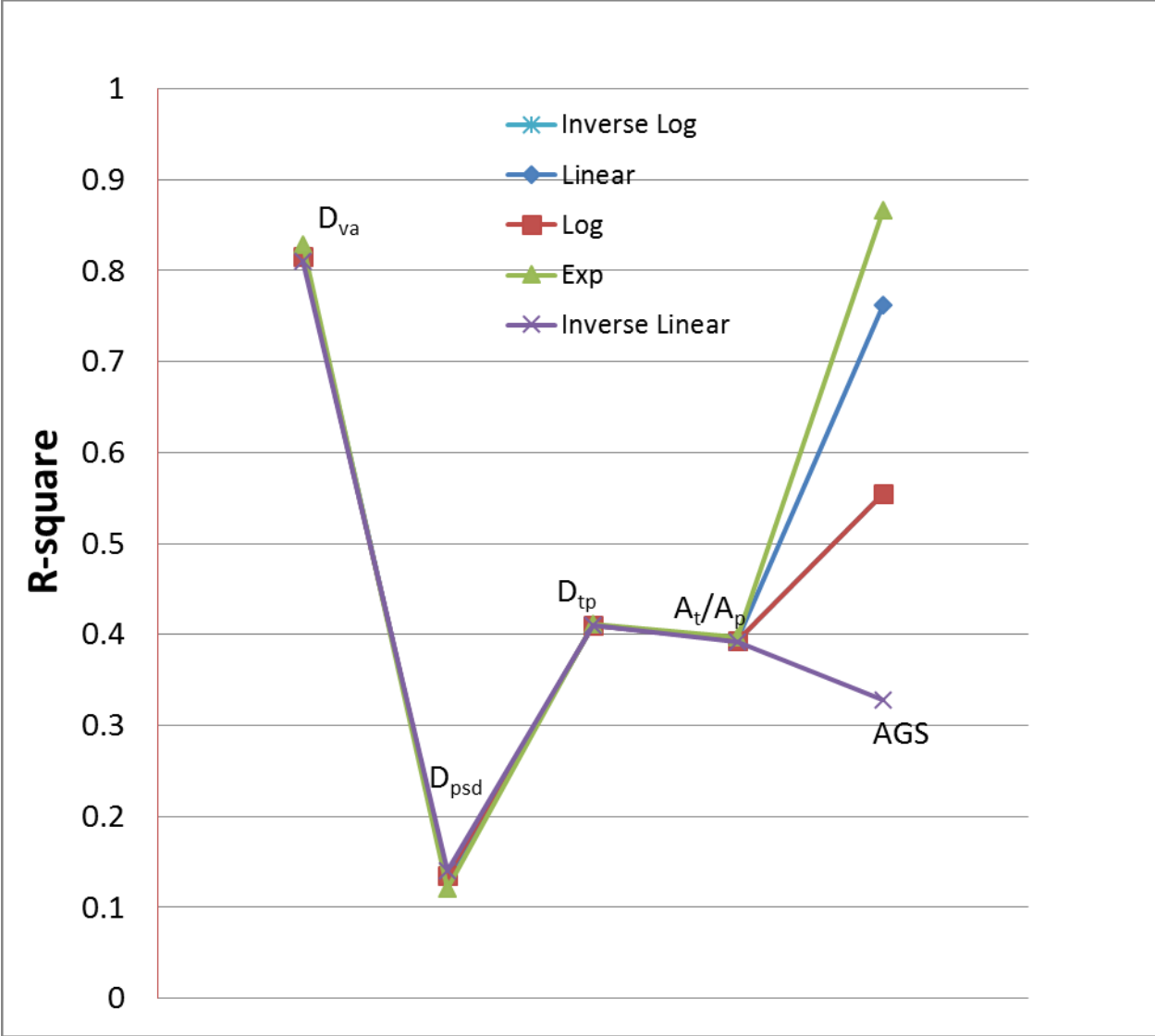


Figure A2—Testing different correlations between five variables and wetted areas for sheared fracture cases for water.

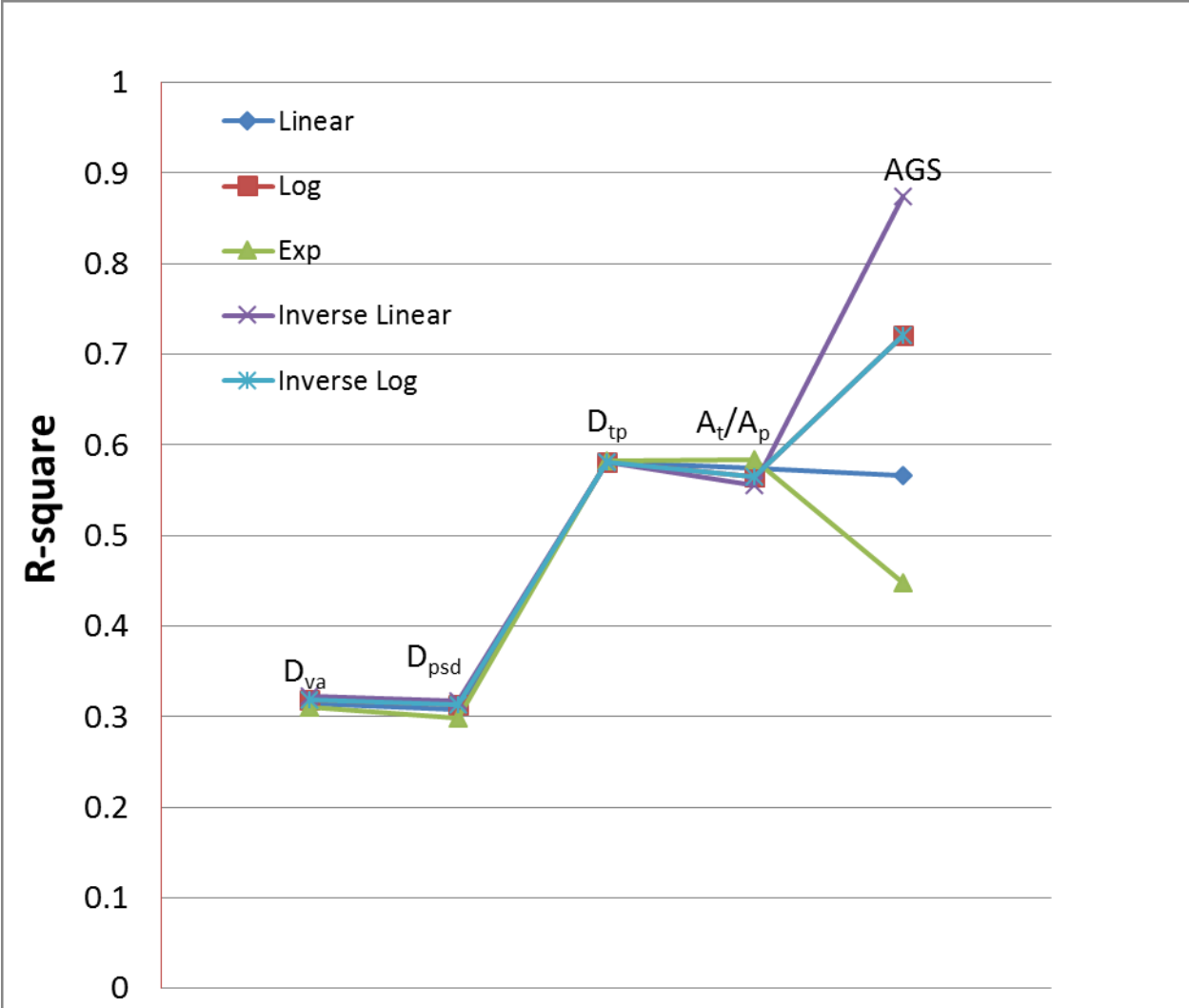


Figure A3—Testing different correlations between five variables and pressure drop for joint fracture cases for water.

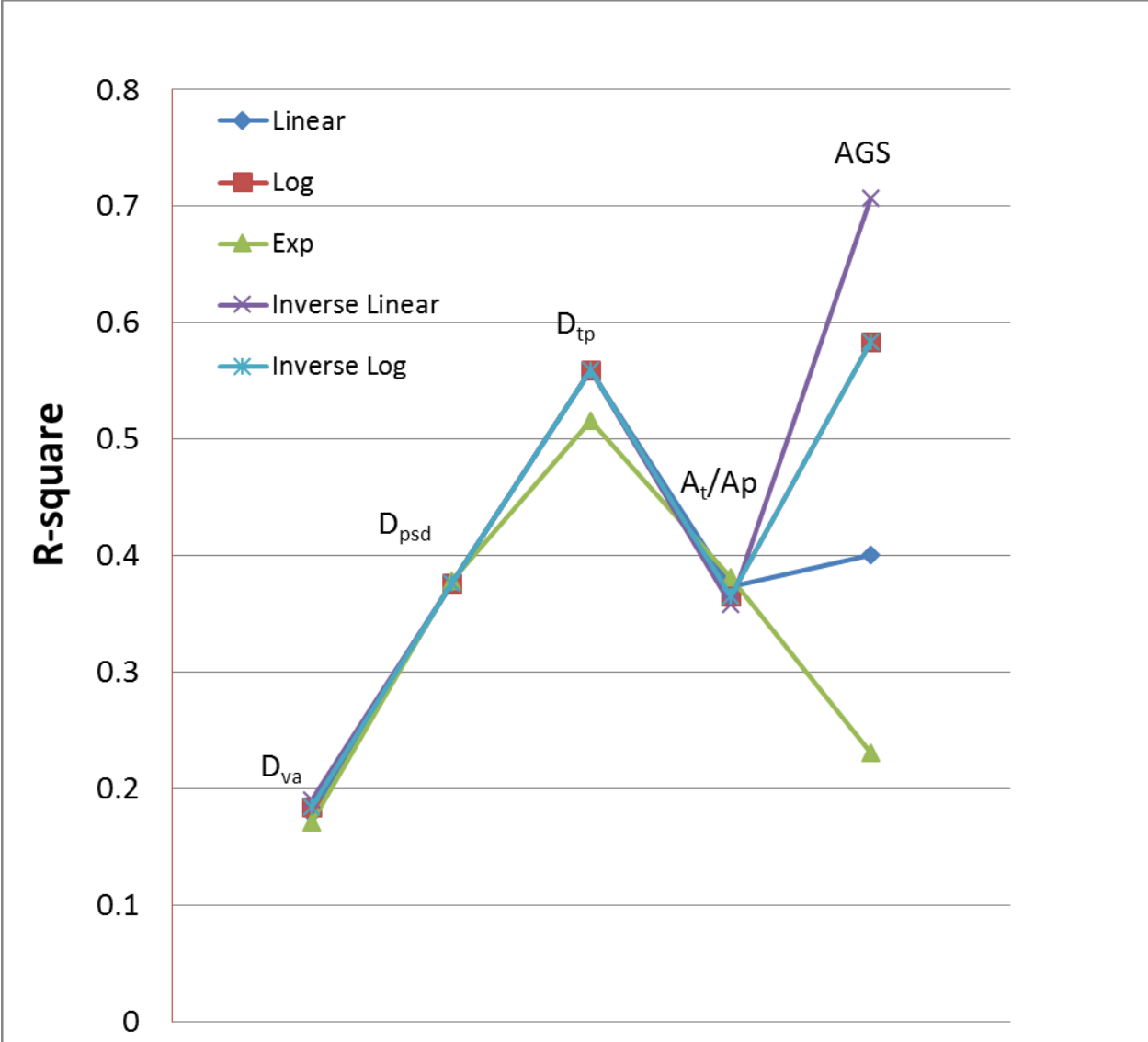


Figure A4—Testing different correlations between five variables and pressure drop for sheared fracture cases for water.

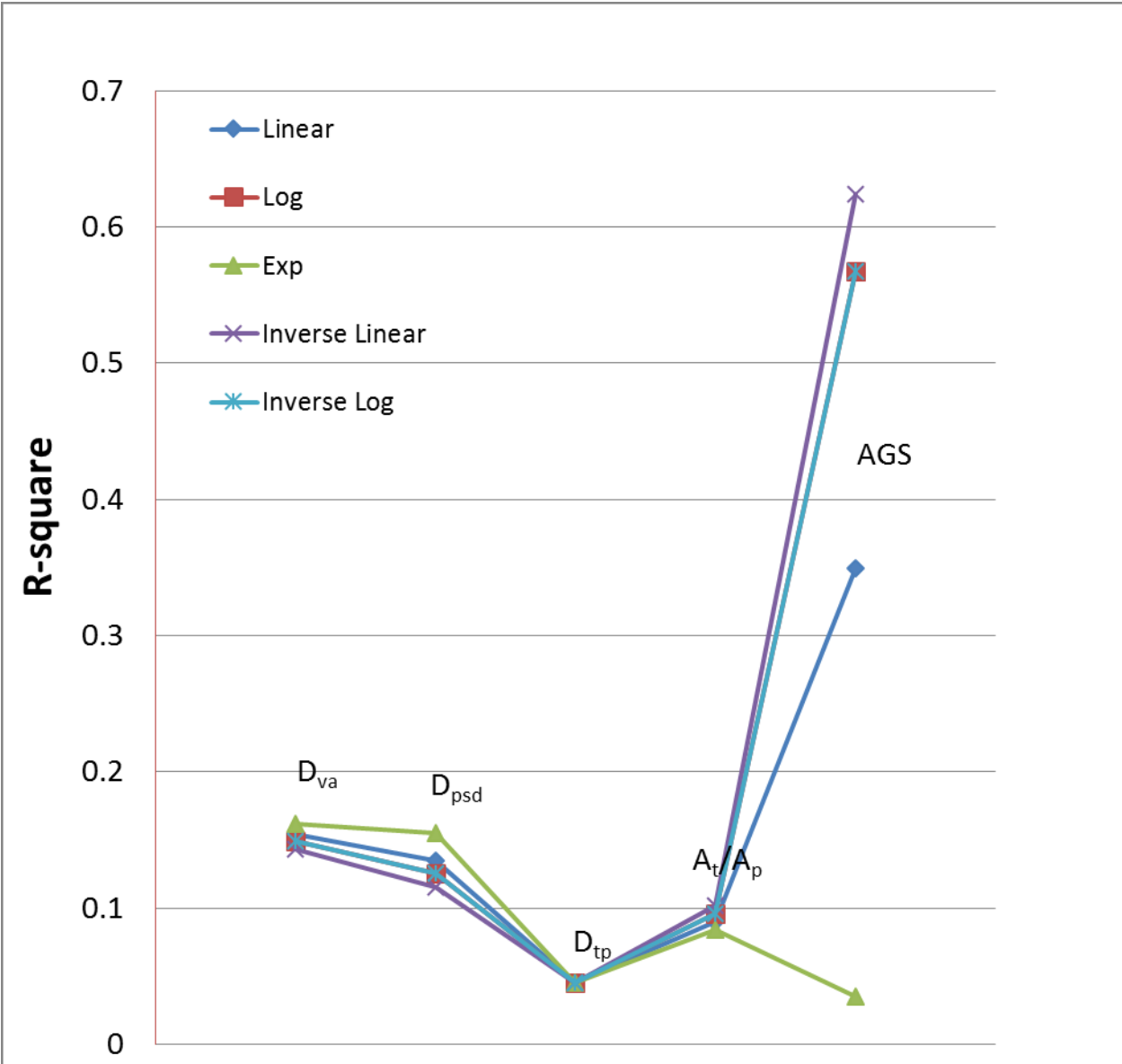


Figure A5—Testing different correlations between five variables and wetted area for joint fracture cases of polymer solution.

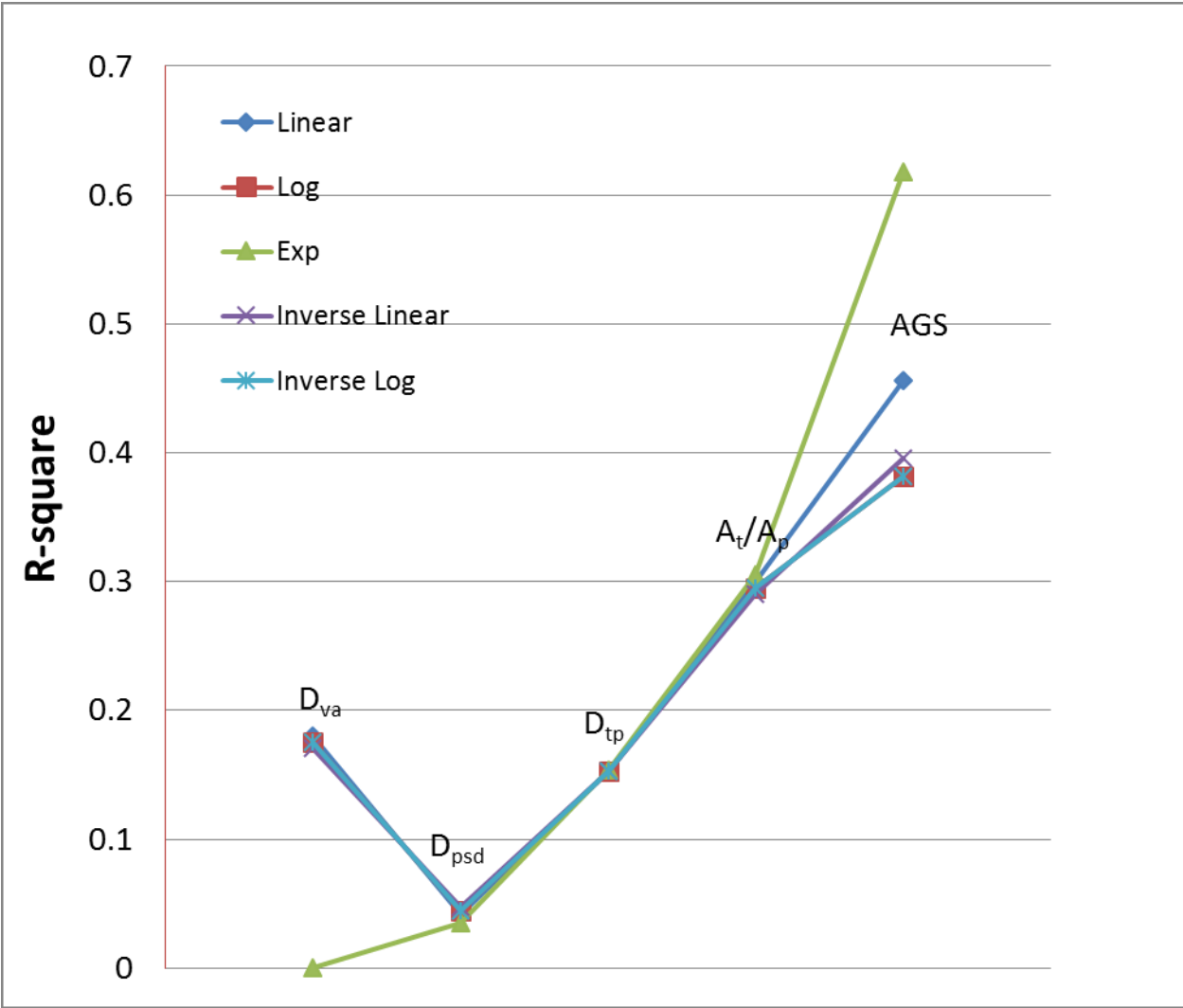


Figure A6—Testing different correlations between five variables and pressure drop for joint fracture cases of polymer solution.

Equation	Number of variables	Coefficients	R ²
$\%WA = a \frac{1}{D_{va}} + b e^{D_{psd}} + c \frac{1}{D_{tp}} + d \frac{1}{\frac{A_t}{A_p}} + e \frac{1}{AGS}$	5	a -417.34 b -4.89 c -285.15 d -53.30 e -2.72	0.99
$\%WA = a \frac{1}{D_{va}} + b \frac{1}{D_{tp}} + c \frac{1}{\frac{A_t}{A_p}} + d \frac{1}{AGS} + e$	4	a 351.18 b -9153.45 c -123.32 d -2.22 e 4250.98	0.74
$\%WA = a \frac{1}{D_{va}} + b \frac{1}{\frac{A_t}{A_p}} + c \frac{1}{AGS} + d$	3	a 337.57 b -52.61 c -1.85 d -136.10	0.73
$\%WA = a \frac{1}{D_{va}} + b \frac{1}{AGS} + c$	2	a 315.10 b -1.57 c -167.80	0.72
$\%WA = a \frac{1}{AGS} + b$	1	a -1.59 b 70.469	0.07
$\%WA = a \left(\frac{1}{D_{va}} \right) + b$	1	a -29.17 b 151.55	0.08

Table A1-Correlations obtained for wetted area – joint fracture cases for water.

Equation	Number of variables	Coefficients	R ²
$\%WA = ae^{D_{va}} + b \frac{1}{D_{psd}} + ce^{D_{tp}} + de^{\frac{A_t}{A_p}} + ee^{GR}$	5	a -88.31 b 379.42 c 25.28 d 14.98 e 0.93	0.93
$\%WA = ae^{D_{va}} + be^{D_{tp}} + ce^{\frac{A_t}{A_p}} + de^{AGS} + e$	4	a -48.26 b -2.60 c -2.75E-02 d -5.86E-04 e 268.06	0.69
$\%WA = ae^{D_{va}} + be^{D_{tp}} + ce^{AGS} + d$	3	a -48.26 b -2.74 c -5.56E-04 d 269.04	0.69
$\%WA = ae^{D_{va}} + be^{AGS} + c$	2	a -48.47 b 0.00 c 249.37	0.69
$\%WA = ae^{AGS} + b$	1	a 0.80 b 71.12	0.30
$\%WA = ae^{D_{va}} + b$	1	a -48.40 b 249.11	0.69

Table A2-Correlations obtained for wetted area – sheared fracture cases for water.

Equation	Number of variables	Coefficients	R ²
$D = a \frac{1}{D_{va}} + b \frac{1}{D_{psd}} + ce^{D_{tp}} + de^{\frac{A_t}{A_p}} + e \frac{1}{AGS}$	5	a -0.14 b 0.22 c -3.94E-03 d 2.62E-02 e 7.97E-03	0.91
$PD = a \frac{1}{D_{va}} + be^{D_{tp}} + ce^{\frac{A_t}{A_p}} + d \frac{1}{AGS} + e$	4	a -0.20 b -0.43 c 9.38E-02 d 8.75E-03 e 3.08	0.88
$PD = ae^{D_{tp}} + be^{\frac{A_t}{A_p}} + c \frac{1}{AGS} + d$	3	a -0.27 b 0.10 c 8.21E-03 d 1.78	0.82
$PD = ae^{\frac{A_t}{A_p}} + b \frac{1}{AGS} + c$	2	a 5.56E-02 b 8.07E-03 c -0.13	0.82
$PD = a \frac{1}{AGS} + b$	1	a 9.23E-03 b 3.22E-02	0.76
$PD = a \left(\frac{1}{D_{va}} \right) + b$	1	a -0.24 b 0.23	0.10

Table A3-Correlations obtained for pressure drop – joint fracture cases for water.

Equation	Number of variables	Coefficients	R ²
$PD = a \frac{1}{D_{va}} + be^{D_{psd}} + cD_{tp} + de^{\frac{A_t}{AP}} + e \frac{1}{AGS}$	5	a 417.28 b -4.90 c -123.25 d 19.06 e -2.73	0.99
$PD = ae^{D_{psd}} + bD_{tp} + ce^{\frac{A_t}{AP}} + d \frac{1}{AGS} + e$	4	a -6.179 b 14.84 c -0.32 d 4.49E-03 e -28.75	0.99
$PD = aD_{tp} + be^{\frac{A_t}{AP}} + c \frac{1}{AGS} + d$	3	a 18.59 b -0.39 c 4.83E-03 d -36.14	0.84
$PD = aD_{tp} + b \frac{1}{AGS} + c$	2	a 2.46 b 5.88E-03 c -4.91	0.57
$PD = a \frac{1}{AGS} + b$	1	a 7.29E-03 b 1.76E-02	0.50
$PD = a \ln(D_{va}) + b$	1	a 7.63E-02 b -6.36E-02	0.03

Table A4-Correlations obtained for pressure drop – sheared fracture cases for water.

Equation	Number of variables	Coefficients	R ²
$\%WA = ae^{Dva} + be^{Dpsd} + ce^{Dtp} + d \frac{1}{\frac{A_t}{A_p}} + e \ln AGS$	5	a -24.72 b -1.87 c 40.49 d -121.19 e 5.16	0.76
$\%WA = ae^{Dva} + be^{Dpsd} + c \frac{1}{\frac{A_t}{A_p}} + d \ln^{AGS} + e$	4	a -25.11 b -1.94 c -149.40 d 5.16 e 329.76	0.78
$\%WA = ae^{Dva} + be^{Dpsd} + c \ln^{AGS} + d$	3	a -13.66 b -1.98 c 3.92 d 150.25	0.54
$\%WA = ae^{Dva} + b \ln^{AGS} + c$	2	a -9.41 b 3.50 c 113.24	0.40
$\%WA = a \ln^{AGS} + b$	1	a 3.17 b 77.88	0.32
$\%WA = ae^{Dva} + b$	1	a -5.31 b 97.10	0.03

Table A5—Correlations obtained for wetted area - joint fracture cases with polymer solution.

Equation	Number of variables	Coefficients		R ²
$PD = ae^{D_{va}} + b \frac{1}{D_{psd}} + ce^{D_{tp}} + de^{\frac{A_t}{A_p}} + ee^{AGS}$	5	a	0.13	0.50
		b	-0.56	
		c	-3.87E-03	
		d	9.59E-02	
		e	-7.77E-03	
$PD = ae^{D_{va}} + be^{D_{tp}} + ce^{\frac{A_t}{A_p}} + de^{AGS+e}$	4	a	7.34E-02	0.66
		b	-6.10	
		c	1.17	
		d	-5.88E-03	
		e	42.20	
$PD = ae^{D_{va}} + be^{\frac{A_t}{A_p}} + ce^{AGS} + d$	3	a	8.06E-02	0.48
		b	0.11	
		c	-6.63E-03	
		d	-0.15	
$PD = ae^{\frac{A_t}{A_p}} + be^{AGS} + c$	2	a	0.20	0.46
		b	-5.33E-03	
		c	-9.98E-02	
$PD = ae^{AGS} + b$	1	a	-5.41E-03	0.38
		b	0.49	
$PD = ae^{D_{va}} + b$	1	a	-6.65E-02	0.03
		b	0.71	

Table A6—Correlations obtained for pressure drop - joint fracture cases with polymer solution.

CHAPTER 4: QUANTITATIVE AND VISUAL ANALYSIS OF PROPPANT TRANSPORT IN ROUGH FRACTURES AND APERTURE STABILITY

This paper is a modified and improved version of SPE 173385, which was presented at the SPE Hydraulic Fracturing Technology Conference held in Woodlands, Texas, USA, 3-5 February 2015. A version of this chapter has been submitted to the journal for publication.

Preface

The consensus reached in the literature is that the roughness of fractures plays a crucial role on proppant transport affecting the aperture sustainability and conductivity of hydraulic fractures. To clarify this, an experimental scheme and analysis are presented in this paper. Propping agents were introduced into seven different transparent fracture replicas obtained from different origin rock samples (granite, marble, and limestone) at a high rate mimicking hydraulic fracturing process conditions. The inlet pressure was continuously monitored to quantify the permeability changes due to proppant distribution. Corresponding images were collected to trace the transport of proppants and their behavior was correlated to the measured permeability change. Experiments were repeated on joint (perfectly mating) and horizontally displaced (sheared-unmating) models using water and polymer solution.

Existing closure areas controlled by roughness dictated proppant movement and permeability change significantly in both joint and displaced type fractures. To quantify this effect, fracture permeability and proppant distribution (area saturated with sands) were correlated to three fractal methods (variogram, power spectral density, and triangular prism) and the ratio of total and planar fracture surface areas. Correlation types differ for water and polymer solution. Joint and displaced type fractures also showed differences in permeability change and sand distribution for certain type of rocks, especially at the higher variogram fractal dimensions. It was also observed that the grain size of the rock as a roughness parameter controls the distribution of the sands.

1. Introduction

A highly permeable flow path is the primary goal of hydrocarbon recovery through hydraulic fracturing, which strictly depends on the transport and distribution of proppant injected with the fracking fluid (Coulter et al. 2004; Terracina et al. 2010; Kassis and Sondergeld 2010; Ribeiro and Sharma 2012, 2013). The transportation of proppants is controlled by aperture distribution, which is formed as the result of rough surfaces (Fredd et al. 2000), and closures that could develop due to fracture -shear- displacement (van Dam and de Pater 1999).

Traditionally, fluid flow in fracture networks is represented by fluid flow in a single rock fracture, which is based on the assumption of two parallel (smooth) plates and described by cubic law (Gangi 1978; Kranz et al. 1979; Tsang and Whitherspoon 1983). Similarly, studies on the mechanics of proppant transport and fracturing design treatments were conducted using the parallel plate model (Babcock et al. 1967; Raymond and Binder 1967; Novotny 1977; Penny 1987). Real rock fractures, however, have a rough surface with variable apertures and asperities that control the tortuosity of fluid path. This type of flow medium may result in deviations from cubic law (Brown 1987; Renshaw 1995). Also, Tsang (1984) showed that the flat surface models might result in much higher flow rates than obtained in rough-walled fracture models.

Shear displacement coupled with surface roughness could cause a decrease in the contact areas yielding significant changes in fracture permeability (Yeo et al. 1998; Lee and Cho 2001; Auradou et al. 2006; Koyama et al. 2007; Nemoto et al. 2008; Watanabe et al. 2008). In this case, the permeability of rough-walled rock fractures may reduce with applied vertical stress (Bernabe 1986; van Dam, 1999; He et al. 2013). The degree of the change in fracture permeability in the presence of proppants should also be clarified considering fracture roughness with applied horizontal and/or vertical stresses. Visual support is especially needed to clarify the roughness effect on proppant transport. In recent attempts, single (Develi and Babadagli 2015) and multiphase (Babadagli et al. 2015a-b) flow in transparent replicas of fractures obtained from different types of rocks were analyzed visually and quantitatively using different fractal roughness parameters. Using the same models, Raimbay et al. (2015) studied the effects of roughness on the conductivity of fractures at hydraulic fracturing conditions.

The objective of this study is to provide a fundamental understanding of the transportation of propping agents in a single fracture obtained from different rock samples (granite, marble, limestone) and to represent different degrees of roughness. To achieve this, transparent replicas of original rock fractures were prepared and proppant distribution and its effect on fracture permeability was investigated visually and quantitatively for joint and sheared fractures in comparison with flat models. Proppants (natural sands) were injected with water and Xanthan Gum at a concentration of 0.1 lbm/gal. The inlet pressure was continuously monitored in order to analyze the stability of the aperture. The change in the permeability due to roughness was quantitatively described with visual supports for fractures of different lithologies. Using the inlet pressure and images acquired, fracture permeability and proppant distribution (area saturated with sands) were correlated to three fractal methods (variogram, power spectral density, and triangular prism) and the ratio of total and planar fracture surface areas. Correlation types differ for water and polymer solution.

2. Experimental Methodology

Different rock samples such as granite, marble, and limestone of 20x20x20 cm were fractured under indirect tensile tests (similar to the Brazilian test). The fractures created were then replicated using silicone rubber and transparent plastic through a series of casting and molding processes. Thus, model fractures of 20x20x5 cm in size were reproduced from the originals (**Fig. 1**). The solid transparent plastic upper parts of the models were facilitated to achieve flow visualization. The bottom parts were non-transparent silicone rubber. The detailed preparation procedure of fracture models can be found in Develi and Babadagli (2015). Two types of fractures were tested: (1) perfectly mating joint and (2) sheared (slightly displacing the top part of the models) fractures. Fracture surface roughness was digitized and then quantified through fractal dimension measurements of the surface data by variogram (D_{va}), power spectral density (D_{psd}), and triangular prism analyses (D_{tp}) as defined in Develi and Babadagli (1998, 2015). The ratio between total and planar fracture surface areas (A_t/A_p) was used as another roughness indicator. The estimated values of fractal dimensions and areal ratios are given in **Table 1**.

The schematic diagram of experimental set-up is shown in **Figure 2**, which contains a model

holder, progressive cavity pump, pressure transducer, and a camera. The model holder represents a base where one of the single fracture models was placed and sealed. The fluid with propping agent was injected through an attached 500 ml reservoir in order to uniformly introduce it into the model and create a 2-D displacement. The reservoir was connected to progressive cavity pump where the fluid and proppants were blended by mixer at the top of pump and introduced together into the reservoir. In the line between the reservoir and pump, a pressure transducer was attached in order to continuously measure the pressure drop. This continuous monitoring of pressure drop was achieved through a data acquisition system. At the same time, pictures were taken to correlate proppant distribution with pressure change. To be able to distinguish the fluid and solid (proppant) phases, a fluorescent dye was added to fluid injected and a UV light was used to make the dyed fluid visible.

Experiments were carried out by injecting water and polymer solution (Xanthan Gum, XG) with propping agents into joint and shear displaced fractures placed horizontally. XG was prepared at a concentration of 0.03% (W/W). As a propping agent, natural sand in a size range of 300-400 μm was used at a concentration of 0.1 lbm/gal. 5 mm shear displacement was provided in unmatting experiments. A mixer was used continuously to blend the sand with the fluid in a tank, which was installed at the top of the pump to avoid settlement of sand particles.

In all experiments, pressure drop was measured while fluid with proppant was injected at a constant flow rate. A constant “aperture” was applied in all cases using a spacer with a size of 3mm. All models have the same length, therefore, the cross-sectional area can be assumed to be the same. Then, the pressure at the given rate can be used to estimate the permeability according to the Darcy’s law:

$$k * A = \frac{\mu * L * q}{\Delta P} \quad (1)$$

Through the images obtained during experiments, the area saturated with sand particles was measured in all models. All images were scaled to the same number of pixels and processed to binary images. **Figure 3** shows the images of two fracture models extracted from the original photos given in **Figure 4**. Areas with settled sand were distinguished and measured from areas

saturated with fluid and dry areas using ImageJ program (Rasband 1997-2005). Later, percentage of embedded sand area was calculated for water and XG in joint and sheared models using the following equation:

$$SSA(\%) = \frac{\text{Sand saturated area}}{\text{Total area}} \times 100 \quad (2)$$

Fracture model	Rock type	D _{va}	D _{psd}	D _{tp}	A _t /A _p
FR. 1	Beige limestone with abundant coarse fossil shells	1.373	2.277	2.012	1.145
FR. 2	Micritic, pink, semi re- crystallized limestone	1.263	2.558	2.007	1.079
FR. 3	Microfossiliferous pisolitic beige limestone	1.303	2.266	2.007	1.061
FR. 4s	Coarse grained white marble	1.39	2.418	2.009	1.098
FR. 5	Amphibole granite	1.299	2.335	2.008	1.083
FR. 6	Micritic cemented, beige limestone with abundant fossils	1.29	2.3	2.010	1.115
FR. 7	Medium-coarse grained white marble	1.326	2.321	2.006	1.072
Flat	-	1	2	2	-

Table 1— Lithology of the rock samples and the roughness parameters for the surfaces of model fractures.

D: fractal dimension; Subscripts – va: variogram analysis, psd: power spectral density, tp: triangular prism; A_t/A_p: ratio of total and planar fracture surface areas.

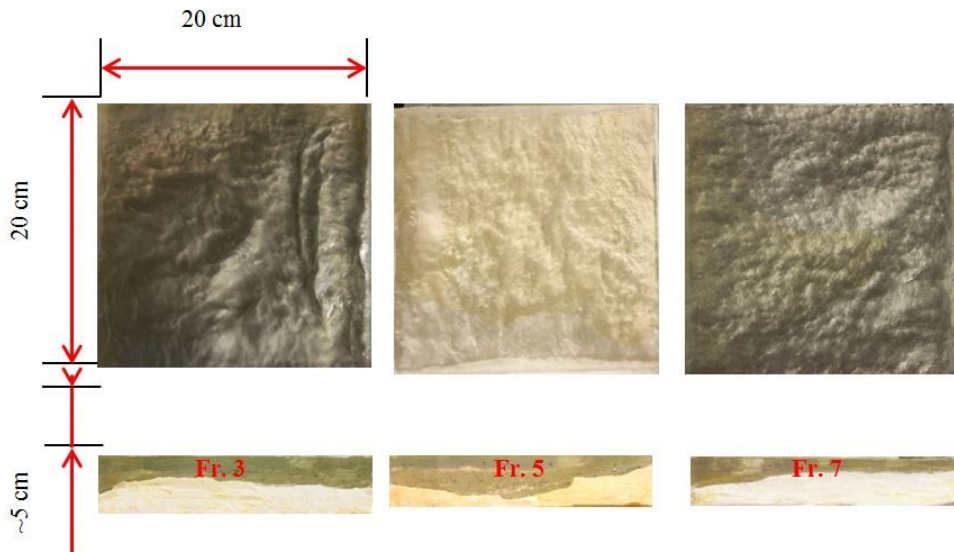


Figure 1—Top and side views of fracture models

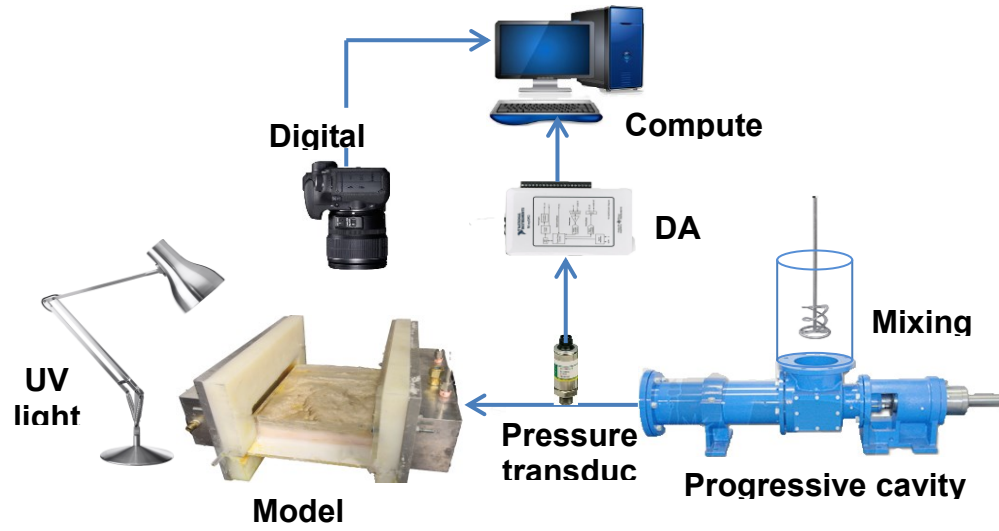


Figure 2—Schematic of experimental set-up.

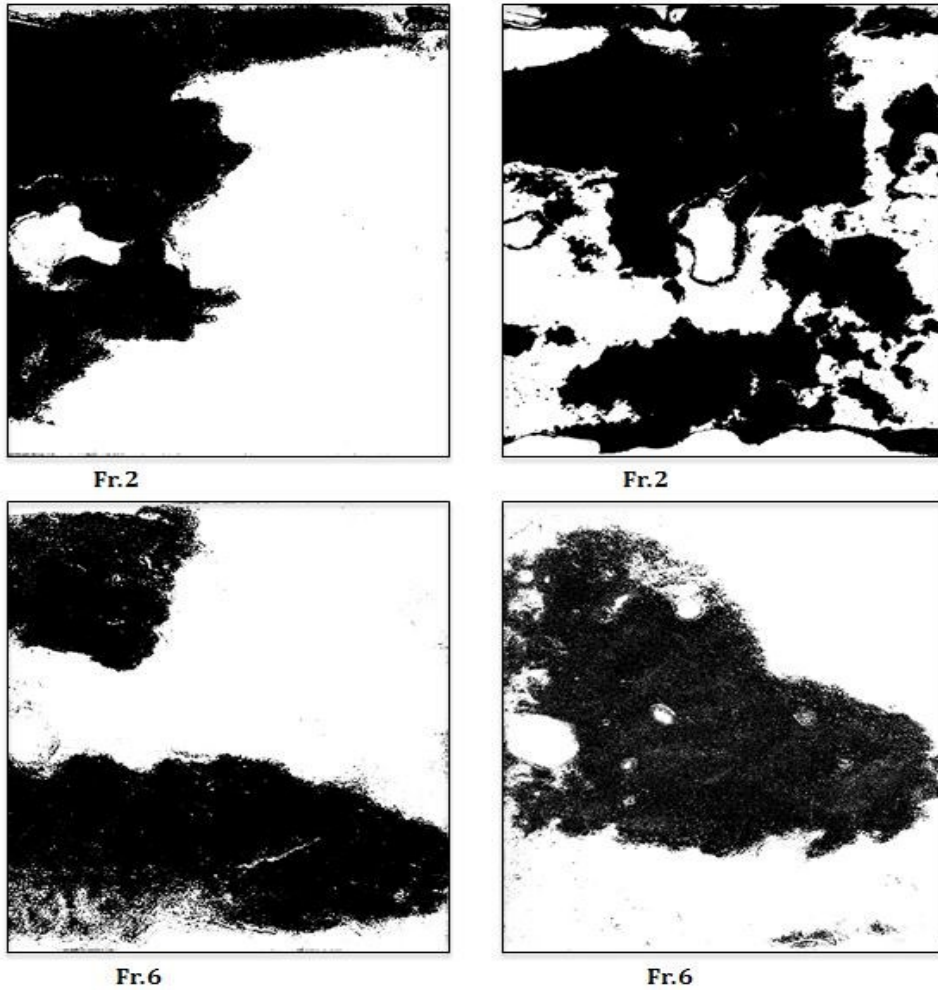


Figure 3—Images of embedded sand particles (black: sands - white: dry and injected fluid saturated areas); Xanthan Gum solution.

3. Results and Discussion

Experiments were conducted using water and polymer solutions (Xanthan Gum, XG) and two modes of fractures (joint and horizontally displaced-sheared). In each case, three fractal dimensions—i.e., variogram (D_{va}), power spectral density (D_{psd}), and triangular prism (D_{tp}) and the ratio between total and planar fracture surface areas (A_t/A_p) were correlated to pressure drop and sand saturated areas.

3.1 Effect of Fluid Type on Proppant Transportation Ability

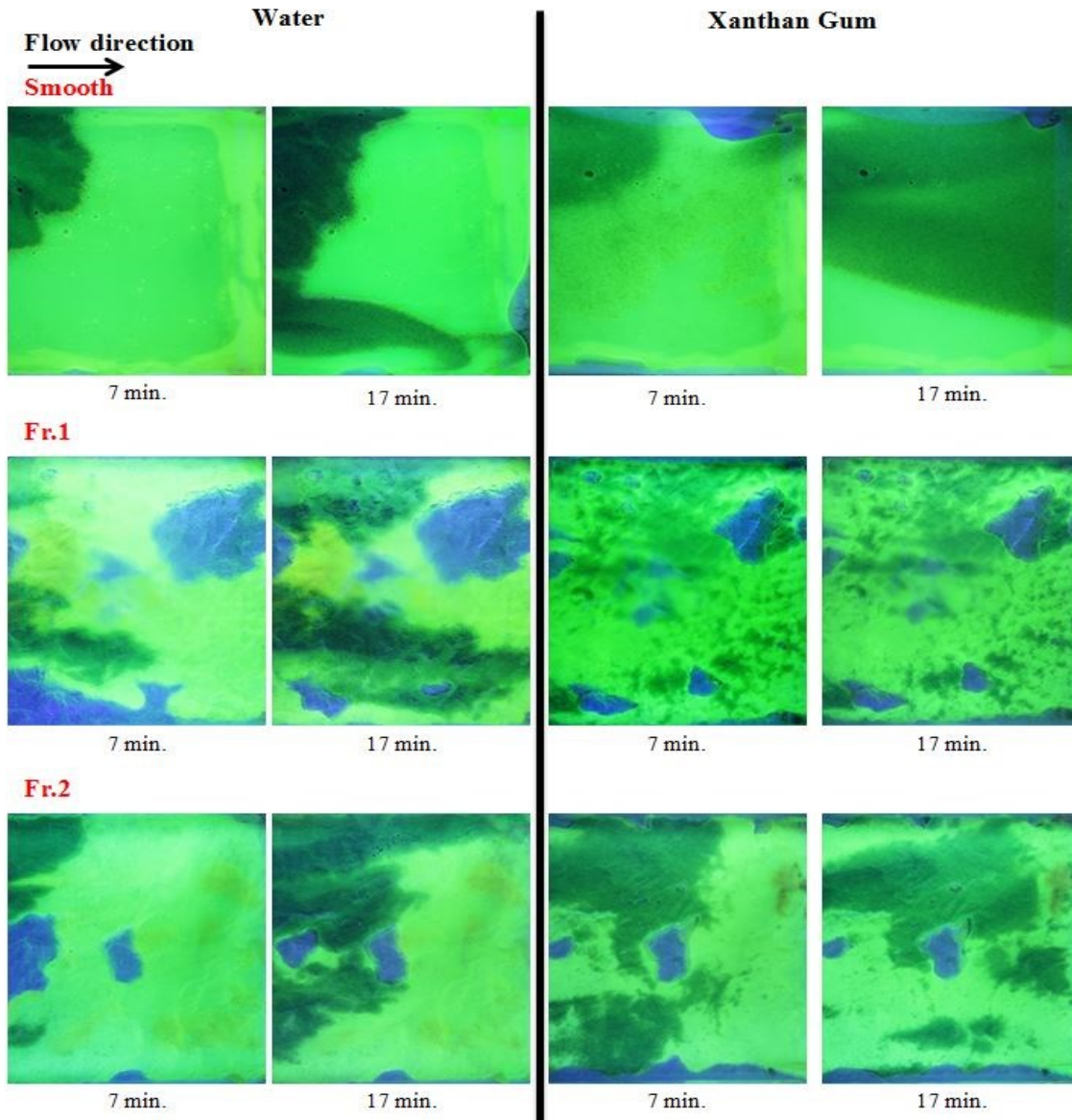
Water + propping agent. Propping agents with water were injected at a constant flow rate (1.3 l/min) with continuous recording of pressure drop along the fracture models while taking corresponding pictures. **Figure 4** shows proppant distribution in the smooth fracture and rough fracture models where blue areas are closures (non-conductive medium), green areas are fracking fluid, and black areas are proppants (sand particles). As can be observed, the distribution of propping agents (black areas) was variable based on the roughness characteristics of rocks. In all fracture models, sand did not reach the end of the fracture and settled along the fracture due to poor transportation of water.

The intensity of the black areas in the smooth fracture model indicates that the sand particles formed packed multilayer at the inlet of the model, while in the rough fracture models, sand particles formed a partial monolayer. Roughness affected not only the permeability but also controlled the distribution of proppants remarkably. Meanwhile, the smooth fracture model showed lower hydraulic conductivity due to intensive packing of propping agents. The best proppant transportation and thereby the accumulation of proppants, which is needed to sustain the permeability, was optimally achieved for the limestone samples (Fr. 1, Fr. 2, and Fr. 3).

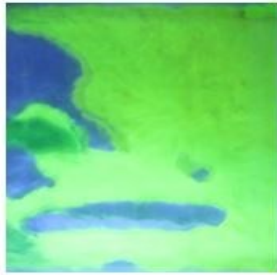
The poorest sand transportation (and distribution) was observed in granite (Fr. 5) and marble (Fr. 7) where proppant progressed through a single channel. Sample Fr.4s also yielded a good sand distribution but they were made of different materials; i.e., both sides were solid transparent unlike the others with the bottom parts made of non-transparent rubber.

Figure 5 shows the pressure drops recorded during the water+proppant experiments. The stabilization point was quickly reached in all cases and the rough-walled fractures yielded higher

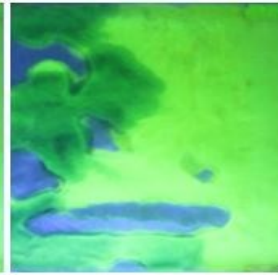
conductivities than the smooth fracture model. Similar observations were also reported by Briggs et al. (2014). Granite (Fr.5) had the lowest conductivity and, hence, resulted in the highest pressure drop among all seven rough rock models. The models were ranked from the lowest to the highest permeability as follows: Fr. 1, Fr. 7, Fr. 6, Fr. 2, Fr. 3, and Fr.4s.



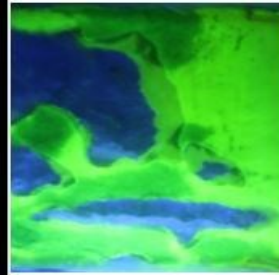
Fr.3



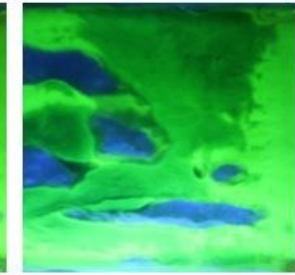
7 min.



17 min.

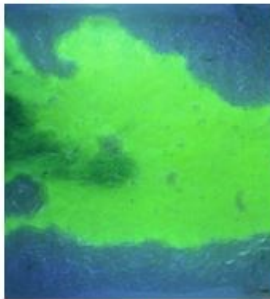


7 min.

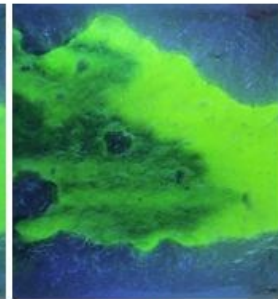


17 min.

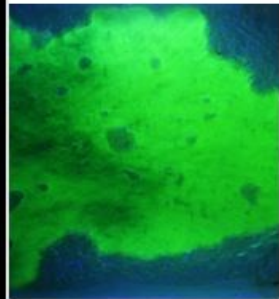
Fr.4s



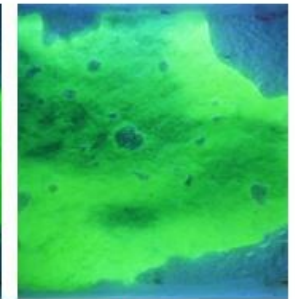
7 min.



17 min.



7 min.



17 min.

Fr.5



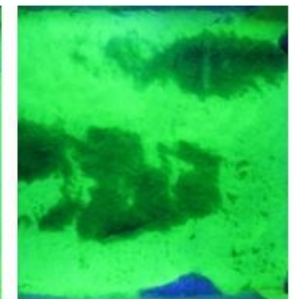
7 min.



17 min.



7 min.

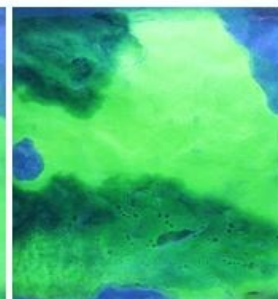


17 min.

Fr.6



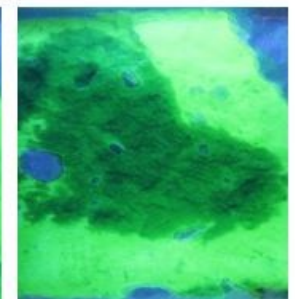
7 min.



17 min.



7 min.



17 min.

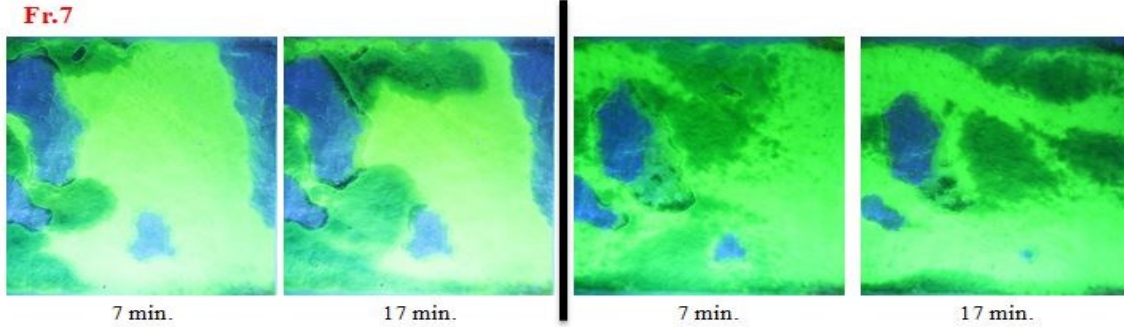


Figure 4—Planar view of water and polymer (Xanthan Gum) solution flow in joint-type (mating) fractured models given in Table 1. Blue areas correspond to air, yellow is dyed water/polymer solution, and black is embedded sand.

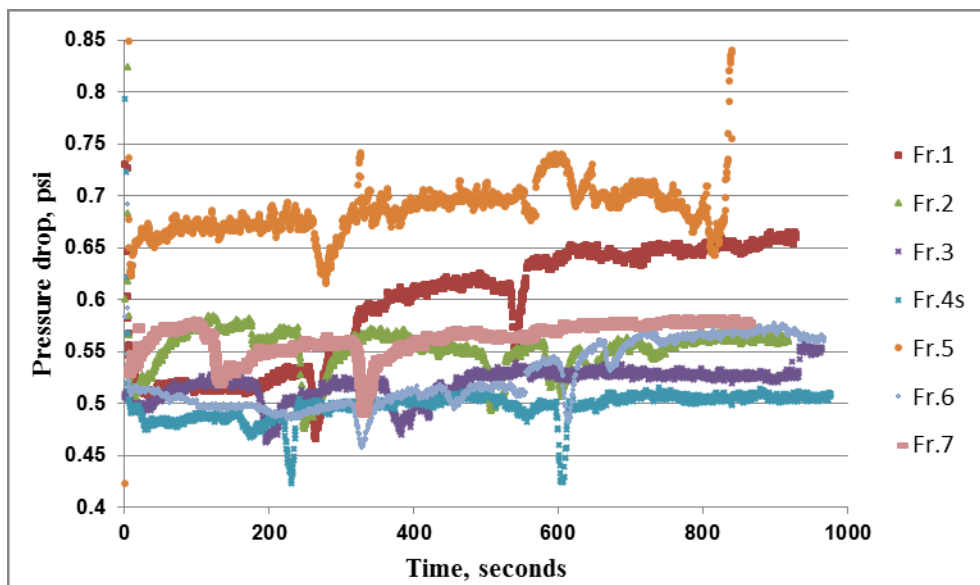
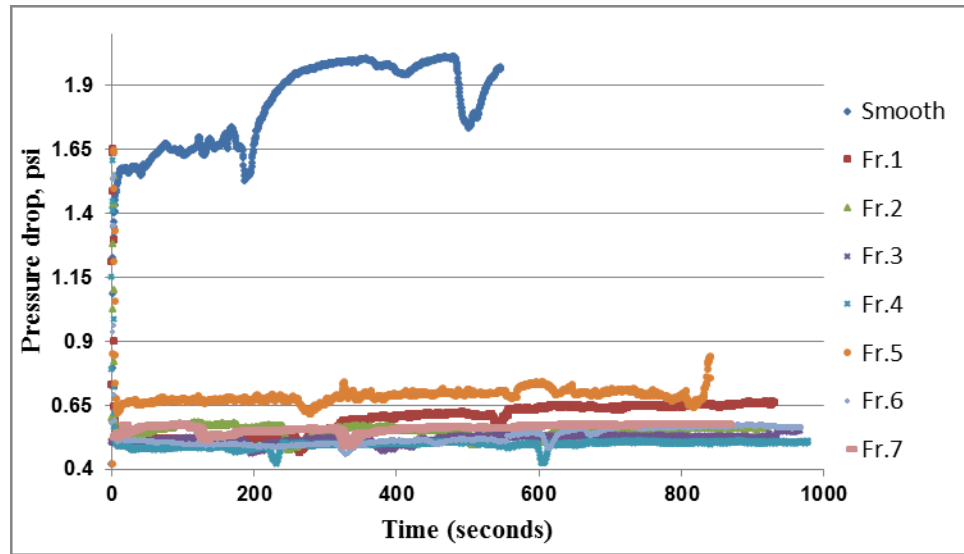


Figure 5—Pressure drop while proppants transported by water in the samples listed in Table 1 and a flat (smooth) fracture. Upper graph shows all these samples and the smooth samples case is excluded in the bottom graph for a better view of pressure drops in rough fractures.

Xanthan Gum + propping agent. A polymer solution prepared by a 0.03% (W/W) Xanthan Gum addition to water was mixed with sand and injected into the joint fractures. In all experiments with the polymer fluids, the injection rate was the same as the one used for water experiments (i.e., 1.3 l/min). In comparison to sand injection with water (left images in Fig. 4), closure (unwetted) areas (i.e., area where there was no through sand transport) decreased significantly when sand was injected with polymer as shown in (right images in Fig. 4). With increased viscosity of fracturing fluid, the fracture aperture increased, leading to the diminishing of the closure areas (blue areas). The amount of propping agents transported with polymer fluid in all fracture models was several orders of magnitude higher than the transported with water. In addition, proppants were transported all the way to the end of the fractures and distributed more uniformly. In rough fracture models, the proppant distribution was also controlled by the roughness characteristics of the rock, similar to the sand transport with water. However, proppants were distributed more uniformly when transported by polymer fluid than with water.

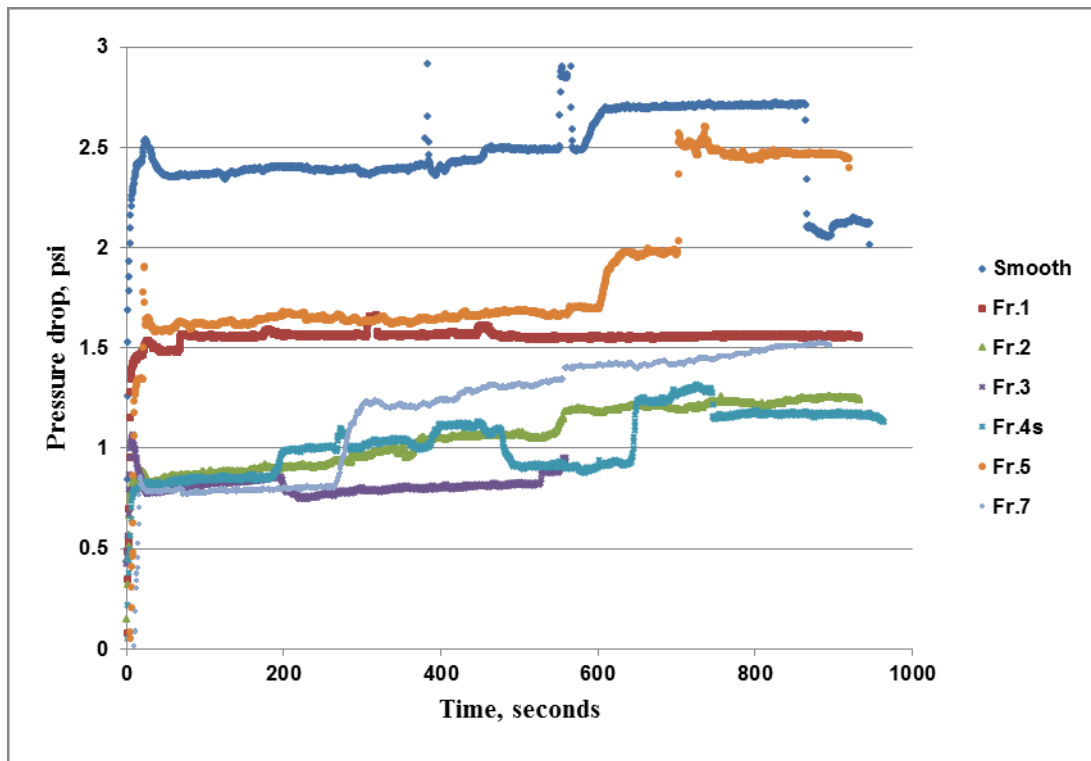
Generally, one may conclude that polymer solution have much better sand transport ability than water. Similar observations were also reported by Boyer et al. (2014). Increasing viscosity of the polymer solution results in more sand suspended in the solution while, at the same time, more drag forces are exerted on the sand particles with flow. Both mechanisms are expected to contribute to effective sand transport along the fractures.

Unlike the sand transport with water, continuous transport of propping agents in rough fracture models were observed with polymer fluid, especially in marble and granite cases. When sand was transported by polymer solution, one of the most uniform sand distribution cases was obtained in granite (Fr. 5). This is opposite to what we observed when the sand was transported by water. In one of the limestone cases (Fr. 3) where we saw the best transportation of proppant with water, the sand did not even reach the tip of the fracture model when it was transported by polymer fluid.

Increased transport and better distribution of sand, however, did not cause any significant change in permeability. As shown in **Figure 6**, higher pressure drop than water was observed in polymer flow, mainly because of the higher viscosity of polymer solution. But the trends are the same; i.e., the lowest hydraulic conductivity was obtained for the smooth fracture model and then

granite (Fr. 5) and a limestone sample (Fr. 1) etc. Although sand did not reach the tip of the limestone fracture model, placed proppants were not washed away and created a stable fracture aperture in limestones (Fr. 1, Fr. 2, Fr. 3) (Fig. 4).

In conclusion, although the polymer solution distributed the sands better than water, it generally followed a similar displacement pattern (Fig. 4) and, thereby, similar trends of permeability change to the water case (Fig. 6). This means that the smooth model showed the lowest permeability (highest pressure drop) and the rough samples were ranked from the lowest to the highest permeability as Fr. 5, Fr. 1, Fr. 7, Fr. 2, Fr. 4s, Fr. 3, which is very similar to the water case. Note that model Fr. 6 was not included in this analysis due to experimental failure.



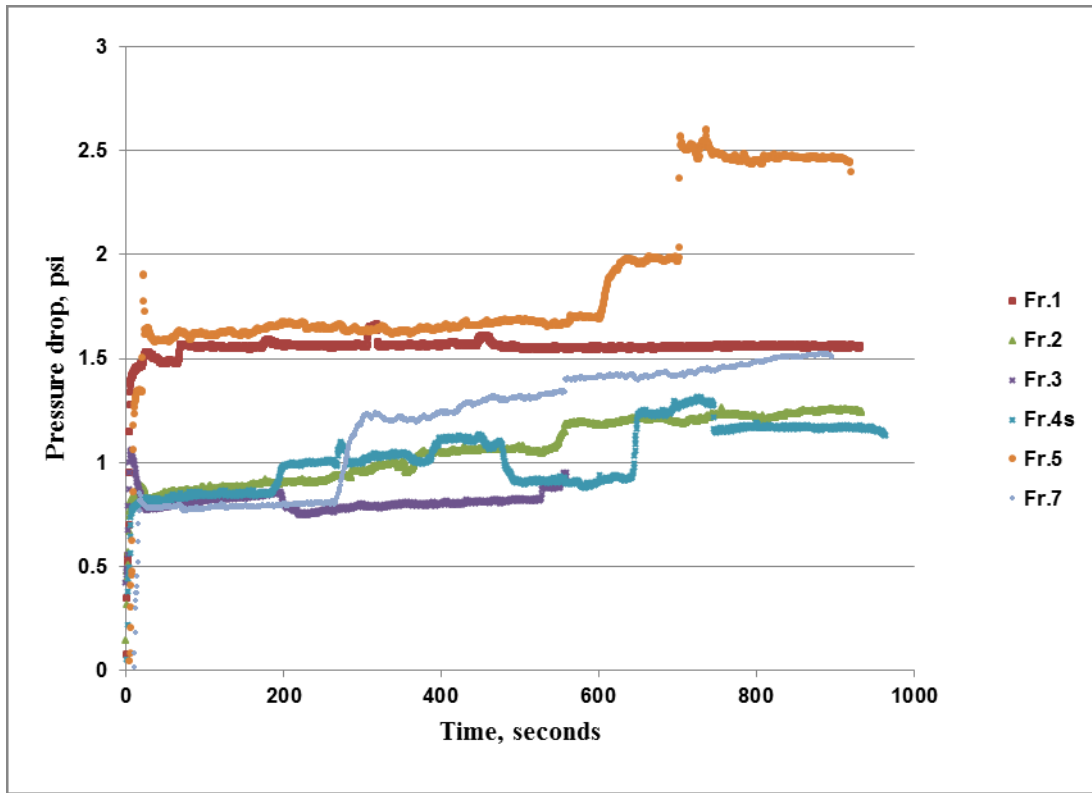


Figure 6—Pressure drop while proppants transported by Xanthan Gum solution in rough fracture models and a flat (smooth) model. Upper graph shows all the samples and the smooth samples case is excluded in the bottom graph for a better view of pressure drops in rough fractures.

3.2 Quantitative Analysis

The data given in Figures 4-6 were used for a quantitative analysis and the pressure drops (**Fig. 7**) and area saturated with sand were plotted against (**Fig. 8**) D_{va} , D_{psd} , D_{tp} and A_t/A_p . Typical trends are illustrated by dotted lines and different symbols are used to indicate the samples falling into different trends. Although the pressure drop values were much higher in case of the polymer solution, both proppant carrying fluids resulted in a similar pressure drop behavior. The (D_{va}) plots showed two groupings: (1) smoother fractures and three limestones with lower D_{va} , and (2) rougher fractures, typically marbles and granite, and the roughest sample of all, Fr. 1. Increasing D_{va} showed lower pressure drop characteristically for both fluids (Figs. 7a and 7b). Interestingly, the trend changes in a “cut-off” point of D_{va} at ~ 1.3 . The same value was also reported in Raimbay et al. (2014 and 2015) for the pressure drop cases for water/polymer solution flow with and without sands. Note that in their case, the sands were not directly injected with the fluids but already placed into the model before the injection of the fluid phase (water or polymer solution) was started.

The behavior was a bit more erratic when pressure drop was plotted against D_{psd} (Figs. 7c and 7d). Different trends were observed but were not consistent with the behavior seen in the D_{va} plots. D_{tp} and A_t/A_p plots showed a similar behavior as they represent similar characteristics of fracture roughness (self-similarity). In both cases the granite sample (Fr. 5) showed an off-trend behavior. The trend of increasing pressure drop with increasing fractal dimension was clearer in the cases of polymer solution (Figs. 7f and 7h).

Areas saturated with sand showed different behavior for the water and polymer solution cases. Specifically, when $D_{va} > 1.3$, increasing fractal dimension yielded increasing and decreasing sand filled areas for water (Fig. 8a) and polymer solutions (Fig. 8b), respectively. Similar to the pressure drop case, no characteristic trend was observed when the area saturated with sand was plotted against D_{psd} . Note that in both cases, Fr. 5 was off-trend.

D_{tp} and A_t/A_p plots showed a similar behavior (comparing Figs. 8e and 8f with Figs. 8g and 8h) but the trends were different for the water (Figs 8e and 8g) and polymer solution cases (Figs. 8f and 8h). As similar to the D_{va} cases given in Figures 8a and 8b, increasing fractal dimension yielded increasing and decreasing sand areas for water (Fig. 8a) and polymer solutions (Fig. 8b), respectively. Fr. 5 was off-trend in both D_{tp} and A_t/A_p cases for water (Figs. 8e and 8g, respectively).

Overall, D_{va} , D_{tp} and A_t/A_p can be used to estimate the sand distribution and permeability correlations. Combination of these three roughness parameters can be implemented in mathematical derivations as they represent different characteristics of fracture surface roughness; i.e., D_{va} (self-affinity) and D_{tp} and A_t/A_p (self-similarity).

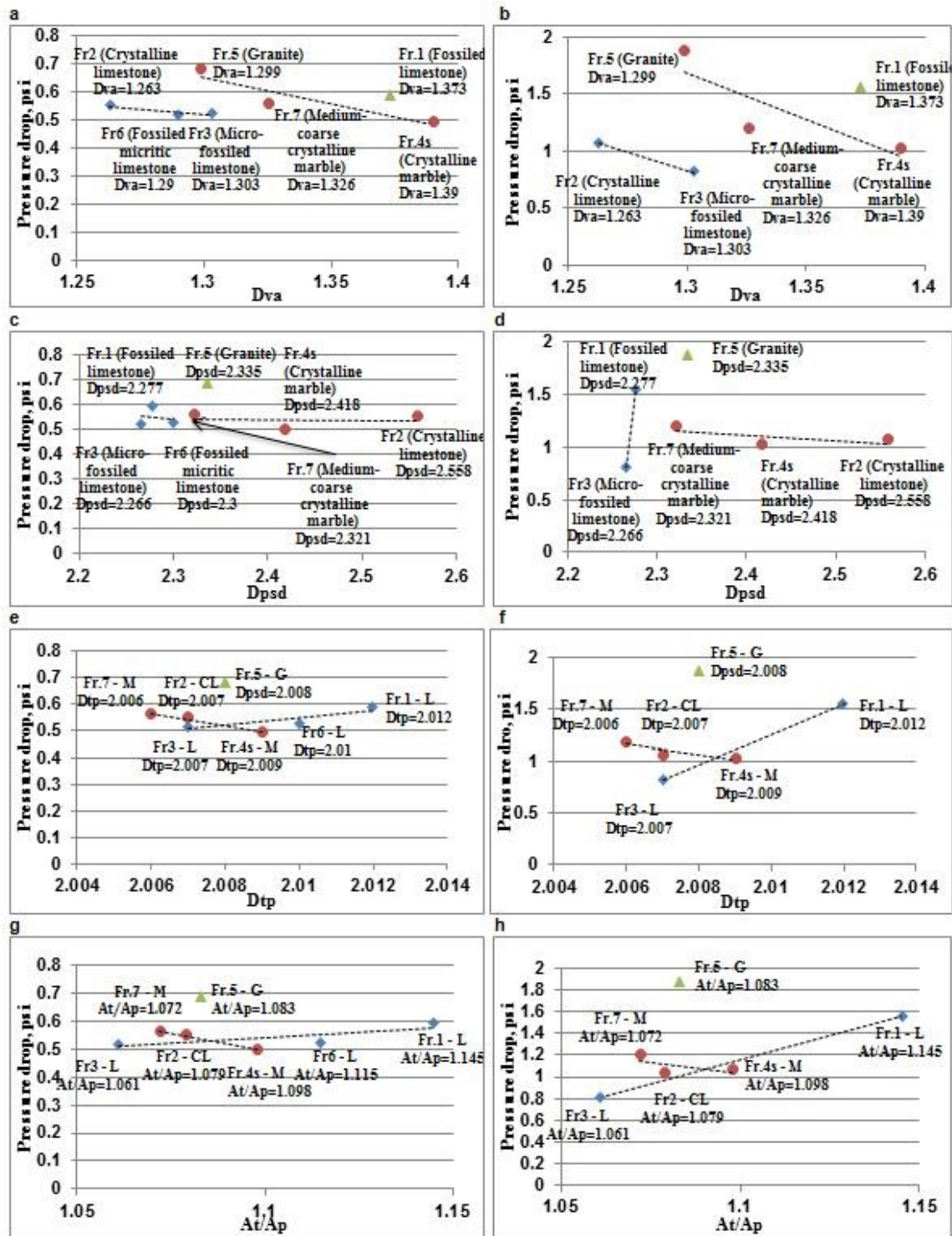


Figure 7—Pressure drops (permeability) correlated to different roughness parameters (variogram analysis, power spectral density and triangular prism fractal dimensions, and ratio of total fracture surface area to planar area) for seven fracture models. Fluid injected: Water (left column) and XG solution (right column). Fracture type: Joint.

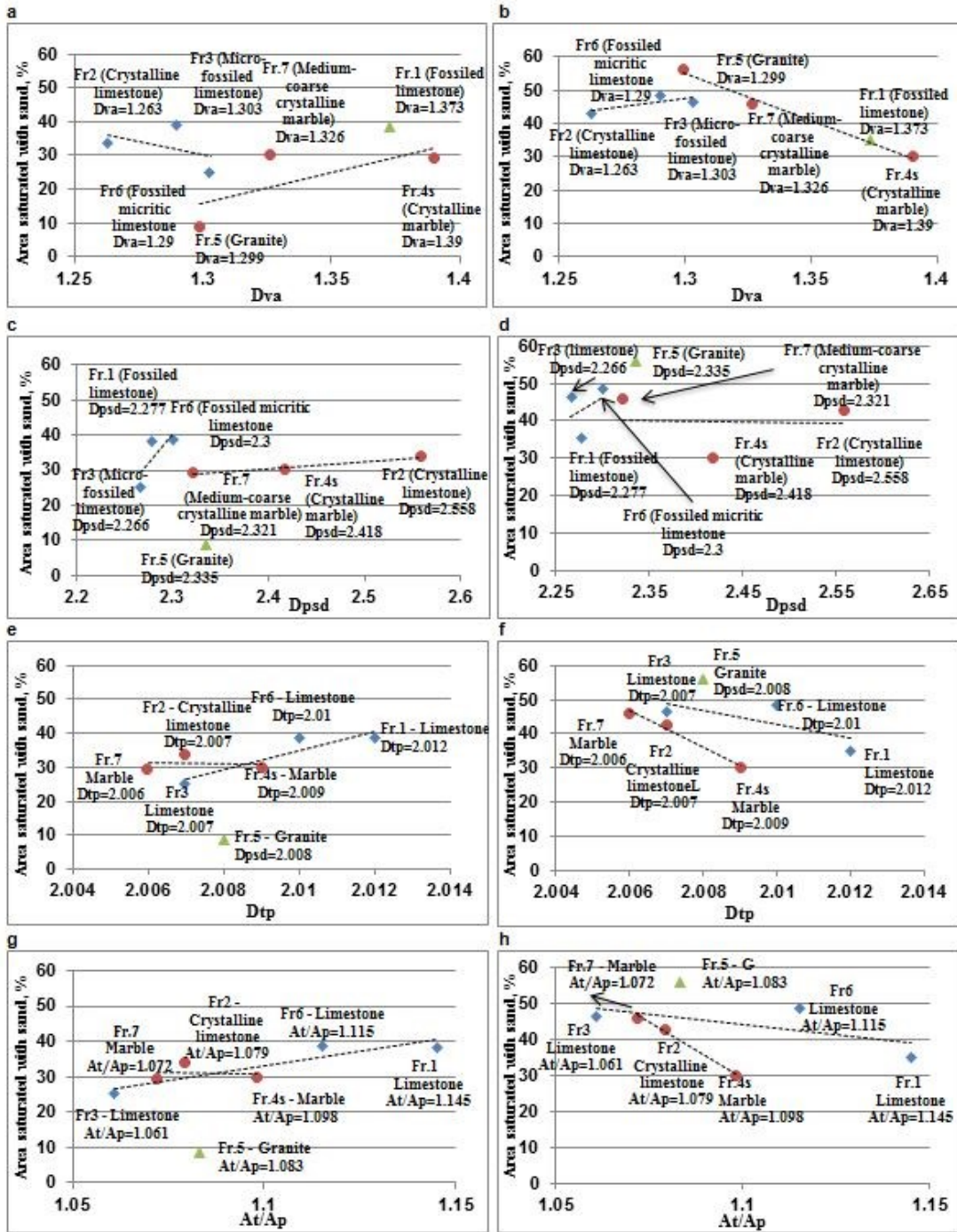


Figure 8—Wetted areas correlated to different roughness parameters (variogram analysis, power spectral density and triangular prism fractal dimensions, and ratio of total fracture surface area to planar area) for seven fracture models. Fluid injected: Water (left column) and Xanthan Gum solution (right column). Fracture type: Joint.

3.3 Effect of Fracture Type (Joint and Horizontally Displaced - Sheared) on Proppant Transportation Ability.

A 5 mm displacement was applied horizontally to all models (sheared) and water and Xanthan

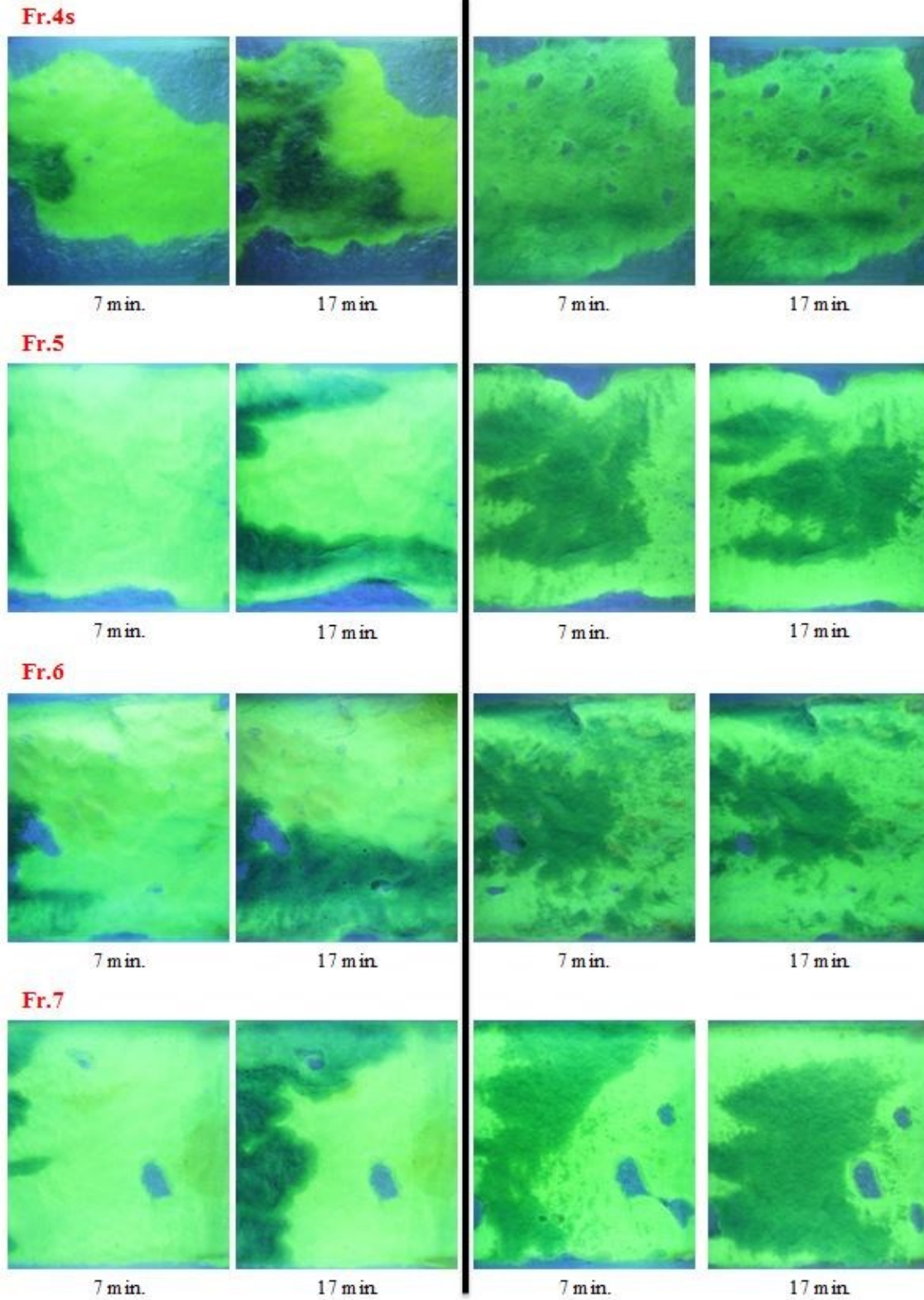
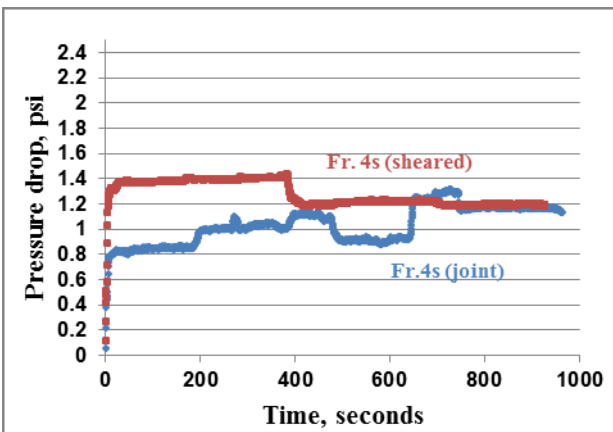
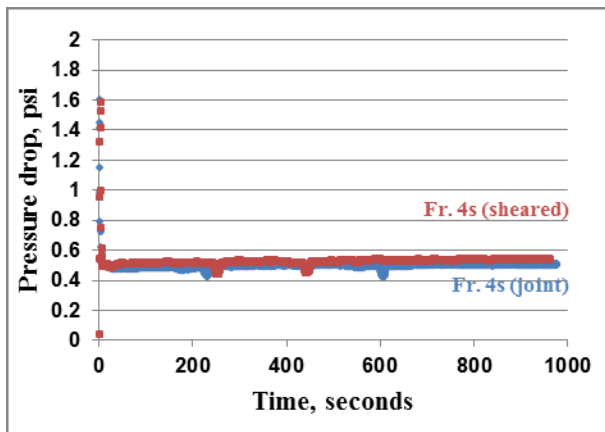
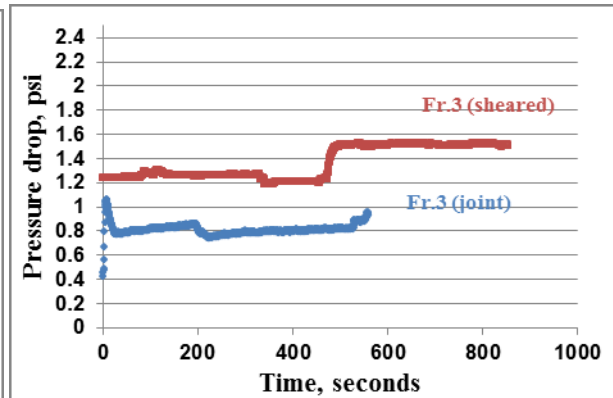
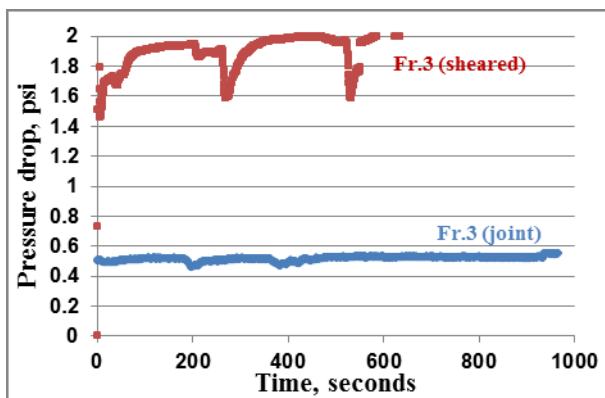
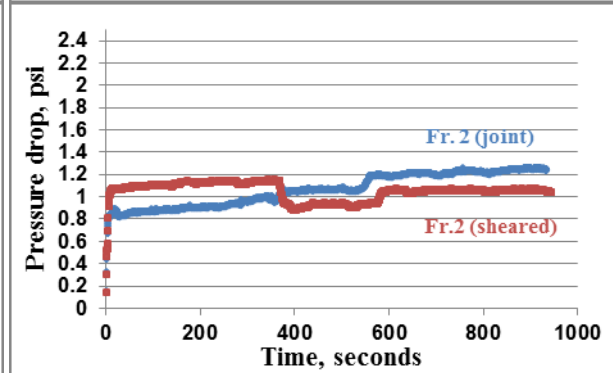
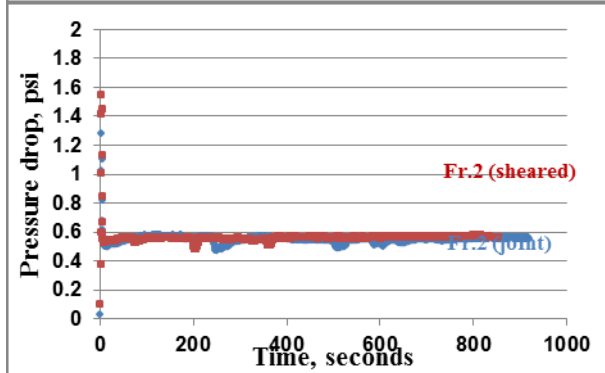
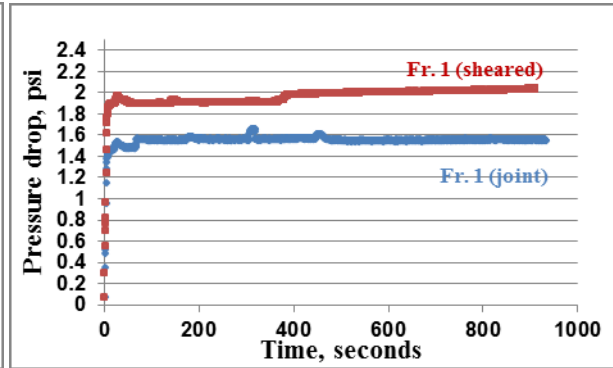
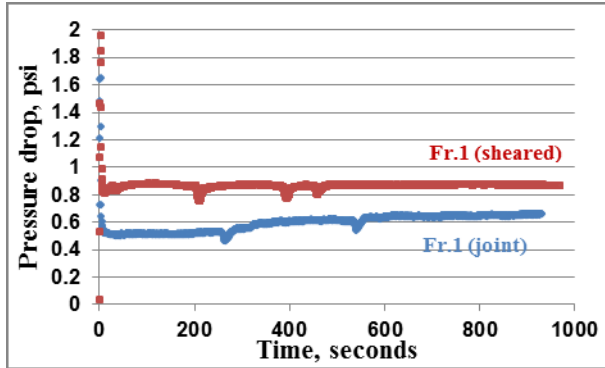


Figure 9—Planar view of water and polymer (Xanthan Gum) solution flow in horizontally displaced (sheared-unmating) fracture models. Blue areas correspond to air, yellow is dyed water/polymer solution, and black is embedded sand.



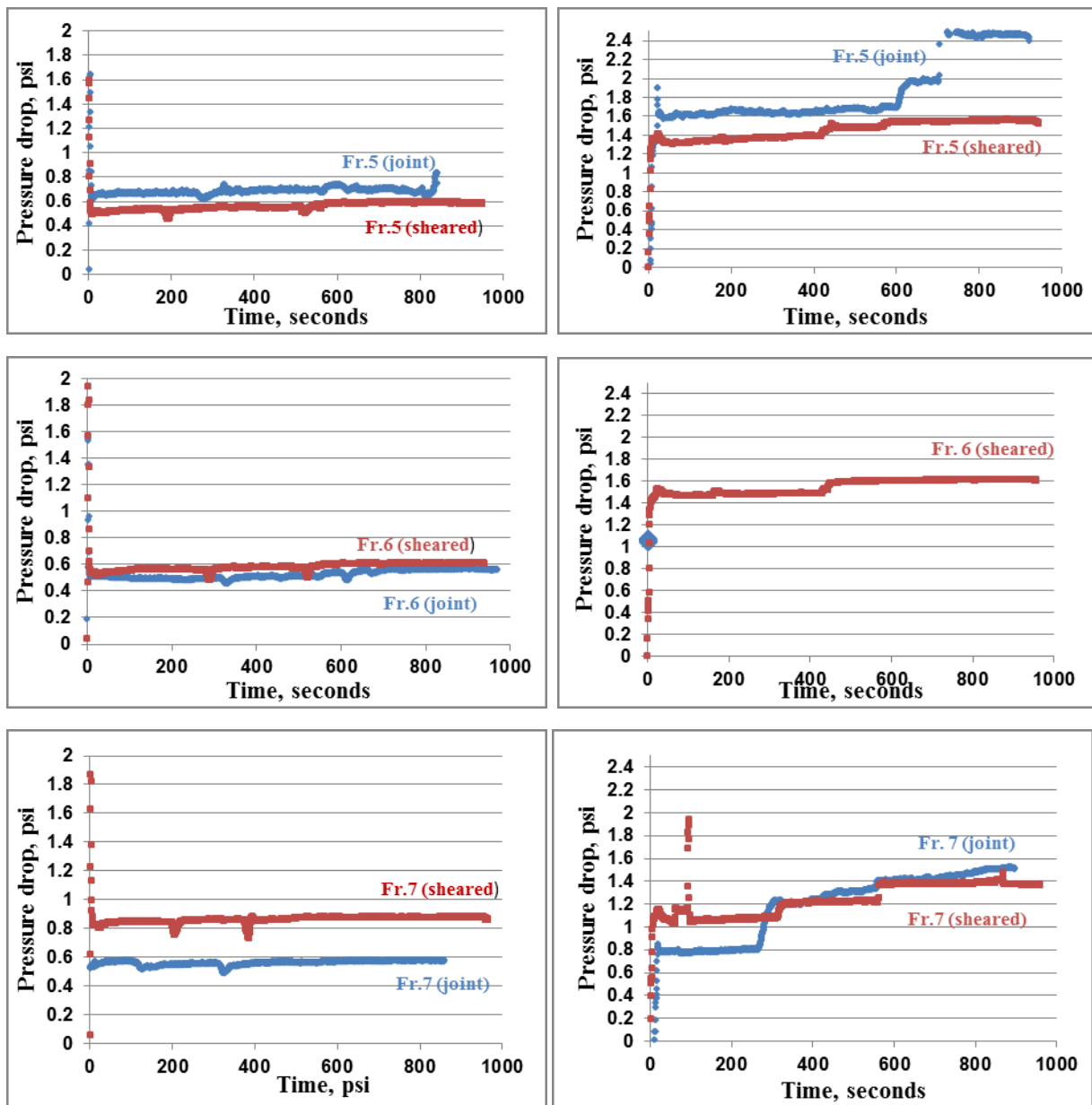


Figure 10—Pressure drop while proppants transported by water (left plots) and Xanthan Gum solution (right plots) on joint-type (mating) and sheared (horizontally displaced-unmating) fracture models. Only an initial value (indicated by a blue circle) of pressure was recorded for the polymer solution of the joint model of Fr. 6 due to mechanical failure.

In addition to visual analysis given above, a quantitative study was performed to distinguish the differences between the joint and sheared models. For this purpose, pressure drops of both cases were compared in Figure 10. Water and polymer solution showed similar differences in pressure drop (permeability) for the joint and sheared models for all cases. Interestingly, the pressure drop values for water and polymer solution were -numerically- close to each other unlike the

joint model cases. Typically, sheared models yielded higher pressure drop (decreased conductivity) except the Fr. 5 (granite) case. The difference is more critical in the cases of Fr. 1, Fr. 3, and Fr. 7. These samples possessed high D_{va} values representing severe roughness.

For a better understanding of the permeability change (or proppant distribution implicitly) with shearing and the effect of roughness on this, the pressure drop values after stabilization were plotted against the four roughness parameters (D_{va} , D_{psd} , D_{tp} and A_t/A_p) in **Figure 11**. The difference between the joint and sheared model became distinguishable after a threshold value of $D_{va} \approx 1.3$ for both water (Fig. 11a) and polymer solution cases (Fig. 11b). The difference was greater for the lower values of D_{psd} as seen in Figures 11c and 11d for both fluids, respectively. No clear trend was observed for the cases of D_{tp} and A_t/A_p (Figs. 11e through 11h). Hence, D_{va} and D_{psd} could be used to incorporate the shear effect on the permeability change in the computational models.

Similar plots were generated for the area saturated with sand (**Fig. 12**). No distinct correlations were observed for all four roughness parameters. In all water cases, sheared models typically yielded higher sand saturated areas (except Fr. 1, which was the roughest model with the highest D_{va} , D_{tp} and A_t/A_p). The differences between the joint and sheared models were quite systematic (left plots in Fig. 12). An opposite behavior was observed in the case of polymer solution (right plots in Fig. 12). With exception of one case (Fr. 4s, the model with both sides of solid transparent material), all joint models yielded larger areas of sand saturation.

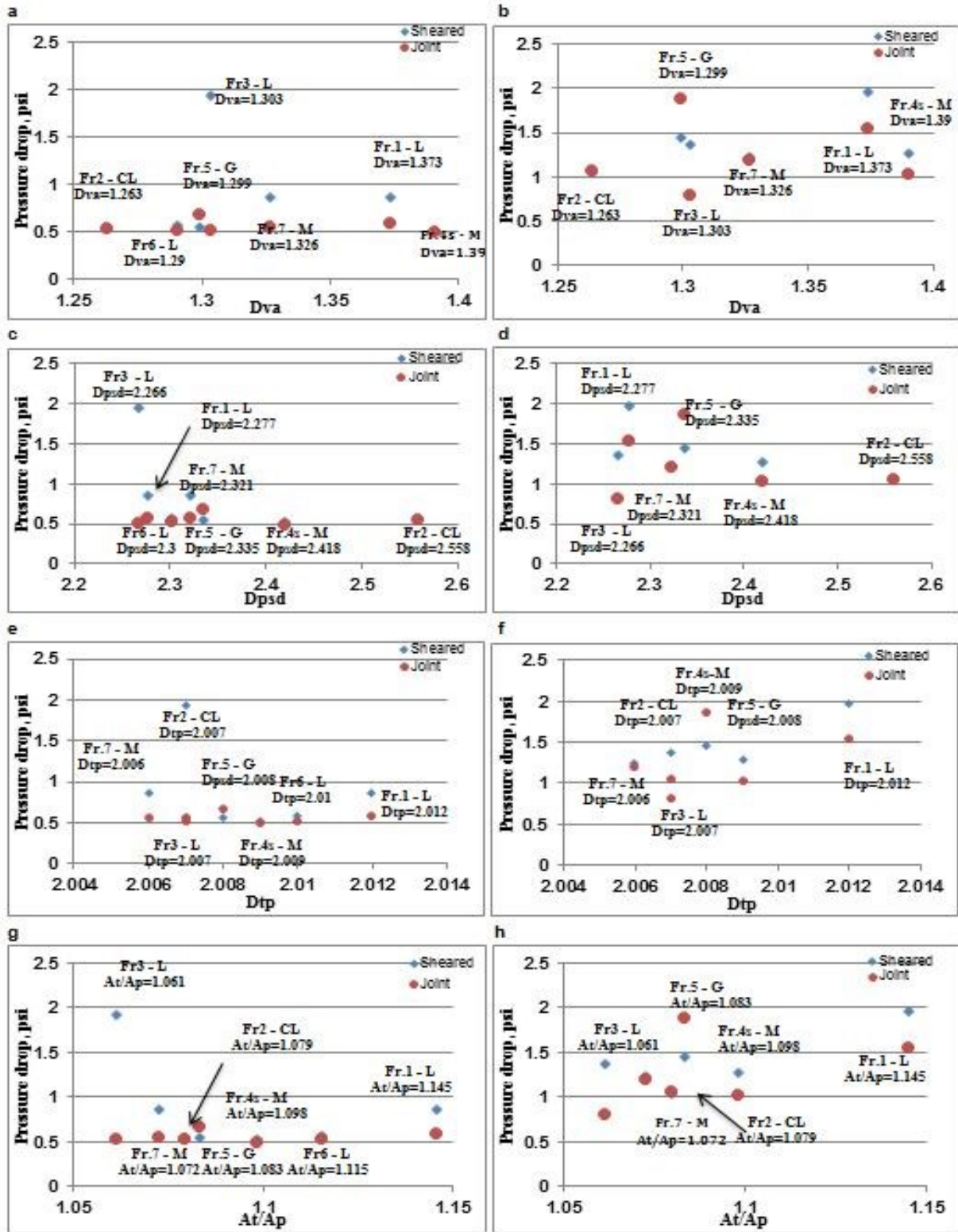


Figure 11—Pressure drop (permeability) correlated to different roughness parameters (variogram analysis, power spectral density and triangular prism fractal dimensions, and ratio of total fracture surface area to planar area) for seven fracture models. Fluid injected: water (left column) and XG (right column). Fracture type: Joint and Sheared. M: Marble, L: Limestone, G: Granite, CL: Crystallized Limestone.

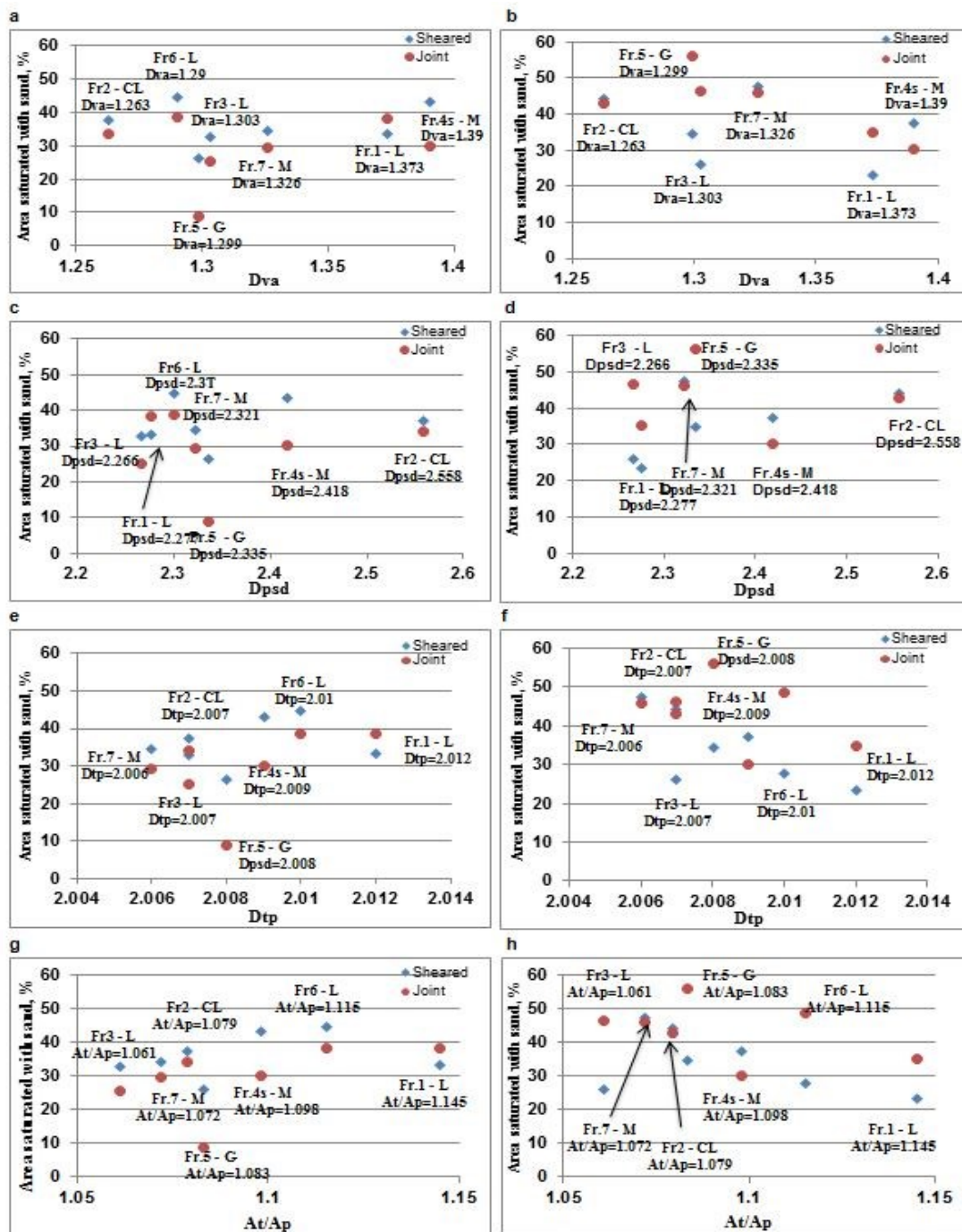


Figure 12—Wetted areas correlated to different roughness parameters (variogram analysis, power spectral density and triangular prism fractal dimensions, and ratio of total fracture surface area to planar area) for seven fracture models. Fluid injected: water (left column) and XG (right column). Fracture type: Joint and Sheared. M: Marble, L: Limestone, G: Granite, CL: Crystallized Limestone.

4. Conclusions

1. Effectiveness of proppant transport and distribution in fractures was found to be controlled by both roughness characteristics of the rock surface and transport ability of fracturing fluids. Also, in general, polymer fluid distributed the sand in fractures much better than water.
2. Sand transport and distribution efficiency in fractures showed some variability depending on the surface characteristics of the rocks. When injected with water, sands were transported and distributed better in limestones unless the roughness was large. When sands were injected with polymer, however, they were better transported and distributed in marble and granite.
3. Surface roughness not only controlled the flow path of fluid but also the placement stability of proppants. In smooth fracture model, sands distributed more uniformly and packed as multilayers. In rough fractures, however, sands distributed non-uniformly and formed a -partial- monolayer. Sand placed in fracture with polymer fluid was more stable in limestone than in marble and granite, i.e., proppants kept moving throughout the injection in marble and granite samples.
4. Smooth fracture model had a lower hydraulic conductivity than rough-walled fracture models. The sheared fracture case demonstrated a significant change in proppant distribution/accumulation and, thereby, hydraulic conductivity of fracture. This change was controlled by the roughness characteristics of fracture surfaces determined by lithology.
5. It was also found that D_{va} , D_{tp} , and A_t/A_p can be used to estimate the sand distribution and permeability correlations. Combination of these three roughness parameters can be implemented in mathematical derivations as they represent different characteristics of fracture surface roughness; i.e., self-affinity (D_{va}) and self-similarity (D_{tp} and A_t/A_p). D_{va} and D_{psd} can be used to incorporate the effect of shear on the permeability change in the computational models.
6. No distinct correlations were observed between the four roughness parameters and area saturated with sand. In all water cases, sheared models typically yielded higher sand saturated areas (except Fr. 1; the roughest model with the highest D_{va} , D_{tp} and A_t/A_p) and

the differences between the joint and sheared models were quite systematic. An opposite behavior was observed in the case of polymer solution (except in the Fr. 4s case -the model with both sides of solid transparent material), all joint models yielded larger areas of sand saturation.

Acknowledgments

This research was conducted under the second author's (TB) NSERC Industrial Research Chair in Unconventional Oil Recovery (industrial partners are CNRL, SUNCOR, Petrobank (Touchstone Exp.), Sherritt Oil, APEX Eng., PEMEX, Statoil, Saudi Aramco and Husky Energy), the Helmholtz Alberta Initiative (HAI) project funded by the Alberta Government. The first author (AR) is thankful to JCS "Center for International Programs," funded by the government of the Republic of Kazakhstan for the MSc scholarship granted. The fourth author (KD) thanks the Scientific and Technological Research Council of Turkey (TÜBİTAK) for his postdoctoral scholarship through the BİDEP program. We gratefully acknowledge these supports.

References

- Auradou, H., Drazer, G., Boschan, A. et al. 2006. Flow Channeling in a Single Fracture Induced by Shear Displacement. *Geothermics* **35**: 579-588. <http://doi:10.1016/j.geothermics.2006.11.004>.
- Babadagli, T., Raza, S., Ren, X. et al. 2015a. Effect of Surface Roughness and Lithology on the Water-Gas and Water-Oil Relative Permeability Ratios of Oil-Wet Single Fractures. *Int. J. of Multiphase Flow* **75**: 68-81.
- Babadagli, T., Ren, X. and Develi, K. 2015b. Effects of Fractal Surface Roughness and lithology on Single and Multiphase Flow in a Single Fracture: An Experimental Investigation. *Int. J. of Multiphase Flow* **68**: 40-58.
- Babcock, R.E., Prokop, C.L., and Kehle, R.O. 1967. Distribution of Propping Agents in Vertical Fractures. University of Arkansas. API-67-207.
- Bernabe, Y. 1986. The Effective Pressure Law for Permeability in Chelmsford Granite and Barre Granite. *Int. J. Rock Mech. Min. Sci. & Geomech. Abstr.* **23** (3): 267-275.
- Boyer J., Maley D., and O'Neil B. 2014. Chemically Enhanced Proppant transport. Presented at the SPE Annual Technical conference, Amsterdam, The Netherlands, 27-29 October. SPE-170640. <http://dx.doi.org/10.2118/170640-MS>.
- Briggs K., Hill D. and Zhu D. 2014. The Relationship Between Rock Properties and Fracture Conductivity in the Fayetteville Shale. Presented at the SPE Annual Technical Conference, Amsterdam, The Netherlands, 27-29 October. SPE-170790. <http://dx.doi.org/10.2118/170790-MS>.
- Brown, S.R. 1987. Fluid Flow Through Joints: The Effect of Surface Roughness. *Journal of Geophysical Research* **92** (B2): 1337-1347.
- Coulter, G.R., Benton, E.G, and Thomson, C.L. 2004. Water Fracs and Sand Quantity: A Barnett Shale Example. Presented at the SPE Annual Technical Conference and Exhibition, Houston, Texas, 26-29 September. SPE-90891-MS. <http://dx.doi.org/10.2118/90891-MS>.

- Develi, K. and Babadagli, T. 1998. Quantification of Natural Fracture Surfaces using Fractal Geometry. *Math. Geol.* **30** (8): 971-998.
- Develi, K. and Babadagli, T. 2015. Experimental and Visual Analysis of Single-Phase Flow through Rough Fracture Replicas. *Int. J. of Rock Mech. and Min. Sci.* **73**: 139-155.
- Fredd, C.N., McConnell, S.B., Boney, C.L. et al. 2000. Experimental Study of Hydraulic Fracture Conductivity Demonstrates the Benefits of Using Proppants. Presented at the SPE Rocky Mountain Regional/Low permeability Reservoirs Symposium, Denver, Colorado, 12-15 March. SPE-60326-MS. <http://dx.doi.org/10.2118/60326-MS>.
- Gangi, A.F. 1978. Variation of Whole and Fractured Porous Rock Permeability with Confining Pressure. *Int. J. Rock Mech. Min. Sci. & Geomech. Abstr.* **15** (5): 249-257.
- He, J., Ling, K., Pie, P. et al. 2013. A Correlation to Evaluate the Fracture Permeability Changes as Reservoir is Depleted. Presented at the SPE Eastern Regional Meeting, Pittsburgh, Pennsylvania, 20-22 August. SPE-165709-MS.
- Kassis, S. and Sondergeld, C.H. 2010. Gas Shale Permeability: Effects of Roughness, Proppant, Fracture Offset, and Confining Pressure. Presented at the CPS/SPE International Oil & Gas Conference and Exhibition, Beijing, China, 8-10 June. SPE-131376-MS. <http://dx.doi.org/10.2118/131376-MS>.
- Kranz, R.L., Frankel, A.D., Engelder, T. et al. 1979. The Permeability of Whole and Jointed Barre Granite. *Int. J. Rock Mech. Min. Sci. & Geomech. Abstr.* **16** (4): 225-234.
- Koyama, T., Neretnieks, I., and Jing, L. 2007. A Numerical Study on Differences in using Navier-Stokes and Reynold Equations for Modeling the Fluid Flow and Particle Transport in Single Rock Fractures with Shear. *International Journal of Rock Mechanics & Mining Sciences* **45** (7): 1082-1101.
- Lee, H.S. and Cho, T.F. 2002. Hydraulic Characteristics of Rough Fractures in Linear Flow under Normal and Shear Load. *Rock Mechanics and Rock Engineering* **35** (4): 299-318. <http://doi:10.1007/s00603-002-0028-y>.
- Mei, Y., Economides, M.J., Chenji, W. et al. 2013. Hydraulic Fracture Design Flaws – Proppant Selection. Presented at the SPE Annual Technical Conference and Exhibition, New Orleans, Louisiana, 30 September–2 October. SPE-166299-MS. <http://dx.doi.org/10.2118/166299-MS>.
- Nemoto, K., Watanabe, N., Hirano, N. et al. 2008. Direct Measurement of Contact Area and Stress Dependence of Anisotropic Flow Through Rock Fracture with Heterogeneous Aperture Distribution. *Earth and Planetary Science Letters* **281** (1-2): 81-78. <http://doi:10.1016/j.epsl.2009.02.005>.
- Novotny, E.J. 1977. Proppant Transport. Presented at the 52nd Annual Fall Technical Conference and Exhibition, Denver, Colorado, 9-12 October. SPE-6813-MS. <http://dx.doi.org/10.2118/6813-MS>.
- Penny, G.S. 1987. An Evaluation of the Effects of Environmental Conditions and Fracturing Fluid upon the Long-Term Conductivity of Proppants. Presented at 62nd Annual Technical Conference and Exhibition, Dallas, Texas, 27-30 September. SPE-16900-MS. <http://dx.doi.org/10.2118/16900-MS>.
- Raimbay, A., Babadagli, T., Kuru, E. and Develi, K.** 2014. Effect of Fracture Surface Roughness and Shear Displacement on Permeability and Proppant Transportation in a Single Fracture. Presented at the 2014 SPE Unconventional Res. Conf., Calgary, AB, Canada, 30 Sept.-2 Oct. SPE-171577-MS. <http://dx.doi.org/10.2118/171577-MS>.
- Raimbay, A., Babadagli, T., Kuru, E. and Develi, K.** 2015. Effect of Fracture Surface Roughness, Shear Displacement, Fluid Type and Proppant on the Permeability of a Single Fracture: A Visual and Quantitative Analysis. Submitted to *SPE Res. Eval. and Eng.*, 2015 (in review).
- Rasband, W.S., ImageJ, U. S. National Institutes of Health, Bethesda, Maryland, USA, 1997-2005, <http://rsbweb.nih.gov/ij/docs/user-guide.pdf>.
- Raymond, L.R. and Binder, G.G. 1967. Productivity of Wells in Vertically Fractured Damaged Formations. *Journal of Petroleum Technology* **19** (01): 120-130.
- Renshaw, C.E. 1995. On the Relationship between Mechanical and Hydraulic Apertures in Rough-Walled Fractures. *Journal of Geophysical Research* **100** (B12): 629-636.
- Ribeiro, L.H. and Sharma, M.M. 2012. A New Three-Dimensional, Compositional, Model for Hydraulic Fracturing with Energized Fluids. Presented at the SPE Annual Technical Conference and Exhibition,

- San Antonio, Texas, 8-10 October. SPE 159812-MS. <http://dx.doi.org/10.2118/159812-MS>.
- Ribeiro, L.H. and Sharma, M.M. 2013. Fluid Selection for Energized Fracture Treatments. Presented at the SPE Hydraulic Fracturing Technology Conference, Woodland, Texas, 4-6 February. SPE-163867-MS. <http://dx.doi.org/10.2118/163867-MS>.
- Terracina, J.M., Turner, J.M., Collins, D.H. et al. 2010. Proppant Selection and its Effect on the Results of Fracturing Treatments Performed in Shale Formations. Presented at the SPE Annual Technical Conference and Exhibition, Florence, Italy, 19-22 September. SPE-135502-MS. <http://dx.doi.org/10.2118/0511-0026-JPT>.
- Tsang, Y.W. and Witherspoon, P.A. 1983. The Dependence of Fracture Mechanical and Fluid Flow Properties on Fracture Roughness and Sample Size. *Journal of Geophysical Research* **88** (B3): 2359-2366.
- Tsang, Y.W. 1984. The Effect of Tortuosity on Fluid Flow Through a Single Fracture. *Water Resources Research* **20** (9): 1209-1215.
- Van Dam, D.B. and de Pater, C.J. 1999. Roughness of Hydraulic Fractures: The Importance of In-Situ Stress and Tip. Presented at SPE Annual Technical Conference and Exhibition, Houston, Texas, 3-6 October. SPE-56596-MS. <http://dx.doi.org/10.2118/56596-MS>.
- Watanabe, N., Hirano, N., and Tsuchiya, N. 2008. Diversity of Channeling Flow in heterogeneous Aperture Distribution Inferred from Integrated Experimental – Numerical Analysis on Flow through Shear Fracture in Granite. *Journal of Geophysical Research* **114** (B4). <http://doi:10.1029/2008JB005959>.
- Yeo, I.W., De Freitas, M.H., and Zimmerman, R.W. 1998. Effect of Shear Displacement on the Aperture and Permeability of a Rock Fracture. *Int. J. Rock Mech. Min. Sci. & Geomech. Abstr.* **35** (8): 1051-1070.

CHAPTER 5: CONCLUSIONS AND RECOMMENDATIONS

Conclusions

Based on the results of the thesis study, the following conclusions can be offered:

- Rough walls of fracture combined with rock type of fracture affects fluid flow and controls permeability of fractures.
- In joint fractures, with increasing degree of roughness in limestone models, permeability of fracture decreases and, in contrast, marble's permeability increases with increasing roughness.
- In horizontally displaced fractures, permeability in limestone increases with increasing roughness; however, in marble with increase of roughness permeability decreases.
- Results of the fractal analyses including the effect of roughness and grain size showed that in joint type fractures, grain size and fractal dimension are important parameters in modeling hydraulic behavior of single fractures. It was seen that with the increasing fractal dimension and grain size, planar area wetted with fluid increases and pressure drop decreases, indicating increase in permeability of fracture.
- In comparison with joint fractures, in horizontally displaced or shear fracture models, area saturated by the injected fluid was systematically higher.
- Among all four fractal dimensions (variogram analysis, D_{va} ; triangular prism, D_{tp} ; power spectral density analysis, D_{psd} , and ratio total to planar areas, A_t/A_p) variogram analysis (D_{va}) showed the best correlation.
- It was found that in addition to roughness characteristics, fluid type or viscosity should be considered in the computational modeling studies of fluid flow. Flow behaviour characteristic (mainly viscosity) is almost equally important as roughness on fluid distribution (wetted area) and especially conductivity (pressure drop).
- Effectiveness of proppant transport and distribution is controlled by both roughness characteristics and transport ability of fracturing fluid.
- Polymer solution distributed proppants more uniformly while water settled proppants in the inlet of fracture and seeped through the model.
- Sand placed by polymer solution was more stable in limestone models than in marble and granite.

- Sand was transported and distributed better in limestone fractures while it was injected with water; however, in marble and granite fractures sand was better transported and distributed with polymer solution.
- Accumulation of sand in smooth model was packed or creating multilayer (thicker) type of settlement while in the rough models, sand was settled as a monolayer (thinner).
- Smooth fracture model had a lower hydraulic conductivity than rough-walled fracture models.
- The sheared fracture case demonstrated a significant change in proppant distribution/accumulation and, thereby, hydraulic conductivity of fracture. This change was controlled by the roughness characteristics of fracture surfaces determined by lithology.

Recommendations

- In this study experiments with one size of sand injection were carried out. In the way forward, it is recommended to inject different size of sand and along with planar distribution of sand measurement, which will give better understanding in relation to sand size within roughness characteristics and its influence to conductivity of fracture.
- In this research the overburden stress was not applied. It is recommended to apply overburden stress in two different fracture types (joint and horizontally displaced) and measure permeability in the presence of propping agents.
- The effect of fracture orientation on transportation and distribution of propping agents will play an important role. It is recommended to inject propping agent in vertical fractures with /against gravity and observe placement of the proppants with its effect to pressure drop.
- Gas injection in the presence of propping agents (which can be injected using different type of fracturing fluid) will provide understanding of the amount of fluid remaining in fractures after fracturing operation (i.e., load recovery during flow back).

- Experiments using different size of propping agent with altered wettability will also be useful to determine the amount of fracturing fluid that can be recovered combined with effect of roughness characteristics.